Global Sensitivity Analysis for Terrestrial Carbon Cycle Simulations Under Present and Future Climate Conditions

by

Raj Deepak Suruli Nagarajan
B.Tech., SRM Institute of Science and Technology, 2011
M.Tech., Savitribai Phule Pune University, 2018

A Dissertation Submitted in Partial Fulfillment of the
Requirements for the Degree of

DOCTOR OF PHILOSOPHY

in the School of Earth and Ocean Sciences

We acknowledge and respect the Lək̓^{w}əŋən (Songhees and X^{w}sepsəm/ Esquimalt) Peoples on whose territory the university stands, and the Lək̓^{w}əŋən and W̱SÁNEĆ Peoples whose historical relationships with the land continue to this day.

Global Sensitivity Analysis for Terrestrial Carbon Cycle Simulations Under Present and Future Climate Conditions

by

Raj Deepak Suruli Nagarajan
B.Tech., SRM Institute of Science and Technology, 2011
M.Tech., Savitribai Phule Pune University, 2018

Supervisory Committee

Dr. Christian Seiler, Co-Supervisor
(School of Environmental Studies, Queen's University;
School of Earth and Ocean Sciences, University of Victoria)

Dr. Adam H. Monahan, Co-Supervisor
(School of Earth and Ocean Sciences, University of Victoria)

Dr. Joe R. Melton, Departmental Member
(Climate Research Division, Environment Climate Change Canada;
School of Earth and Ocean Sciences, University of Victoria)

Dr. Julie Zhou, Outside Member
(Department of Mathematics and Statistics, University of Victoria)

ABSTRACT

In this dissertation, I assessed the sensitivity of the land surface carbon, water, and energy fluxes to variations in model input parameters when simulated by a land surface model (LSM). The terrestrial biosphere currently uptakes approximately 30% of anthropogenic CO_2 emissions. LSMs project that the biosphere will continue to take up carbon till early to mid 22^{nd} century, making it a net carbon sink. These carbon sink projections are important for improving the future carbon predictions and informing mitigation strategies. But, there are substantial uncertainties in the strength of the simulated sink. For instance, the spread in the inter-model carbon sink is 1 to 3.2 PgC yr^{-1} during 2014-2023 (Global Carbon Budget), and 2 to 7 PgC yr^{-1} for the end of the 21^{st} century (Intergovernmental Panel on Climate Change's Sixth Assessment Report).

Some of the mentioned uncertainties in the simulated carbon sink arises from parameter uncertainties. While parameter tuning can help reduce these uncertainties, optimizing all input parameters in a complex, non-linear LSM is computationally prohibitive. Identifying influential parameters and understanding their influence on the model output(s) is an essential step before tuning the parameters. The influence of parameter uncertainties on the terrestrial carbon cycle output variables can be assessed using global sensitivity analysis (GSA). In this dissertation, I apply a two-step GSA to the output variables simulated by an LSM, the Canadian Land Surface Scheme Including Biogeochemical Cycles (CLASSIC).

This research is divided into three parts, each applying GSA to CLASSIC output variables under different conditions. The questions asked are: (1) Is there a common set of parameters that substantially influence the majority of ecosystem output variables simulated at an eddy covariance site?, (2) Which parameters substantially affect the uncertainty of the historical carbon sink for different biomes?, and (3) Which parameters substantially affect the uncertainty of future carbon sink projections for different biomes?

Through GSA's first step, a coarse sampled screening test, I found that only 15–17% of input parameters show appreciable influence on any of the simulated output variables. Through the second fine sampled quantitative analysis, I further narrowed this subset, and identified between two and 15 parameters as the most influential for different output variables and statistical measures. The influential parameters varied depending on the meteorological forcing used. The maximum rate at which CO_2

is used during photosynthesis ($vmax$) and the loss of light along the canopy depth (kn) are the most recurring influential parameters across all forcing scenarios, and statistical measures. Additionally, other photosynthetic parameters, as well as those related to rooting and phenology, play an important role when CLASSIC is forced using reanalysis and Earth system model data. The sensitivity of the terrestrial carbon sink to the uncertainty in $vmax$ reduces by the end of the 21^{st} century. In many cases the analysis is unable to rank the most influential parameters because of large sampling variations in the sensitivity indices.

GSA is a stepping stone before performing model optimization. However, the computational demands of GSA are substantial. In this study, performing GSA for just seven grid cells required approximately 25 CPU years. Scaling such analyses to a global level using the full model would be computationally prohibitive. However, advancements in machine learning and emulator-based approaches present a promising alternative for GSA and optimization efforts, drastically reducing computational costs by requiring fewer input-output simulations than the full model. These innovations could enable large-scale assessments of parameter uncertainty, ultimately leading to more robust predictions of the terrestrial carbon sink, which will help in the shaping of better mitigation efforts.

Contents

List of Tables

List of Figures

ACKNOWLEDGEMENTS

This dissertation is the outcome of six years' worth of journey, filled with hard work. I am grateful to everyone who has stood by me through these years, especially during the times when I did not believe in myself.

First and foremost, to Christian and Adam. Thank you for being the best supervisors a researcher could ask for. Thank you for your unwavering support since day one, when I took a leap of faith to pursue my Ph. D. Thank you for your invaluable mentorship and support for both within and out of this journey. I could not have done a better job without your supervision.

I sincerely appreciate my committee members Joe and Julie for providing me with constructive criticism and thoughtful suggestions, which have greatly improved the quality of my work.

I am grateful for all the members of the CLASSIC group. Vivek, Joe, and Paul, your valuable input for parameter uncertainties and model expertise has helped me become a better modeller. Gesa, thank you for your help with the numerous errors I had encountered. Mike, I highly appreciate your help with the model's technicalities during my initial stage. Charles, I enjoyed working with you. It was good to know and connect with someone who was on a very similar boat as I was. Every other member is also appreciated in terms of their knowledge about the model, even if I have had minimal interactions.

I am deeply grateful to Ed for his technical support and computing expertise. Without his help, I would not have made any computational progress, let alone complete 25 CPU years' worth of (bug-free) simulations. I also sincerely appreciate my peers Jo, Liang, Ruth, Kyle, Ameneh, Camille, Dan, Julia, and everyone else in the Climate lab, for their patience and understanding, especially when I occupied all the nodes and processors. Thank you for being amazing colleagues. You can definitely generate a "Blame Raj" folder. Jia-Xuan, Patrick Duke and Parsa, thank you for cheering loudly for me.

My friends near and far, thank you for rooting for me. Ross, thank you for being a mental support when things got out of hand. I look forward to expanding our friendship to many more years to come. Dan, thank you for the numerous photo walks that we went on. I really needed them, especially when I was stressed out these past few months, while writing this document. Singu and family, thank you for being my family here. Prathyusha, Prerna, and Harish, you all made the transition from

India to here, feel less of a burden. We've seen each other grow through the thick and thin of academic life. Miles, thank you for making the house feel less of a house and more of a home. Samay and Kavi, your phone calls through these years always felt like a soothing balm; thank you for standing by me in this chapter of my life and many more to come. And to my numerous other friends who have supported me through and through, I thank you from the depths of my heart.

Darcey, thank you for being a person I connected with on a very fine level. You were the beacon to my ship caught in a storm, and I am glad I could be that person for you as well. I wish you all the peace in the world. Trevor, thank you for being more than a friend, and showing me a new world.

Mom, Dad, brother, and everyone in my family, thank you for trusting me to live a life by myself. Thank you for your unconditional love, patience, and encouragement. Homesickness is a thing and I did not realise it until after I stepped out (of course!). I have grown to be a better person who can hold his ground, and I know you are proud of me.

And lastly, a thank you to myself. I have been on high waves and on low tides through this journey. I have had times where I doubted myself, thought I was not fit, and talked bad about myself, be it due to imposter syndrome or even worse, self doubt. I am more than that. I am proud of the work I have done in this research and on myself. I am proud to stand tall like a tree, like the forests I study in this research work. "*Raj, you have come a long way, and you are more level-headed than you were a few years ago. I am proud of you, and the person you have become.*"

Chapter 1

Introduction

1.1 The Carbon Cycle

We are part of the carbon cycle and we are disrupting it at a tremendous pace. Carbon is the fundamental building block of life and is present in a majority of things we consume and interact with, including ourselves, the food we eat, the air we breathe, plants and animals, oceans, transportation, fuels, and some rocks and minerals. The carbon that exists today has been cycling through Earth's systems for billions of years, moving from one carbon stock to another (Figure 1.1). One such carbon stock is the atmosphere, which held a global average of 855 GtC between 2014 and 2023 (Friedlingstein et al., 2024). Carbon continuously gets exchanged between the atmosphere, land, and ocean.

Atmospheric CO_2 is absorbed by the terrestrial biosphere and the ocean, cycles through organisms via the food chain, and transfers within various parts of the the ocean and the ocean floor. In both terrestrial and aquatic environments, microorganisms feeding on decomposing organic matter, along with respiration from plants and animals, release carbon back into their surroundings. On land, wildfires also contribute to carbon emissions. Some carbon is sequestered as dying plants and carbon-rich ocean sediments become buried beneath Earth's surface, eventually returning to the atmosphere through geological processes such as subduction and volcanic outgassing. Since industrialization, large-scale fossil fuel extraction and combustion for energy, along with limestone use in cement production, have released vast amounts of stored carbon into the atmosphere at an extreme rate. There was a near carbon balance during the Holocene period, but the release of copious amounts of CO_2 into

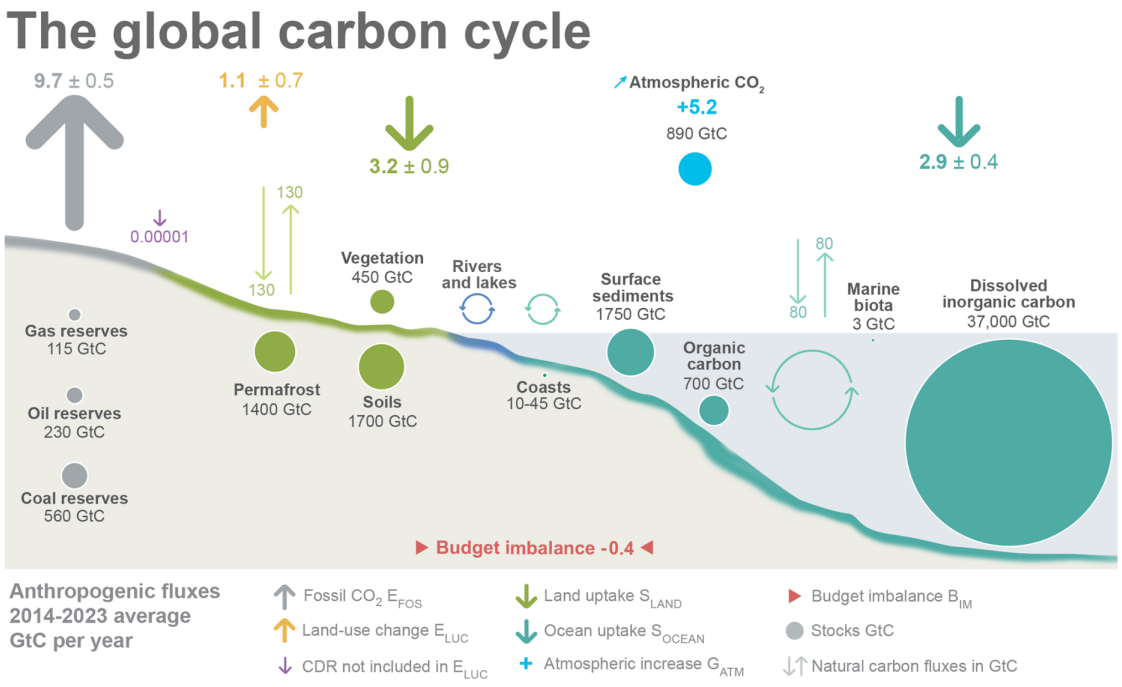

Figure 1.1: A schematic representation of the carbon cycle perturbation due to anthropogenic activities for the decade 2014-2023 (Friedlingstein et al., 2024).

the atmosphere has disrupted the carbon budget since then.

1.2 The Terrestrial Carbon Sink

The atmospheric carbon sink consists of the terrestrial biosphere, the ocean from shallow waters to deep depths, and underground hydrocarbon reserves (Global Carbon Budget 2024 assessment; GCB; Friedlingstein et al., 2024). Over many millennia, the terrestrial biosphere has functioned as a net carbon sink, absorbing more carbon from the atmosphere than it releases. Through photosynthesis, plants capture atmospheric CO_2 and store it as biomass in leaves, stems, and roots, contributing to a global average of 450 GtC of the 3,550 GtC stored in the terrestrial biosphere during 2014–2023. Simultaneously, respiration by living plant cells, microbial decomposition of organic matter, and natural disturbances such as wildfires contribute to CO_2 emissions. The balance between carbon uptake and release within the terrestrial biosphere fluctuates across diurnal, seasonal, decadal, and millennial timescales.

Anthropogenic activities such as land-use change (excluding processes like afforestation), human-induced wildfires, and fossil fuel combustion serve as substantial

sources of atmospheric carbon. These additional sources disrupt the natural carbon budget. Since the Industrial Revolution (1850) to the present day, atmospheric CO_2 concentrations ($[CO_2]$) have risen from 284.32 ppm to 424 ppm (2024) due to anthropogenic emissions (Friedlingstein et al., 2024). The GCB assessment shows the terrestrial biosphere has absorbed about 30% of anthropogenic CO_2 emissions over the past decade. Earth system models (ESMs) project that while the total land carbon uptake will continue to rise with increasing emissions, the fraction of emissions sequestered through photosynthesis will decline by the late 21st century (Canadell et al., 2023). However, the strength of the terrestrial carbon sink remains highly uncertain, both in present-day estimates and future projections, as simulated by land surface models (LSMs).

1.3 Land Surface Modelling

LSMs are integral components of ESMs, designed to simulate the exchange of mass, energy, and momentum between the land surface and the atmosphere. Over the decades, LSMs have progressively incorporated more processes to better represent the terrestrial biosphere as illustrated in Figure 1.2 (Fisher & Koven, 2020). Through the evolution process, these models have become complex over the decades. Highly complex models require input parameters to interact and/or require a large number of input parameters. Some parameters lack direct observational constraints, leading to uncertainties that propagate through the model and affect the reliability of simulated outputs.

One such LSM is the Canadian Land Surface Scheme Including Biogeochemical Cycles-version 1.0 (CLASSIC; Melton et al., 2020), which serves as the terrestrial component of the Canadian Earth System Model (CanESM; Swart et al., 2019). As illustrated in Figure 1.3, CLASSIC simulates a wide range of processes and is highly complex. CLASSIC is one of the 17 participants in the Trends and Drivers of the Regional Scale Terrestrial Sources and Sinks of Carbon Dioxide (TRENDY) project (Sitch et al., 2024). The GCB assessments (e.g., Friedlingstein et al., 2023, 2024) analyse the TRENDY models to provide one of the most comprehensive estimates of global carbon fluxes. Additionally, ESMs such as the CanESM participate in the Coupled Model Intercomparison Projects (CMIP) to simulate future environmental conditions, including projections of the terrestrial carbon sink. The outcomes from CMIP are used in the Intergovernmental Panel on Climate Change Assessment

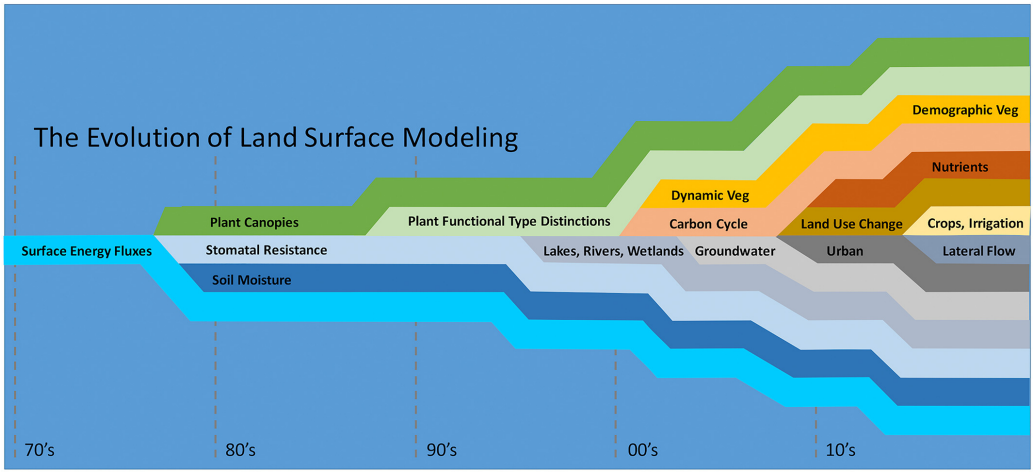

Figure 1.2: A representation of evolution of land surface model processes, depicting increasing complexity from 1970's to 2010's (Fisher & Koven, 2020).

Reports (e.g., the Sixth Assessment Report; Lee et al., 2023). Even after decades of evolution, broad inter-modal uncertainty ranges are noticed for the present and future terrestrial carbon sink simulated by LSMs (Arora et al., 2019; **?**; **?**). Most signatories of the Paris Agreement stated that the land carbon sink would be utilized to help achieve mitigation targets for reducing greenhouse gas emissions (Horowitz, 2016). Given its influential role in mitigation plans, assessing current carbon fluxes, and projecting future changes, reducing uncertainties in the output variables simulated by an LSM is essential.

1.4 Global Sensitivity Analysis

LSMs require a wide range of inputs, such as meteorological data, atmospheric CO_2 concentration ($[CO_2]$), land cover change, initial conditions, and parameter values. However, many of the input parameter values are not well constrained due to a lack of observations, and uncertain inputs lead to uncertain outputs. One way to reduce uncertainties in the output variables is through parameter tuning, where uncertain input parameters are adjusted to improve the model's performance. When parameters are allowed to vary, each parameter or combination of parameters accounts for a fraction of the total model output variation. However, tuning all input parameters in a highly complex model like CLASSIC is computationally prohibitive. Understanding how input parameter uncertainties influence model outputs is essential for improving

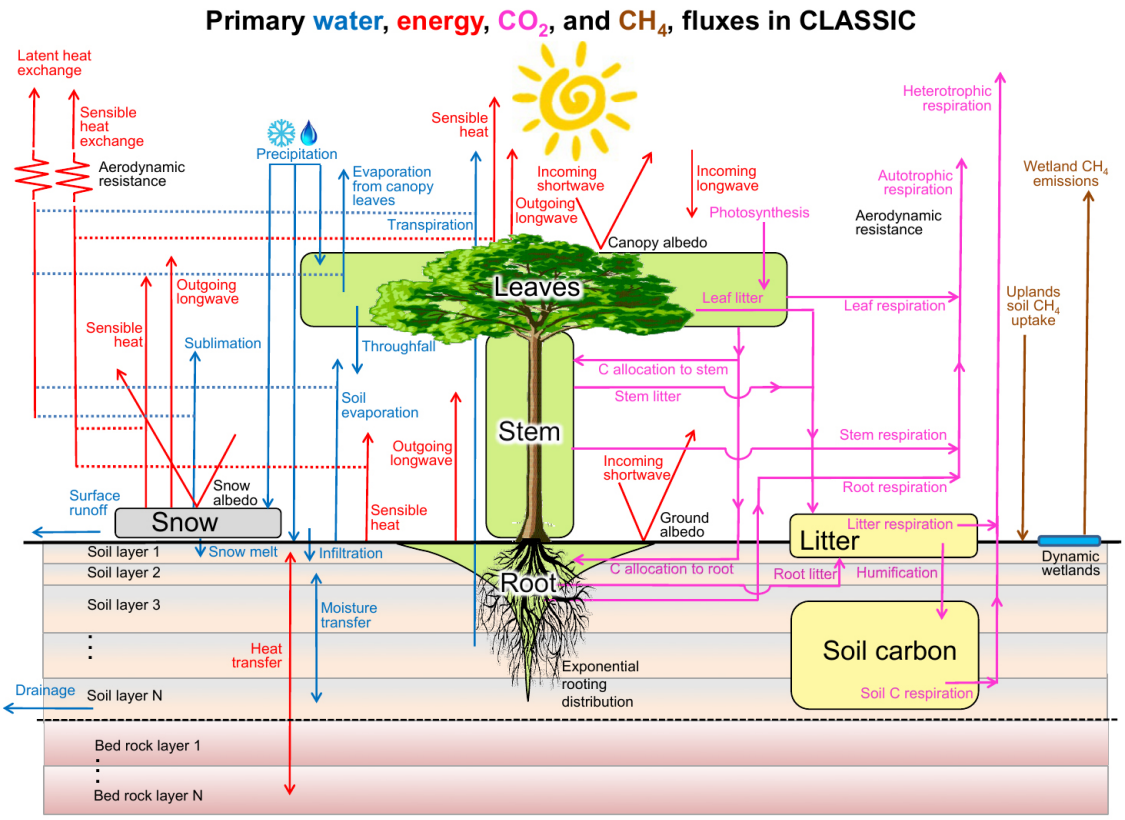

Figure 1.3: Schematic representation of different processes simulated by CLASSIC (Melton et al., 2020).

the model's performance. Identification of influential parameters allows optimization efforts to focus on a small subset of parameters. Global sensitivity analysis (GSA) allows for the quantification of parameter value uncertainties' impact on model output variables, thereby identifying a small subset of highly influential parameters (Saltelli et al., 2004; Wagener & Pianosi, 2019).

Global sensitivity analysis (GSA) quantifies the uncertainties in the output variables due to uncertainties in the input parameters. In the research work presented, GSA is used to evaluate the sensitivity of carbon cycle variables to parameter uncertainty using CLASSIC. There are no previous GSA studies performed on the outputs simulated by CLASSIC. By identifying the most influential parameters through GSA, this research aims to enhance the understanding of the LSM and provide insights for future model development and optimization. GSA can help identify a subset of the most influential parameters, allowing for a better optimization process (e.g., Baker et al., 2022; McNeall et al., 2023, 2020; Petropoulos et al., 2014). By narrowing down

the number of parameters to be tuned, GSA facilitates model refinement while reducing computational costs. While the results of GSA will be discussed in detail, model optimization itself is beyond the scope of this work.

1.5 Research Questions

Previous LSM studies have evaluated parameter uncertainty in terrestrial carbon cycle variables through GSA methods (e.g., Y. Li et al., 2022; Ma et al., 2020; Pappas et al., 2013; Zhu & Zhuang, 2014). Most of these studies relied on outputs from eddy covariance sites, which provide observed meteorological data. However, these data are too short to simulate carbon stocks (e.g., the soil carbon pool), that eventually affect long-term carbon sink dynamics. The TRENDY protocol recommends running LSMs in a fully transient mode over extended periods to examine the terrestrial carbon balance. In transient simulations, models respond dynamically to changing environmental conditions. To study the carbon sink under such conditions, meteorological data from reanalysis or ESMs can be used.

GSA has not yet been conducted for CLASSIC using output variables simulated at an eddy covariance site. No GSA studies have quantified parameter uncertainty in the historical terrestrial carbon sink, nor have they assessed the uncertainty in future carbon sink projections. This research is the first to evaluate the uncertainty of both present and future terrestrial carbon cycle variables simulated by CLASSIC. The study is structured into three main chapters, each applying GSA under different conditions. The research questions addressed in the work presented here, include:

1. Is there a common set of parameters that substantially influence the majority of ecosystem output variables simulated at an eddy covariance site?

2. Which parameters substantially affect the uncertainty of the historical carbon sink for different biomes?

3. Which parameters substantially affect the uncertainty of future carbon sink projections for different biomes?

1.6 Dissertation Outline

The GSA methodology is consistent across the three main chapters. The analysis perturbs all parameters within their respective uncertainty ranges and runs CLASSIC for each unique parameter combination. Since quantitatively assessing the sensitivity of any output variable simulated by CLASSIC to all input parameters is computationally prohibitive, the GSA is conducted in a two-step process. First, a qualitative screening method is used to identify an influential subset of parameters for a range of output variables, including carbon cycle variables and turbulent heat fluxes. The top-ranked parameters from this screening are then analyzed using a quantitative variance-based method. This two-step approach reduces computational expense while maintaining a systematic evaluation of the sensitivities.

Chapter 2 establishes the framework for performing GSA on all input parameters in CLASSIC. The analysis is conducted for a single eddy covariance measurement site in the Amazon rainforest, characterized by homogeneous evergreen broadleaf trees (Pastorello et al., 2020). This study identifies the most influential parameters for a wide range of output variables, and focuses on the uncertainties of the carbon uptake term as an example. This study did not simulate the long-term carbon sink, as capturing the long-term dynamics requires extended transient simulations that account for the carbon exchange between the atmosphere and biosphere, which are not available from the eddy covariance site.

To address questions related to the uncertainty in the historical carbon sink, long transient simulations spanning centuries were conducted. In Chapter 3, CLASSIC is forced with reanalysis data at seven grid cells each located in a different biome. This chapter also accounts for CO_2 emissions from wildfires, increasing the number of parameters considered compared to Chapter 2. This chapter mainly assesses the sensitivity of the historical carbon sink to influential parameters for two statistical measures.

Chapter 4 quantifies the sensitivity of carbon cycle variables to influential parameters under a future climate condition. CLASSIC is forced with the output data from CanESM5. By incorporating transient conditions, this chapter provides a comprehensive understanding of how input parameter uncertainties influence carbon sink projections over time. The influential parameters obtained are compared for the projected future carbon sink, and the difference between the future and historical mean carbon sinks.

Chapter 5 provides a compilation of the findings and summaries of the three main chapters. This chapter also answers the broad research questions mentioned earlier. Future avenues for GSA studies performed on the outputs of LSMs and how it will be helpful for future research are also provided in this chapter.

The contents of Chapter 2 have been published in Atmosphere-Ocean (S. N. et al., 2024). Contents of Chapters 3 and 4 have been submitted for peer review in the same journal as two separate manuscripts.

The following chapter answers the question “Is there a common set of parameters that drive the majority of ecosystem output variables simulated at an eddy covariance site?”

Chapter 2

Global Sensitivity Analysis at an Evergreen Broadleaf Eddy Covariance site

Land surface models have become indispensable for understanding the role of the terrestrial biosphere in the global climate system. However, the ability of LSMs to reproduce observed carbon, water, and energy fluxes varies considerably among models. Some of these deficiencies are attributed to parameter uncertainties. Global sensitivity analysis (GSA) quantifies model output uncertainties caused by the uncertainty in model inputs. Our study conducts, for the first time, a GSA for the Canadian Land Surface Scheme Including Biogeochemical Cycles (CLASSIC). Focusing on a site in the humid tropics, we evaluate the model's sensitivity for a wide range of ecosystem variables (17 in total). Considering a total of 90 parameters, we identify the top five most influential parameters using the qualitative Morris method per output variable. These influential parameters are then analyzed using the quantitative Sobol' method. The analysis shows that the maximum carboxylation rate parameter has the greatest influence on almost all output variables considered. The impact of the maximum carboxylation rate is partially regulated by the canopy extinction coefficient's uncertainty. The results of this research will guide future efforts to optimize the model's performance more efficiently, focusing on a small subset of the 90 parameters.

The contents of this chapter appeared in Atmosphere-Ocean Journal as *A Global Sensitivity Analysis of Parameter Uncertainty in CLASSIC* (S. N. et al., 2024).

2.1 Introduction

Land Surface Models (LSM) are components of climate models that simulate the exchange of mass, energy, and momentum between the land surface and the atmosphere. The complexity of LSMs has increased over time as more processes have been added (Fisher & Koven, 2020; Pitman, 2003). Sellers et al. (1997) proposed a classification for LSMs based on their degree of complexity. They characterize the first generation of LSMs as those using a simple surface energy balance equation and processes related to a combined surface-vegetation layer (Manabe, 1969). The second generation of LSMs took the first generation a step further by dividing the surface-vegetation layer into a separate soil and vegetation layer. This approach recognizes that the canopy cover shields a fraction of the ground from incoming solar radiation. Additionally, moisture diffusion into multiple soil layers and the impact of snow cover on the soil are also considered (Deardorff, 1978). The third generation of LSMs include a representation of carbon fluxes through stomatal conductance, photosynthesis, and respiration (Farquhar et al., 1980). The next generation of LSMs included carbon pools, allowing climate models to simulate an interactive global carbon cycle. Further processes include competition among plant functional types, wildfires, and land cover changes (Lawrence et al., 2019). The role of nutrients in photosynthesis has been incorporated through the addition of nitrogen (Lawrence et al., 2019) and phosphorous cycles (Goll et al., 2017; Reed et al., 2015; X. Yang et al., 2014). The increasing complexity of LSMs creates the demand for advanced methods of model evaluation, including a systematic approach for assessing model sensitivity.

Some of the uncertainties seen in the output variables are due to uncertainties in the input parameters, as these parameters are not well constrained due to a lack of observations. Sensitivity analysis can be used to quantify these uncertainties in the output variable caused by uncertainties in the input parameters. Two types of sensitivity analysis are commonly used: local sensitivity analysis, and global sensitivity analysis (GSA). Local sensitivity analysis evaluates the effect on model output of small changes in input parameter values around a base point (e.g., local derivatives), and is typically performed one parameter at a time. In contrast, GSA computes the importance of parameters based on changes in model output(s) over the full uncertainty

range of parameter values for multiple input parameters simultaneously (Saltelli et al., 2008). GSA is an important step for model development and optimization, which can be done by constraining very few parameters with optimal values using observations (Bagnara et al., 2019; J. Li et al., 2016; Y. Li et al., 2022; Ma et al., 2020; Zhu & Zhuang, 2014). LSM groups have used GSA methods to identify parameters that are influential on output variables by studying a single eddy covariance site (Ma et al., 2020; Tang & Zhuang, 2009; Verbeeck et al., 2006), multiple sites (Alton et al., 2006; Arsenault et al., 2018; Hou et al., 2015; Y. Li et al., 2022; Pappas et al., 2013; Rosolem et al., 2012; Zhu & Zhuang, 2014) or by using global model data (J. Li et al., 2016; X. Lu et al., 2013). The results of these studies consistently show that most of the model output uncertainty associated with parameters is governed by very few parameters. The most influential parameters for the model output variables net ecosystem exchange, gross primary productivity (GPP), sensible heat flux, and latent heat flux are frequently identified as maximum carboxylation rate ($vmax$), quantum efficiency, specific leaf area, parameters related to stomatal conductance, and roughness length (Alton et al., 2006; Arsenault et al., 2018; J. Li et al., 2016; Y. Li et al., 2022; X. Lu et al., 2013; Ma et al., 2020; Rosolem et al., 2012; Zhu & Zhuang, 2014). Other studies have identified influential parameters such as the Clapp and Hornberger b parameter, soil respiration parameters, the canopy extinction coefficient (kn), and the scaling parameter from leaf to canopy (J. Li et al., 2013; Pappas et al., 2013; Verbeeck et al., 2006). The differences can be due to the choice of models, sites, sensitivity approaches, and/or parameter uncertainty ranges.

The Canadian Land Surface Scheme Including Biogeochemical Cycles (CLASSIC; Melton et al., 2020) is the land surface component of the Canadian Earth System Model (CanESM; Swart et al., 2019) and has undergone decades of development. There has been no prior GSA conducted on CLASSIC. Conducting such an analysis is important for understanding the importance of various parameters and how different processes are affected based on parameter uncertainty interactions. Additionally, GSA provides valuable insights to support ongoing model development efforts and tuning.

In the present study, we use GSA methods to identify the most influential parameters for a broad range of model outputs, including variables that form part of the carbon, water, heat, and radiation fluxes simulated by CLASSIC at a single eddy covariance FLUXNET2015 site in the humid tropics. We consider 90 independent parameters in a screening test to identify a subset of parameters that are then used in

a quantification test, wherein the effects of variations in input parameters on various model outputs such as gross primary productivity, autotrophic and heterotrophic respiration and transpiration rates, latent and sensible heat fluxes are studied. We also study the interactions of uncertainty ranges of the two most influential parameters on all model output variables.

The Methods section provides an overview of CLASSIC, the input parameters along with their uncertainty ranges, the chosen FLUXNET2015 site, and the GSA techniques and sampling method employed. The Results section presents findings from the GSA methods, and the importance and interactions of the two most influential parameters' uncertainty ranges on all processes. The Discussion section covers insights gained from this analysis, limitations in this study, the implications for parameter tuning, and the relevance of GSA to the terrestrial biosphere modelling community.

2.2 Methods

2.2.1 CLASSIC

CLASSIC can be used both in a coupled mode inside CanESM, and offline as a standalone model. The model is composed of two main components, namely the Canadian Land Surface Scheme (CLASS; Verseghy, 2017) and the Canadian Terrestrial Ecosystem Model (CTEM; Melton & Arora, 2016). CLASS simulates physical processes such as radiation, heat, and water fluxes of the land surface vegetation, soil, and snow. CTEM is the dynamic vegetation model in CLASSIC that simulates biogeochemical processes such as photosynthesis, phenology, allocation of carbon to the live carbon pools, canopy conductance, and tissue turnover (Arora & Boer, 2005); maintenance, growth and heterotrophic respiration (Melton et al., 2015) and dynamic root distribution (Arora & Boer, 2003). For the present study, for the current model configuration, some processes, such as competition, land use change, fire, moss, and the turbation of carbon in the soil, have been deactivated, as these processes are either not relevant for the site considered or are under active development in the model. CLASSIC has 134 input parameters, of which only parameters that are site-relevant (91) are considered in this study. The processes represented by these parameters are generally non-linear and are obtained empirically.

For our analysis, the model is run in the offline mode, and has been spun up to

a state of equilibrium with the observed meteorological data obtained from the site. The spin-up is performed separately for each combination of input parameter values. The spin-up starts from a bare ground state, where the leaf, stem, root, litter biomass and soil carbon pools are each set to values of zero. The model is determined to be in an equilibrium state if the annual soil carbon changes are less than 0.1% and/or the absolute net biome productivity value for the last two sets of spin-up years is less than 2×10^{-12} kgC m^{-2} year^{-1}. To reach equilibrium, we spin the model up for 500 years by looping over the available 11-year meteorological dataset, for the FLUXNET2015 site location (described in detail in Section 2.2.2). Once the equilibrium state is attained, the model is run for an additional 11 years using the observed meteorological forcing. The 11-year annual average value of each output variable is chosen for analysis by the GSA methods.

The photosynthesis module of CLASSIC simulates the net canopy-level photosynthetic rate that includes GPP (Eq. A.1-A.8; Melton & Arora, 2016) and autrotrophic respiration fluxes, which are computed from the living components: the vegetation carbon pools (leaf, root, stem). Heterotrophic respiration is the respiration from microbes that decompose litter (dead leaves, stems and roots) and soil organic carbon. The combined carbon pool present on the land is referred to as cLand. The model also simulates variables such as the leaf area index and vegetation height. The net canopy-level photosynthetic rate, along with the atmospheric CO_2 concentration and vapour pressure is used to compute the canopy conductance. Canopy conductance is used by the physical component of CLASSIC to obtain the surface energy budget variables, such as latent heat flux and sensible heat flux; and water cycle variables, such as the total run-off (including drainage through the base of the soil model) per unit area leaving the land portion of the grid cell, and transpiration. The net longwave and net shortwave radiation fluxes and the surface albedo are also simulated by the physical component of CLASSIC.

The response of modelled processes to changes in parameter uncertainties can be studied by identifying the influential parameters. In this study, the following variables have been analyzed using GSA methods: individual carbon cycle components (GPP, autotrophic respiration, heterotrophic respiration, leaf area index, vegetation height, carbon pools of the land, leaf, litter, root, stem, soil); turbulent heat fluxes (latent and sensible heat fluxes); radiation fluxes (net longwave and shortwave); and water cycle components (transpiration and total run-off). The subsections that follow provide further detail on the site selection process, parameter uncertainty ranges, and

sensitivity analysis methods used. A more comprehensive discussion on the model equations used to compute GPP is provided in Appendix A.1.1.

Parameter Uncertainty Ranges

Parameter ranges represent a critical choice for any sensitivity analysis, and these ranges will inevitably affect the sensitivity results (Wallach & Genard, 1998). Of the 134 input parameters, only 91 were used for the GSA (Table A.2), of which 88 are independent parameters, and three are dependent. As mentioned earlier, some parameters were not considered as they correspond to processes that are deactivated in the present model configuration, or are not relevant to our site, or have virtually no uncertainty. The parameter uncertainty ranges were determined in the following ways: $vmax$, a well-documented parameter, has been assigned a specific range based on observations of the evergreen broadleaf plant function type (from the TRY plant traits database; Kattge et al., 2020); 35 parameters (38.5% of the total number of parameters) have been assigned plausible ranges based on our modelling experience and expert advice, and 30 parameters (32.3% of the total number of parameters) have been assigned values based on a literature survey, of which the ranges for the lower and upper temperature thresholds for photosynthesis ($tlow$ and tup) have been modified to include the default values used in CLASSIC. All other parameters for which documented uncertainty ranges are not available (28.5% of the total number of parameters) were assigned ±10% ranges, except for the lower temperature threshold used to estimate cold stress-related leaf loss rate ($lwrtrsh$). The parameter $lwrtrsh$ was assigned a ±2 K range, as including a ±10% range would correspond to an unnatural range of 45-50 K (Table A.2).

All parameters considered in GSA methods must be independent, and thus the three dependent parameters, namely, the base allocation parameters for carbon (*epsilonl, epsilons, epsilonr* in Table A.2) have to be converted to independent variants. The dependent parameters are transformed using the spherical coordinate system to achieve the required parameter independence (Eq. A.10-A.12). With just two spherical parameters, the three dependent parameters can be converted to independent parameters. This transformation further reduces the total number of independent parameters used in the screening test to 90. Details about the spherical coordinate conversion used in this article are available in Appendix A.1.2.

2.2.2 Site Selection

The FLUXNET2015 database provides measurements from 204 eddy covariance sites around the world (Pastorello et al., 2017). CLASSIC has been evaluated for the performance at 31 sites (Melton et al., 2020), of which 17 have various degrees of gap-filling (Pastorello et al., 2020). Multiple selection criteria have been considered before choosing a site for our analysis. These include the gap-filling score, age of the forest, time from previous catastrophic disturbance, available number of years of measured meteorological data, and homogeneity of the landscape and vegetation.

The site chosen for this study is a tropical wet primary forest (evergreen broadleaf forest) located in French Guiana, South America (5°16'54"N, 52°54'44"W; Pastorello et al., 2017). The site is surrounded by over 400 ha of undisturbed forest, in the northernmost region on the Guiana Plateau with small hills ranging from 10 to 40 m a.s.l. This forest site is home to old-growth trees, with the oldest trees over 300 years of age. The average canopy height is 35 m, with an overgrowth of 5 m. The flux tower is 55 m tall, and the sensors are placed 3 m above the top of the tower. The positioning of the sensors are such that there is little disturbance to the upper canopy, with the presence of over 1 km of forest cover in the direction of the prevailing winds (Bonal et al., 2008). The tower was erected in 2003 and continuous meteorological data such as atmospheric pressure, precipitation, specific humidity, atmospheric temperature and horizontal winds; and fluxes such as net radiation, GPP, ecosystem respiration, and net ecosystem exchange are available for 11 years from 2004 to 2014 (Pastorello et al., 2017). The data obtained from this site has the least gap among a wide range of sites, as 121 out of 132 months are available (Pastorello et al., 2020).

FLUXNET2015 sites measure various fluxes between the land and the atmosphere, typically employed for model optimization. The reader should note that our study does not involve any optimization. Instead, we use the observed meteorological data from the FLUXNET2015 site as the forcing for our model, which is forced from a bareground state. Spinning up and running the model separately for each set of parameter uncertainty values is important for computing differences in outputs during GSA sensitivity measure calculations.

2.2.3 Global Sensitivity Analysis

GSA can be described as the class of statistical methods where the relationship between variations in the input parameters and variations in single or multiple output

variables can be quantified across the specified uncertainty range of multiple input parameters (Saltelli et al., 2004). GSA methods can be used to identify parameters that individually do or do not influence the model outputs, as well as identify the interactions among parameters.

Morris Elementary Effects Method

Pareto's principle is an empirical observation stating that in general the variability of model output is largely determined by the uncertainty of only a few parameters (Box & Meyer, 1986). If variations of a parameter over its range of uncertainty induce larger output variations than comparable variations of other parameters, the input parameter is influential (Wagener & Pianosi, 2019). The method of distinguishing influential parameters from those with least impact is referred to as screening or qualitative GSA. The Morris elementary effects method, proposed by (Morris, 1991) and later modified by (Campolongo & Braddock, 1999), is a screening test based on the one-at-a-time design. This method perturbs only one parameter between consecutive steps in a realization/simulation, generating a random walk through the parameter space (Eq.A.14-A.15). Multiple realizations of such random walks are performed to sample the parameter space for all parameters. The ratio of difference of any two consecutive random walks to the step size is an elementary effects value. Statistical measures, such as the absolute mean and standard deviation of the elementary effects value from multiple evaluations, are the sensitivity measures used to determine the influence of the parameters on the model output(s). The elementary effects method is simple, and effective at identifying the set of important parameters among all parameters considered and distinguishing between those with negligible effects (small absolute mean and standard deviation values), linear effects (large absolute mean and small standard deviation values), and non-linear effects (large absolute mean and standard deviation values) on the model output variable(s). While the method can allow parameters to be ranked according to the type of effect, it cannot quantitatively assess the individual importance or parameter interactions.

The statistical measures mean (μ), absolute mean (μ^*), and standard deviation

(σ) are given by (Saltelli et al., 2008):

$$\mu_i = \frac{1}{r}\sum_{j=1}^{r}(EE_i^j), \tag{2.1}$$

$$\mu_i^* = \frac{1}{r}\sum_{j=1}^{r}\left|EE_i^j\right|, \tag{2.2}$$

$$\sigma_i = \sqrt{\frac{1}{r-1}\sum_{j=1}^{r}(EE_i^j - \mu_i)^2}, \tag{2.3}$$

where r is the total number of realizations, and EE_i^j is the elementary effects value for the i^{th} parameter and j^{th} realization. We have used the Euclidean distance (κ) from the origin and points (μ_i^*,σ_i) as the sensitivity measure to identify the influential parameters (Eq. A.19). The influential parameters will have a larger value of κ, which is indicative of greater sensitivity of the output variable to the parameter(s). Details about the hypercube, step-size, and random-walk trajectory used by the Morris method, are provided in Appendix A.1.3.

To compute one elementary effects value for a single parameter, two points in the unit hypercube are necessary. For n parameters, which yields n elementary effects values, $(n+1)$ model evaluations are required. In addition, r realizations/trajectories result in a total of $r \times (n+1)$ evaluations (Saltelli, 2002; Saltelli et al., 2004). In this study, 90 independent parameters and 80 realizations were used for the elementary effects method, requiring 7280 runs. The top five influential parameters for each of the output variables were obtained from the elementary effects method, which were further analyzed to quantify their individual contributions and interactions using the Sobol' variance-based GSA method. The screening test robustly identifies the most influential parameters, but the ranking of less influential parameters experiences substantial sampling variability. From our experience with the Morris method, there is no perfect way to select the subset of parameters for the Sobol' method, as the same selection procedure applied to two sets of realizations in the screening test would produce the same most influential parameters but would differ in some of the less influential parameters. When repeating the screening test with a different set of realizations, we find that those parameters which are not robustly identified as influential have negligible contribution to the variance-based sensitivity analysis to which we now turn.

Sobol' Analysis

A GSA method used to quantify the uncertainty of output variables due to the uncertainty in input parameters is the Sobol' method, based on a variance decomposition. The influence of individual parameters on the output can be determined by calculating the variance of conditional expectation ($V[E(\cdot|\cdot)]$). To study variations in the output with the uncertainty in a single input parameter ($Y|x_i$), the output can be split into subsets based on quantile ranges of the i^{th} parameter's uncertainty range. For each quantile slice, an average can be computed, representing the conditional expectation ($E_{x_{\sim i}}(Y|x_i)$) of the output when the i^{th} parameter is held constant, while the expectation is estimated by sampling over all other ($\sim i$) parameters. The variance of the conditional expectation, $V_{x_i}[E_{x_{\sim i}}(Y|x_i)]$, quantifies the influence of a single parameter on the output variable when all other parameters change. We use the first-order and total-order sensitivity indices (SI) in this study to quantify influential input parameters and their interactive effects. The first-order SI for the i^{th} parameter (SI_{1_i}) is given as (Saltelli et al., 2008):

$$SI_{1_i} = \frac{V_{x_i}[E_{x_{\sim i}}(Y|x_i)]}{V(Y)}, \tag{2.4}$$

where $V(Y)$ represents the output variance. The total-order SI for the i^{th} parameter (S_{tot_i})is given as (Saltelli et al., 2008):

$$SI_{tot_i} = 1 - \frac{V_{x_i}[E_{x_i}(Y|x_{\sim i})]}{V(Y)}, \tag{2.5}$$

where $V_{x_i}[E_{x_i}(Y|x_{\sim i})]$ represents the variance of the conditional expectation of the output when all parameters other than the i^{th} are varied, while the expectation is estimated by sampling over the (i^{th}) parameter. SI_{tot_i} close to zero implies that the influence of a parameter is negligible, and an error bar crossing zero implies that even if the mean is away from zero the influence of the parameter is not robust. Fixing the parameter within its uncertainty range will not affect the output variable if $SI_{tot_i} \simeq 0$. We have included the derivation of equations to obtain the sensitivity indices (Eq. A.20-A.24) using the Sobol' method, and a tutorial example in Appendix A.1.4.

To compute the first-order and total sensitivity indices using the Sobol' variance-based method, a total of $N \times (k + 2)$ model evaluations are required, where N is the number of perturbation points for each parameter (Saltelli et al., 2008). The com-

putational cost to run each perturbation is the main drawback of variance methods. As the dimensionality (k) increases, more points have to be sampled to evaluate the whole variability space. The parameter values are drawn randomly from their range, so a large number of realizations is necessary to adequately cover the parameter space. In this study, 14 parameters and 512 perturbation points were used for the Sobol' analysis, resulting in a total of 8192 model evaluations.

Various sampling techniques can be used to perform variance-based GSA, but in this study, quasi-random numbers were used. Quasi-random or Quasi-Monte Carlo (QMC) methods were employed to improve sampling of the whole variability space of each parameter (Morokoff & Caflisch, 1994; Niederreiter, 1978, 1992; Sobol', 1998). QMC methods consider the position of previously generated samples to create a spread of samples that are neither random nor completely predictable. These methods utilize an algorithm that generates distributions of points with a low measure of deviation from uniformity, known as low-discrepancy sequences. These methods have low disorderliness and gaps, resulting in efficient utilization of the sampling space. We have used the Sobol' low-discrepancy sequences, which produces successive points in a deterministic pattern, while performing the Sobol' analysis. This sampling technique is known for producing a highly uniform distribution as the sample size increases, making it an efficient method for sampling the input space in variance-based sensitivity analysis (Bratley et al., 1992; Sobol', 1967, 1976). This technique has been shown to be faster than pseudo-random Monte Carlo methods because of its improved sampling of parameter uncertainty ranges (Chan et al., 2000; Kucherenko & Sytsko, 2005; Sobol', 1967; Sobol' & Kucherenko, 2005).

It is important to consider the sampling uncertainty of the outputs when considering model output statistics based on a finite number of runs. In this study, the sampling uncertainties of the sensitivity indices that are computed by the bootstrap confidence intervals span from the 2.5th to 97.5th percentiles. It is possible to have slightly negative values of the Sobol' indices and the confidence intervals due to properties of the estimator used for the sample estimates (Eq. A.20; Saltelli et al., 2008). If the SI values are close to zero, or if zero falls well within the confidence interval of the parameters of interest, it suggests that the parameter might be non-influential, particularly if the interval has a small spread in range.

2.3 Results

2.3.1 Morris Elementary Effects Method

All model variables evaluated in this study are sensitive to fewer than 15% (10 - 11) of the total number of parameters (90; Figure 2.1). The relative sensitivity to each parameter varies among output variables. At least five parameters that are part of the photosynthesis module, especially *vmax*, are highly influential across all output variables (Figure 2.1). At least two parameters that are part of the phenology parameterization are influential across all output variables. Most of the least influential parameters form part of parameterizations related to physical processes and heterotrophic respiration.

The elementary effects method used in this study assesses the relative influence of each parameter on the individual model output variables, rather than quantifying the individual contribution of each parameter to changes in the model outputs. To further investigate the influential parameters, the Morris method was utilized to identify a subset of 14 parameters for more detailed analysis using the Sobol' variance-based decomposition (Table 2.1).

While the allocation fractions are not found to be influential, they are included in the Sobol' analysis along with *rtsrmin* as otherwise the model was found to crash.

2.3.2 Sobol' Analysis

First and Total Order Sobol' Indices

The output values from all the runs were analyzed using the Sobol' method for each of the model output variables considered. We first consider the main order effects, where the SI values denote the conditional variance of the model output(s) for a single conditioning variable. The results indicate that the variance of all model output variables is primarily dominated by only one parameter, *vmax*, which accounts for approximately 50 - 80% of the output variance for all model variables (Figure 2.2a).

For most model outputs, the importance of *vmax* is comparable, as the ranges of confidence intervals of the sensitivity indices overlap. However, for net shortwave radiation (denoted as RSS in the Figures 2.1,2.2), the importance of near-infra-red albedo (*albnir*) and *vmax* are comparable (Figure 2.2a). The parameter defined as *kn* is the second most influential parameter for most output variables except for net

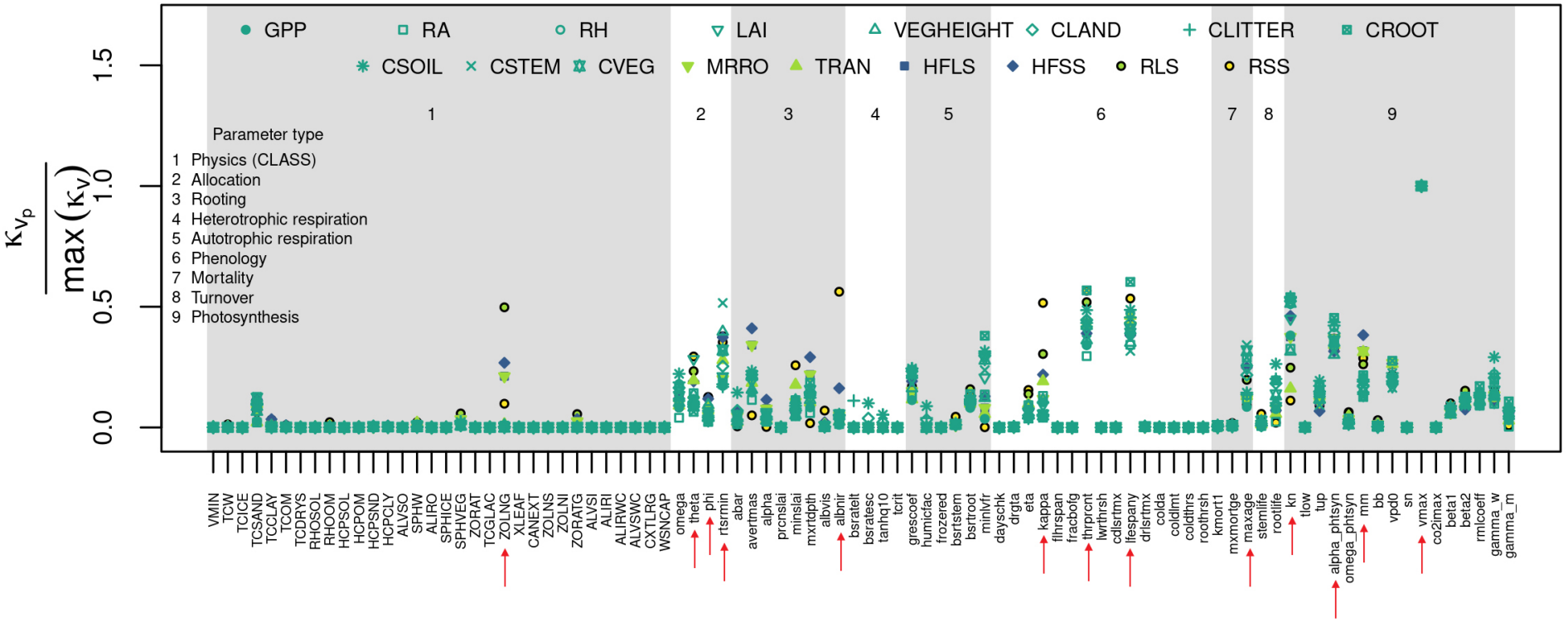

Figure 2.1: Normalized Euclidean distances (κ) of each parameter (p) computed from the sensitive indices (μ^*, σ) of the Morris elementary effects method for the output variables (represented as coloured symbols, v). The κ values were normalized with the maximum distance across parameters for a given output variable, as the output variables have different units. Red arrows denote the parameters in Table 2.1 (*theta* and *phi* are the spherical components of *epsilonl*, *epsilonr*, and *epsilons*).

Table 2.1: List of parameters selected for Sobol' analysis, their minimum and maximum uncertainty ranges, default values, units, and description.

Parameter	**Min.**	**Max.**	**Default**	**Unit**	**Description**
vmax	10.0e-06	80.0e-06	35.0e-06	$molCO_2 m^{-2} s^{-1}$	Max. carboxylation rate
lfespany	0.6466	2.5979	1.50	years	Leaf life span
alpha_phtysn	0.05	0.120	0.08	$\mu molCO_2$ $(\mu mol\ photon)^{-1}$	Quantum efficiency
kn	0.4	0.7	0.50	-	Canopy light extinction coefficient
rtsrmin	0.1	1	0.16	-	Minimum rootshoot ratio for support and stability
thrprcnt	30	60	40	%	Percentage of max. leaf area index that can be supported, used as a threshold for determining leaf phenology status
avertmas	0.1	8.7	2.45	kgC m^{-2}	Average root biomass
ZOLNG	-6.908	-0.5108	-4.605	-	Natural log of roughness length of soil
albnir	20.7	25.3	23	-	Near IR albedo
maxage	100	2100	600	years	Maximum plant age. used to calculate intrinsic mortality rate.
mm	9	15	12	-	Used in photosynthesis-stomatal conductance coupling.
kappa	1.44	1.76	1.6	-	Exponential parameter of allometric relations, required to support green leaf biomass.
epsilonl	0.15	0.5	0.35	-	Base allocation fraction for leaf (epsilon L)
epsilons	0.01	0.1	0.05	-	Base allocation fraction for stem (epsilon S)
epsilonr	0.4	0.8	0.60	-	Base allocation fraction for roots (epsilon R)

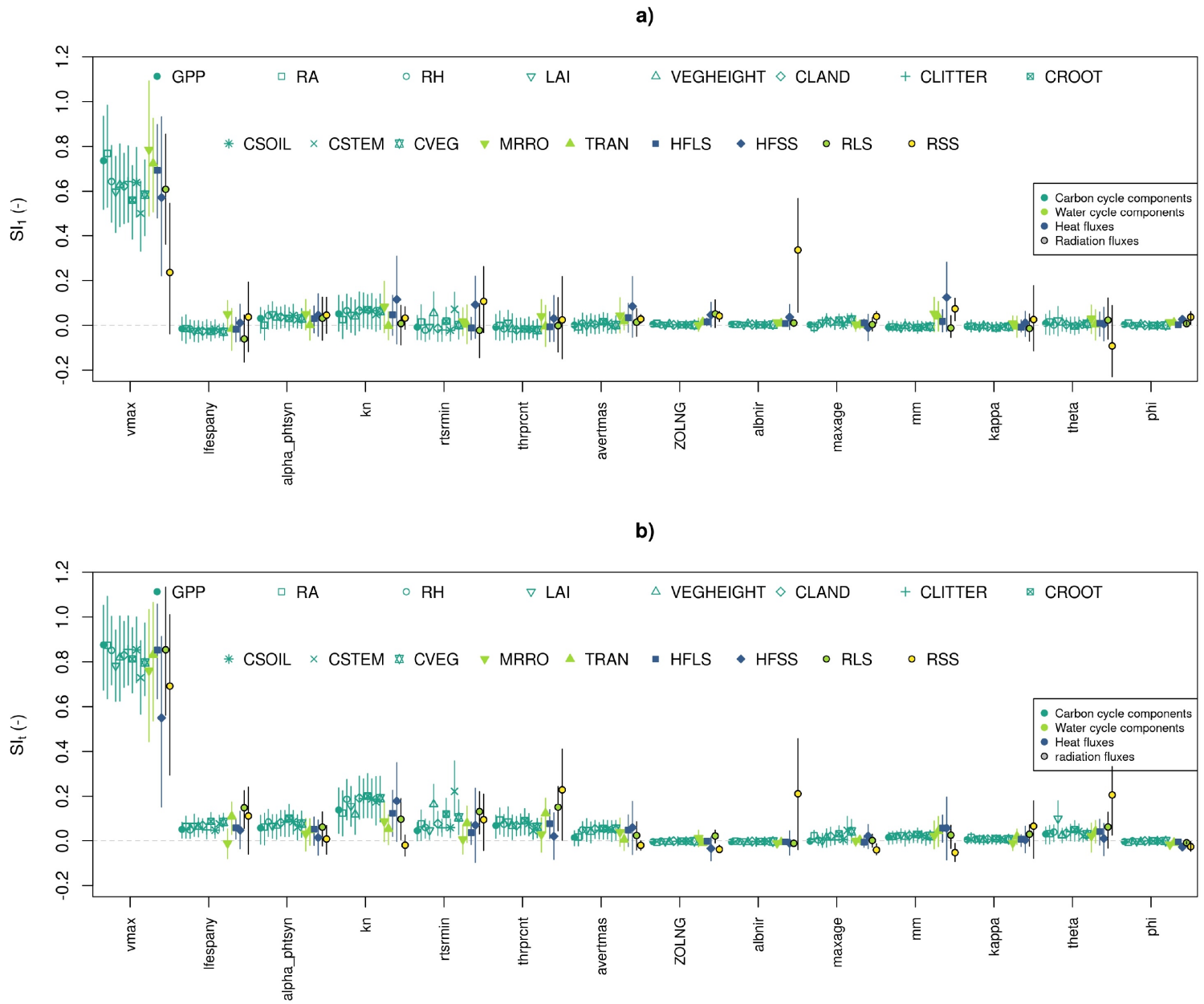

Figure 2.2: First order (a) and total order (b) sensitivity indices, and their confidence intervals for all outputs for the 14 parameters.

shortwave radiation, vegetation height (denoted as vegHeight) and cStem. All other parameters considered have negligible influence on a majority of model outputs, as their SI values are very small. The confidence intervals of the first order SI of all other parameters except for $vmax$, for all variables (except net shortwave radiation), cross zero, indicating that the first order SI values for these parameters cannot robustly be distinguished from zero (Figure 2.2a).

Total order indices include the interactive effects of all the parameters considered (Figure 2.2b). The total order of each output variable includes the first-order effect and is theoretically greater in value for the same set of input parameters analyzed. The ranking of parameters follows similar patterns of importance as of the first order, wherein the photosynthetic parameter $vmax$ has the highest total SI values for all model outputs. This parameter also exhibits the largest interactive features for all output variables (except for total run-off, denoted as MRRO, and sensible heat flux, denoted as HFSS), due to the fact that the strength of the interactions is based on the difference between the total and first-order indices. As most of the output variables behave similarly to each other, we focus on GPP as broadly representative of the GSA. The total variance in GPP explained by $vmax$ is about 88% (confidence intervals 68 to 100%; Figure 2.2b), of which the individual effect is about 75% (confidence intervals 52 to 90%; Figure 2.2a), such that the interactions account to about 13%. Most of the parameters that did not exhibit any first-order influence on the model outputs have some positive interactive effects that are not generally robust (Figure 2.2b), which is indicative of the interactions of each parameter considered with other parameters. For almost all model outputs the interactive effects add on to the first order indices, while for a few model outputs (e.g., sensible heat flux, total run-off and net shortwave radiation) the total order is less than the first order, which cannot be true theoretically, and must be the result of sampling variability in the estimators used for the indices (as shown in Figure A.1).

Interactions of Influential Parameters

Figure 2.3 shows the distributions of GPP variability conditioned on the top four influential parameters from the first-order SI. Values were plotted on conditional distributions along with their variations in conditional means. The distributions illustrate the conditional dependence of the output on individual parameters. As described in the previous section, the influence of the parameter is measured by the

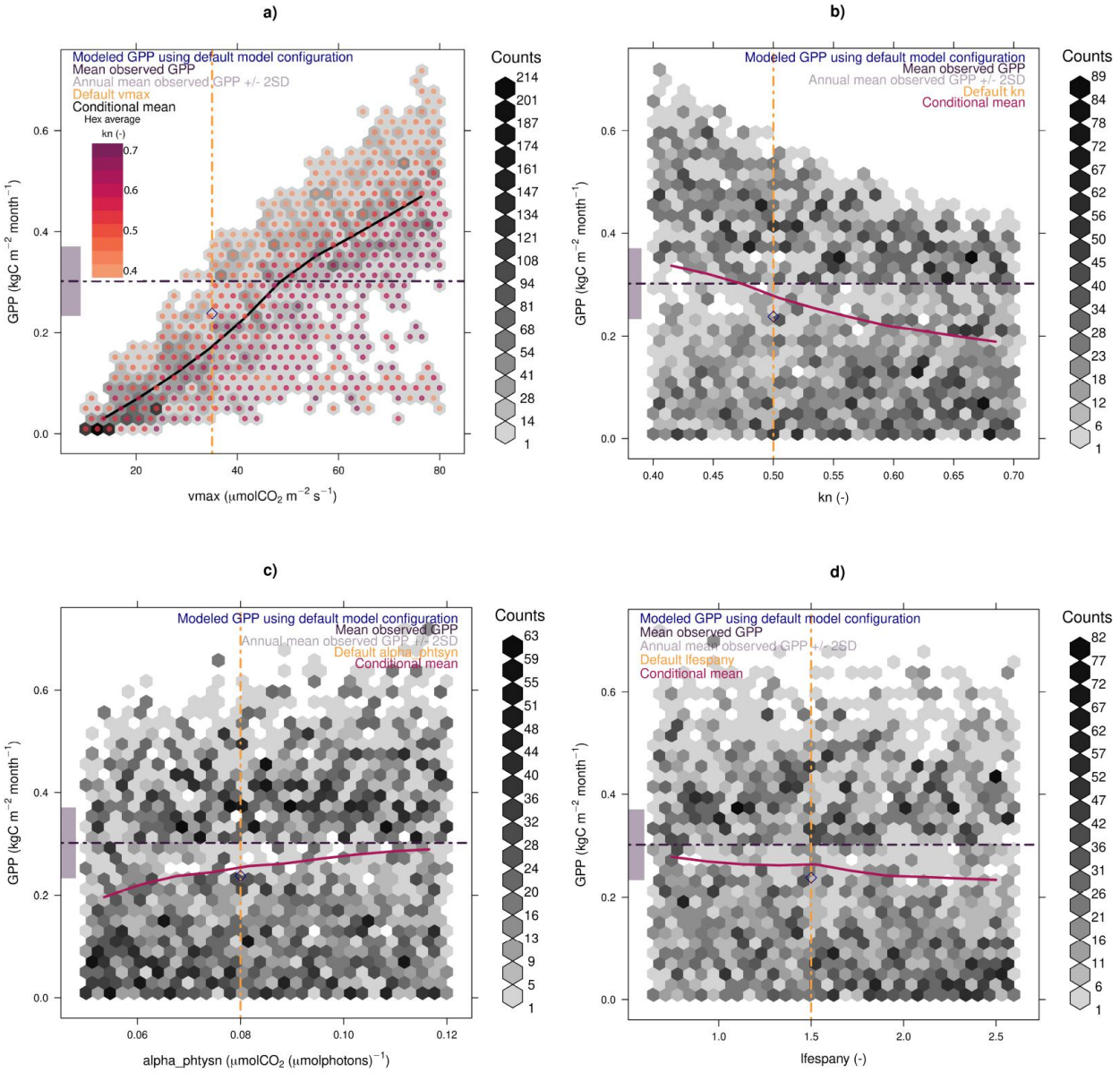

Figure 2.3: Conditional distribution of mean GPP (kgC m^{-2} month^{-1}) for the top-four highly influential parameters. Solid line denotes the conditional expectation. Horizontal black dot-dashed line denotes the mean observed GPP, with the ± 2 standard deviation in grey. The vertical yellow line denotes the default parameter value for evergreen broadleaf plant functional type. Blue diamond corresponds to GPP when simulated with default parameter values and the respective parameter ((a) $vmax$, (b) kn, (c) $alpha\_phtsyn$, and (d) $lfespany$). Coloured stipples in (a) denote the mean kn values for individual hexagonal cells containing multiple simulations.

variance of the conditional mean. If the variance of the conditional mean for the model output is strong for the parameter, that parameter is highly influential. Conversely, if the variance of the conditional mean for the model output is weak for the parameter , that parameter has low influence.

The first four influential parameters for GPP (from highest to lowest first-order SI values) are $vmax$, canopy light extinction coefficient along the depth (kn), quantum efficiency ($alpha\_phtsyn$) and leaf lifespan ($lfespany$; Figure 2.2a). As is illustrated graphically by the variation of the conditional means in each plot (Figure 2.3 a-d), the parameter $vmax$ has the greatest variation in the conditional mean, followed by kn, $alpha\_phtsyn$ (Figure 2.3 a, b and c). The variation of the conditional mean of GPP to $lfespany$ (Figure 2.3d) is the least among the four parameters, reflecting that $lfespany$ has the least influence among the four parameters. The dependencies of the conditional means of GPP on the other parameters are close to zero, as the sensitivity of the output to the inputs reduces as the ranking increases (not shown).

As mentioned in the previous section, the parameter kn represents the rate at which the canopy reduces the availability of light. To investigate interactions between kn and $vmax$, the average kn values for simulations falling within each hexagonal grid have been included as coloured stipples along with the conditional distribution of GPP on $vmax$ (Figure 2.3a). For a given $vmax$ value, the GPP values tend to reduce as the average kn values increase. Figure 2.4 further illustrates the dependence of GPP on $vmax$ and kn for an instantaneous state obtained from the equations S1 - S8. To obtain this state, the output variable leaf area index is fixed, and no soil moisture stress effects are considered. The instantaneous dependence of GPP reflects the pattern seen in the conditional distribution in Figure 2.3(a). The slope of GPP vs $vmax$ reduces as kn values are increased. This analysis shows that even if $vmax$ values are high, GPP may be less depending on the availability of light. Since all output variables are directly or indirectly affected by the vegetative biomass present, all output variables are sensitive to $vmax$ and kn. Our analysis also helps in understanding the importance of interactions between the influential parameters' uncertainty in driving the carbon cycle.

2.4 Discussion and Conclusions

This study screened the influence of 90 independent input parameters in CLASSIC using the Morris elementary effects method and found a small number of influential

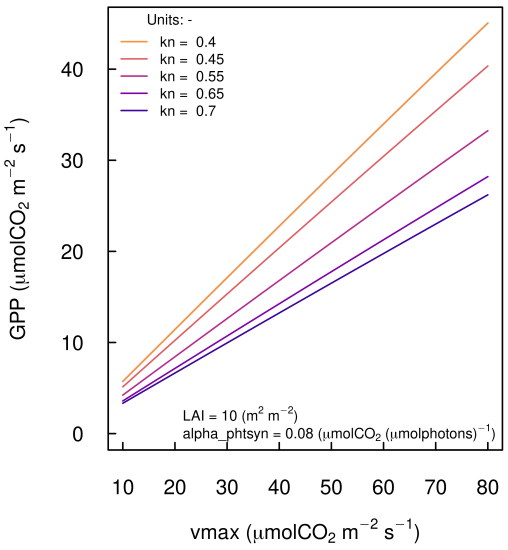

Figure 2.4: Functional dependence of GPP vs $vmax$ and kn for a particular state with site-specific PPFD = 2100 mol photons m^{-2} s^{-1}, 2009 atmospheric $[CO_2]$ = 387.64 ppm, mean atmospheric pressure = 1005.93 hPa, and defined leaf internal $[CO_2]$ (c_i = 240 ppm) and canopy temperature (T_c = 29 °C)

parameters for any given model output. The most influential parameters across output variables, when combined and quantified using Sobol' analysis, a variance-based GSA method, showed that the photosynthetic parameter $vmax$ by far has the greatest impact on the model output variance for all output variables, regardless of the type of variable. The overall importance of photosynthetic parameters is consistent with previous studies that analyzed carbon fluxes, latent heat flux, and carbon pools (Alton et al., 2006; Arsenault et al., 2018; J. Li et al., 2013, 2016; X. Lu et al., 2013; Pappas et al., 2013; Rosolem et al., 2012; Verbeeck et al., 2006).

Remarkably, a wide range of output variables are sensitive to the same set of primarily photosynthetic parameters (e.g., $vmax$ and kn). An upper limit of how much CO_2 a plant can assimilate and how the slope of the reaction rate versus intercellular CO_2 concentration changes is given by $vmax$, while kn determines the amount of light in the depth of the canopy and thereby the absorption of photons as a function of leaf area index. The autotrophic respiration is a function of $vmax$ and the factor for scaling photosynthesis from the leaf to the canopy (fPAR in Eq. A.8), the latter depending on kn, as in Eq. A.9. For heterotrophic respiration to occur, a sustained supply of litter and detritus is required and is provided by the biomass, which is

sensitive to the parameters *vmax* and *kn*. Parameters such as the litter respiration rate (*bsratelt*) and soil carbon respiration rate (*bsratesc*) may be expected to be more influential for heterotrophic respiration but, as shown by the results from Morris elementary effects, are far less influential in comparison to *vmax*. The variance in biomass, in response to photosynthetic parameter variations, affects the amount of carbon that enters the litter pool and ultimately the soil pool, and thus affecting heterotrophic respiration more compared to the variations of individual respiration parameters. We note that there are far more parameters in the model's photosynthesis parameterization compared to respiration, and more complex parameterizations may lead to more uncertainty. We also note that the site in this study is tropical, and soil-related parameters may be of more importance in colder climates where decomposition is slower.

Since the carbon and water cycle are directly linked through stomatal conductance, changes in the two photosynthetic parameters also influence the water cycle outputs, transpiration and total run-off. The photosynthetic parameters affect stomatal conductance and thereby the latent heat flux, which then affects soil moisture. The most influential photosynthetic parameters (*vmax*, *kn*) affect the carbon cycle variables (*GPP*, autotrophic respiration, heterotrophic respiration, leaf area index, vegetation height, and the carbon pools) directly through processes described in Eq. A.1-A.9 and indirectly affect the heat, water, and radiation fluxes through stomatal conductance and plant growth.

The parameter *vmax* dominates the sensitivity of a wide range of output variables simulated by CLASSIC, but the *kn* controls the slope of this dependence (e.g., *GPP* vs. *vmax* as depicted in the previous section). For the tropical site selected in this study, *vmax* and *kn* were the only parameters that had robust interactive effects for various output variables, as observed in the Sobol' method. It is important to note that different biomes may exhibit different interactive effects among various influential parameters.

The uncertainty range for quantum efficiency (*alpha_phtsyn*, Table A.2) in our study is narrower than that used by previous sensitivity analyses of LSMs. This decision was motivated after performing the GSA methods using uncertainty ranges provided by earlier studies (J. Li et al., 2013; X. Lu et al., 2013; Ma et al., 2020; Pappas et al., 2013), where assigning broader ranges to *alpha_phtysn* and *vmax* resulted in *alpha_phtsyn* being much more influential for all model outputs compared to *vmax*. The extreme values of these two photosynthetic parameters interacted to

produce unrealistic low and high biomass states, which are not observed when plant function type-specific and/or narrower ranges are used. Uncertainty ranges must be chosen carefully, as the sensitivity of an output variable strongly depends on the uncertainty range of each parameter, indicating the importance of carefully examining and evaluating the ranges assigned to all parameters. Plant function type-specific uncertainty ranges must be used whenever possible (e.g., from the TRY plant traits database; Kattge et al., 2020), especially if the parameter could be highly influential (e.g., *alpha_phtsyn* and *vmax*).

Insights from GSA allow for the targeted optimization of specific parameters, making the optimization process more efficient. Better optimized parameters in a model should in principle lead to improved output results. Model performance can be optimized by comparing observed output variables with model outputs, using metrics like root mean square error, squared correlation coefficient, and absolute errors. As we have shown in our study, GSA can identify the influential parameters for the output variables simulated by CLASSIC. This knowledge can then be used to optimize CLASSIC model's output variables. Since CLASSIC is the land component of CanESM, improvements in CLASSIC will ultimately enhance CanESM as well. Currently, parameter optimization using a machine learning algorithm is under progress by one of the co-authors.

Our study, like many other GSA studies performed on LSMs, is not without limitations. As mentioned earlier, this research was conducted for a tropical FLUXNET2015 site with 11 years of available observed meteorological forcing. The 11-year period considered for the mean state is too short to represent the historical period, and this affects the mean state of the model. While the site was well suited given a high gap-filling score, the influential parameters identified may vary if a different FLUXNET2015 site is chosen, or if a greater number of available years are considered for GSA.

To address the high dimensionality of the parameter space considered in the study, we performed the GSA in two steps. Various other GSA techniques are available, but by performing the Morris and Sobol' methods sequentially, we were able to screen out parameters that have limited influence on the output variables and quantify the absolute effects of the most influential parameters. We chose to use the first and total-order sensitivity indices to study the individual effects of parameters and their interactive effects. We assume that the difference between total index and first-order index is dominated by interactions between two parameters namely *vmax* and *kn*,

since only these two parameters showed robust differences between the first-order and total-order indices. In such cases, second-order effects could be studied instead of/or in addition to the total-order effects to identify parameters that have interactive effects on the output variables.

Based on the computational load, we chose to use the top five influential parameters from all output variables for the Sobol' method. This number is arbitrary, as even three or ten could be used. Modelers should keep in mind that as the dimensionality increases, so does the number of runs. They should also consider the extent to which the parameter space needs to be studied and will be studied. With 512 perturbation points, the confidence intervals computed through the Sobol' method are broad. The confidence intervals would be smaller if the number of perturbation points were increased. Just like the Morris method, the computational time and parameter search space should be kept in mind while performing the Sobol' method. We did not perform a test with various perturbation sizes due to time constraints. Additionally, this study focuses on the sensitivity of the average annual mean of output variables. The influential parameters may vary if a different statistical measure such as the trend over the period concerned is chosen instead of the mean state.

Our analysis involved performing a large number (15,472) of simulations with CLASSIC. An alternative to ease computational load while performing GSA is to use emulators. Emulators are statistical proxies of complex models such as LSMs or even Earth system models. These models provide a statistical relationship between model input parameters and model output, and are less complex, thereby, are far less computationally demanding. Emulators can be used for identifying optimum parameter ranges, and global sensitivity analysis (Baker et al., 2022; McNeall et al., 2023, 2020; Petropoulos et al., 2014). Using the original model is more reliable than using a proxy when identifying influential parameters.

To conclude, we have identified that for CLASSIC and considering an evergreen broadleaf forest site in French Guiana, the photosynthetic parameters, maximum carboxylation rate ($vmax$) and canopy extinction coefficient (kn), are the most influential among 90 input parameters. This influence is observed across the mean state of 17 output variables representing the budgets of carbon, water, and turbulent energy fluxes. Our findings were derived from a two-step global sensitivity analysis (GSA). The parameter $vmax$ dominates the sensitivity of all the output variables while kn controls the slope of the output variables. Together these two parameters account for a majority of the interactive effects on the output variables.

This finding brings forth the critical importance of $vmax$ (and kn) in LSMs, and that the most influential parameters have to be accurately parameterized to improve model performance and reliability. As mentioned earlier, the influential parameters may vary for different biomes, and for different statistical measures. The main objective of this study was to develop a framework to identify the most influential parameters in CLASSIC using GSA. This study does not delve into optimizing CLASSIC for optimal values or ranges of these influential parameters but forms the basis for future optimization work. We leave the development of an optimization framework for future research. Chapter 3 assesses the impacts of parameter uncertainties on the uncertainty of the historical carbon sink simulated by CLASSIC.

Chapter 3

Global Sensitivity Analysis of the Historical Carbon Sink Across Biomes

The terrestrial biosphere currently acts as a carbon sink, mitigating atmospheric CO_2 increases caused by human activities. However, the sink's strength remains highly uncertain, with recent estimates from terrestrial biosphere models ranging from 1 to 3.2 PgC yr^{-1} during 2014-2023. Some of this inter-model difference is caused by the uncertainty of model input parameters. This study employs global sensitivity analysis to quantify how parametric uncertainty affects the uncertainty of the land carbon sink of the last three decades, as well as its rate of change. Using the Canadian Land Surface Scheme Including Biogeochemical Cycles (CLASSIC) as an example, we conduct a GSA for seven grid cells located in different biomes. While focusing on net biome productivity (NBP), the analysis also considers other variables that are relevant for the carbon cycle. The Morris method screened 124 input parameters, reducing the set to fewer than 20 influential parameters per biome. The Sobol' method quantified the absolute effects of these parameters, revealing that the maximum carboxylation rate ($vmax$) was consistently the most influential across five of the seven biomes for both the mean and trend of NBP. However, due to substantial sampling variability, model tuning should incorporate influential parameters from multiple processes rather than focusing predominantly on $vmax$. Despite extensive sampling using almost 10

CPU years, sensitivity index values showed broad uncertainty ranges, complicating parameter ranking. By pinpointing influential processes, this research advances our understanding of the historical carbon sink's parametric uncertainty and identifies a low-dimensional space of influential parameters suitable for future model tuning efforts.

The contents of this Chapter have been submitted to Atmosphere-Ocean for peer review as "Global Sensitivity Analysis of the Historical Carbon Sink Across Biomes".

3.1 Introduction

The terrestrial biosphere currently functions as a carbon sink, absorbing more CO_2 through photosynthesis than it releases through respiration and disturbance. This enhanced absorption slows the increase in atmospheric CO_2 concentrations ($[CO_2]$) caused by anthropogenic sources (Matthews et al., 2021). According to the Global Carbon Budget 2023 Assessment (Friedlingstein et al., 2024), terrestrial biomes, including tropical, temperate, and boreal forests, have been acting as carbon sinks since the 1960s, absorbing approximately 30% of anthropogenic CO_2 emissions since the mid-1990s. The strength of the carbon sink is given by the difference of photosynthetic uptake, and release of carbon due to ecosystem respiration and disturbances. The Global Carbon Budget 2023 shows that while the strength of the carbon sink has been increasing over the past few decades due to the increased photosynthetic uptake, the relative amount of emissions taken up by the land has remained around 29% over the past decade, with annual variations influenced by climatic factors (Friedlingstein et al., 2024). Despite its critical role, the strength of the carbon sink as measured by the net biome productivity (NBP) remains highly uncertain. Terrestrial biosphere models play a key role in determining the strength of the carbon sink in the global carbon budget. To address the uncertainty of the carbon sink simulated by terrestrial biosphere models, we use the Canadian Land Surface Scheme Including Biogeochemical Cycles (CLASSIC; Melton et al., 2020) as an example and perform a global sensitivity analysis (GSA). CLASSIC is part of the Trends and Drivers of the Regional Scale Terrestrial Sources and Sinks of Carbon Dioxide (TRENDY) project, which is used for the global carbon sink estimation (Sitch et al., 2024). We aim to quantify the uncertainty in the simulated NBP due to parameter uncertainty using GSA. We focus on the sensitivity of NBP but also evaluate the sensitivity of other ecosystem variables relevant for the carbon cycle, including sensible and latent heat

fluxes.

Estimating the uncertainty of CO_2 fluxes remains a challenge due to both modelling and measurement limitations. Much of this difficulty arises from the fact that NBP is the difference of two almost equal fluxes (gross primary productivity and ecosystem respiration rate), along with smaller contributions from ecosystem disturbance. Previous studies have emphasized the complexity of the carbon sink, noting persistent uncertainties in the global terrestrial carbon sink despite advances in modelling and observational techniques (Arora & Scinocca, 2016; Ciais et al., 2013; Friend et al., 2014; Schimel, Stephens, & Fisher, 2015). According to the Global Carbon Budget 2023, the strength of the global carbon sink estimated from terrestrial biosphere models' average is 2.1 PgC yr^{-1} during 2013-2022. The corresponding uncertainty range in the terrestrial carbon sink based on the standard deviation of the inter-model spread over the same period equals 1 to 3.2 PgC yr^{-1} (Friedlingstein et al., 2024). Since all the simulations follow the same modelling protocol, the uncertainty arises from the combined effects of structural and parameter uncertainty (Booth et al., 2012; Dietze, 2017; Fisher et al., 2019; Knorr et al., 2024; Zheng et al., 2018). Studies have found that carbon fluxes simulated by terrestrial biosphere models are influenced by parametric uncertainties (Kaminski et al., 2013; Raoult et al., 2024; Xiao et al., 2014; Xing et al., 2023). Raoult et al. (2024) recently emphasized the importance of identifying influential parameters, so that uncertainties in model outputs related to parametric uncertainties can be reduced. By doing so, their study noted that the outputs simulated by land surface models could be improved. GSA is a valuable method for quantifying how variations in parameter values impact model output (e.g., Bastrikov et al., 2018; Saltelli et al., 2004; Senapati et al., 2016; Wagener & Pianosi, 2019; Y. Yang et al., 2022; Zhang et al., 2019; Zhu & Zhuang, 2014).

Previous studies have assessed the sensitivity of carbon fluxes and turbulent heat fluxes simulated by land surface models to input parameter uncertainties across various biomes using GSA. These assessments often included site-level GSA performed at eddy covariance sites, such as the ChinaFLUX sites (Xing et al., 2023; Q. Yang et al., 2021), and FLUXNET2015 sites (Alton et al., 2006; Arsenault et al., 2018; Hou et al., 2015; Y. Li et al., 2022; X. Lu et al., 2013; Pappas et al., 2013; Ricciuto, Sargsyan, & Thornton, 2018; Rosolem et al., 2012; Zhu & Zhuang, 2014). Other studies have performed GSA at a single grid cell location (Massoud et al., 2019); regional scale (Rodriguez & Espíndola, 2024); and global scale (J. Li et al., 2016). These studies consistently indicate that the outputs are sensitive to only a small subset of input

parameters. Specifically, studies focusing on gross primary productivity, net primary productivity, net ecosystem exchange (or net ecosystem productivity), and leaf area index have found that photosynthetic parameters such as the maximum carboxylation rate ($vmax$), quantum efficiency ($alpha\_phtysn$), and the growth respiration coefficient ($grescoef$) are highly influential (J. Li et al., 2016; Y. Li et al., 2022; Ma et al., 2020; Massoud et al., 2019; Xing et al., 2023; Q. Yang et al., 2021; Zhu & Zhuang, 2014).

These previous GSA studies of land surface models have evaluated 13-87 parameters, and typically focused on short transient simulation times (2-20 years) corresponding to the time periods of observations at the eddy covariance sites after spinning up the model or on the final 20-30 years of the spin-up period (Bagnara et al., 2019; J. Li et al., 2016; Y. Li et al., 2022; X. Lu et al., 2013; Ma et al., 2020; Massoud et al., 2019; Ricciuto et al., 2018; Xing et al., 2023; Q. Yang et al., 2021; Zhu & Zhuang, 2014). None of these studies employed long transient runs to generate output variables for the present, corresponding to the simulation protocol used in the TRENDY project. During the spinup, models reach an equilibrium in the terrestrial carbon cycle, whereas in a transient run, models respond to changing environmental conditions. Studies using shorter transient timescales risk producing incomplete or misleading sensitivity analyses because they may not capture longer-term dynamics that drive the carbon cycle, including the CO_2-fertilization effect or wildfires (Raoult et al., 2024). To assess the NBP, which results from the imbalance of carbon fluxes between the atmosphere and the biosphere, the model must be run in a fully transient mode over extended time periods (as prescribed by the TRENDY protocol).

The TRENDY project is used for the global carbon sink calculation based on various terrestrial biosphere models (Sitch et al., 2024). The project synthesizes different data streams to provide our current best estimate of global carbon fluxes for an evolving environment. CLASSIC is one of the terrestrial biosphere models used in the TRENDY project. In our previous study, we used meteorological data from a single tropical FLUXNET2015 site to drive CLASSIC (Chapter 2). The model underwent a spin-up phase to reach equilibrium by repeatedly cycling through 11 years of meteorological observations for a total of 495 years. Following this, we ran the model for an additional 11 years under transient conditions, and the resulting outputs were used for the GSA. As mentioned in Section 4.1, 11 years is a short time span to quantify the uncertainty of NBP, and thus we did not simulate CLASSIC using the TRENDY simulation protocol.

In the present study, we address the research gap mentioned above, as we are interested in the sensitivity of NBP. To do so, we spin up CLASSIC to equilibrium and then conduct a transient run for the period 1901-2017. We then quantify various output variables related to the carbon cycle using a two-step GSA, as in Chapter 2. The first step is a qualitative screening using the Morris method, and the second is the variance based Sobol' method. We perform the GSA for two statistical measures, the 30-year mean and 30-year trend, where the 30 years correspond to the last three decades of our study period (1986-2017). To study how the sensitivity of the output variables to parameters vary at different biomes, we perform the experiment at seven grid cells, each located within a different biome. The research questions in focus are: (1) what percentage of the total parameters considered are influential?; (2) can we identify the influential parameters for each biome location, for the two statistical measures?; (3) if not, can we group the influential parameters according to the processes? From the previous studies, we expect a big proportion of the input parameters to be non-influential, and we expect parameters such as the $vmax$, canopy light extinction coefficient (kn), $alpha\_phtsyn$, and $grescoef$ to be influential. As NBP is the difference between the net uptake and the net release of carbon, we expect its parametric uncertainty to be high. We also expect more parameters to be influential than previous studies. We may be able to group the most influential parameters based on their related processes if we are unable to identify the influential parameters by rank.

In the following, the Methods section outlines CLASSIC, the experimental design, the input parameters and their uncertainty ranges, the chosen biome grid cells, and the GSA methods used. The Results section documents the outcomes from the Morris elementary effects method, the general uncertainty in NBP due to parametric uncertainty, and the results from the Sobol' method. The Sobol' method contains the results from the sensitivity indices, conditional distribution of NBP when varying $vmax$, and an overview of $vmax$'s influence on all the output variables considered, for the climatological mean and the trend. The Discussion section covers the takeaways, limitations related to sampling uncertainty and parameter interactions, the practical implementation of our findings in current projects, the broader relevance of our research to the terrestrial biosphere modelling community, and concluding remarks.

3.2 Methods

3.2.1 CLASSIC

CLASSIC is the land surface component of the Canadian Earth System Model (CanESM; Swart et al., 2019), and is one of the models used in the TRENDY project. In our study, CLASSIC is run offline using quasi-observed meteorological data as a forcing. One of CLASSIC's components, the Canadian Land Surface Scheme (CLASS; Verseghy, 2017) simulates physical processes such as energy and water fluxes of vegetation, soil, and snow; while the other component, the Canadian Terrestrial Ecosystem Model (CTEM; Melton & Arora, 2016) is the dynamic vegetation model. The Canadian Terrestrial Ecosystem Model simulates biogeochemical processes such as the allocation of carbon to the carbon pools, photosynthesis, phenology, tissue turnover, and canopy conductance (Arora & Boer, 2005); growth, maintenance and heterotrophic respiration (Melton et al., 2015) and dynamic root distribution (Arora & Boer, 2003). The version of the model used here is capable of simulating nine different plant-function types (PFTs; Table 3.1). The minimum, default, and maximum PFT-specific values of *vmax* and *kn*, the two parameters that were found to be influential in Chapter 2 are presented in Table 3.1.

Table 3.1: PFTs in CLASSIC and the corresponding default, minimum, and maximum values of the two most influential parameters obtained from Chapter 2, *vmax* (derived from Kattge et al., 2020) and *kn* (Pappas et al., 2013).

PFT names	*vmax* **Default (min, max)** (μ mol CO_2 m^{-2} s^{-1})	*kn* **Default (min, max)** (-)
Evergreen Needleleaf	42 (16, 123)	0.5 (0.4, 0.7)
Deciduous Needleleaf	47 (37, 54)	0.5 (0.4, 0.7)
Evergreen Broadleaf	35 (13, 80)	0.5 (0.4, 0.7)
Deciduous Broadleaf (Cold)	57 (12, 110)	0.5 (0.4, 0.7)
Deciduous Broadleaf (Dry)	40 (12,110)	0.5 (0.4, 0.7)
C3 Crops	55 (15,125)	0.4 (0.4, 0.7)
C4 Crops	40 (22, 121)	0.48 (0.4, 0.7)
C3 Grass	55 (15, 125)	0.46 (0.4, 0.7)
C4 Grass	15 (15, 121)	0.44 (0.4, 0.7)

Experimental Design

The meteorological forcing used is the Climate Research Unit Japanese 55-year reanalysis version 1.1 (CRUJRAv1.1; Harris, 2019). The dataset is a combination of Japanese Meteorological Agency's reanalysis data (JRA; Kobayashi et al., 2015) adjusted and aligned with Climate Research Unit's (CRU) data (Harris et al., 2014). Population density was obtained from TRENDY and the History Database of the Global Environment (HYDE version 3.3, Klein Goldewijk et al., 2017). The PFT covers per grid cell were prescribed from the European Space Agency Climate Change Initiative (ESA-CCI; CCI, 2018). Lightning flash extent density was from **?**. Forcing data such as precipitation, near-surface air temperature (increase of 1.1°C from 1901 to present day; Lee et al., 2023), and atmospheric [CO_2] (from 295.8 ppm in 1901 to 405.19 ppm in 2017; Friedlingstein et al., 2024) exhibit trends that are caused by anthropogenic greenhouse gas emissions.

The model's experimental design used in our study is similar to that of the TRENDY protocol. The main difference is the transient time period for the meteorological forcing used in our study is from 1901-2017 vs. in the TRENDY protocol is 1700-present. For our model spin-up, we use constant 1901 values for [CO_2], plant-functional type's cover, population density, and annual cloud-to-ground lightning strike rate, and the meteorological forcing data are recycled from 1901 to 1920 (500 years). Equilibrium is reached when annual soil carbon changes fall below 0.1% at each biome grid cell. The transient period is then simulated from 1901–2017 (Table 3.2). Starting our analysis with the data from 1901 is a compromise that allows us to manage computational costs. The spin-up used in our study is for 500 years, which was found to be sufficient to ensure the model has reached equilibrium for all extreme parameter combinations.

On the other hand, the TRENDY protocol uses constant values of [CO_2], land use change, population density, and annual cloud-to-ground lightning strike rate from the year 1700 for the spin-up along with meteorological data from looped data of 1901-1920. For equilibrium conditions, a threshold of 0.05 PgC yr^{-1} for the global net atmosphere-land CO_2 flux is considered. The historical transient period from 1700-present is split into two portions. For the runs starting from 1701 to 1900, varying [CO_2] is used, while the looped meteorological data from 1901-1920 is retained. The rest of the time period from 1901-2019 is simulated with fully transient conditions.

We do not include all state variables when simulating CLASSIC. We do not use

Table 3.2: Summary of the experimental design used in Chapter 3.

Forcing Type	**Forcing based on**	**Spin-up** (500 years)	**Historical** (117 years)
CO_2	TRENDY	1901 (295.8 ppm)	1901-2017 (295.8-405.19 ppm)
Meteorology	TRENDY-CRUJRA	1901-1920	1901-2017
Land cover	ESA-CCI	1901	1901-2017
Population density	TRENDY-HYDE	1901	1901-2017
Lightning strike rate	LIS/OTD	1901	1901-2017

the prognostic nitrogen cycle in our simulations, because *vmax* is predicted, but in our study, *vmax* values are prescribed. The model's performance also generally decreases when the nitrogen cycle is used (Seiler et al., 2024). Additionally, the number of years to reach equilibrium state increases to over 5000 years when the nitrogen cycle is used. Methane cycle, peatlands, and mosses are not included in our study, as they will increase the number of parameters considered, which in turn increases the number of runs and the computational expense. Additionally, these processes are not active in all the biome locations. Since the fractional PFT cover per grid cell are prescribed, competition has not been included.

Output variables

Given the coupling between the carbon cycle and turbulent heat fluxes, and recognizing that tuning for influential parameters of one output variable can adversely impact other outputs, we analyzed a broad set of variables (Table 4.2) to determine the most influential parameters. For the primary analysis, NBP was used, which encompasses multiple carbon fluxes, including gross primary productivity (*GPP*), ecosystem respiration rate (consisting of autotrophic respiration rate (*Ra*) and heterotrophic respiration rate (*Rh*)), and disturbances (that include CO_2 emissions from

Table 3.3: Annual output variables used.

Short name	**Long name**	**Units**
GPP	Gross primary productivity	kgC m^{-2} s^{-1}
Ra	Autotrophic respiration rate	kgC m^{-2} s^{-1}
Rh	Heterotrophic respiration rate	kgC m^{-2} s^{-1}
fFire	CO_2 emissions from wildfire	kgC m^{-2} s^{-1}
NPP	Net primary productivity	kgC m^{-2} s^{-1}
NEP	Net ecosystem productivity	kgC m^{-2} s^{-1}
NBP	Net biome productivity	kgC m^{-2} s^{-1}
cLand	Land carbon pool	kgC m^{-2}
cLitter	Litter carbon pool	kgC m^{-2}
cRoot	Root carbon pool	kgC m^{-2}
cSoil	Soil carbon pool	kgC m^{-2}
cStem	Stem carbon pool	kgC m^{-2}
cVeg	Vegetation carbon pool	kgC m^{-2}
HFLS	Latent heat flux	W m^{-2}
HFSS	Sensible heat flux	W m^{-2}

wildfires (*fFire*) and land-use (E_{LUC})), expressed as:

$$NBP = GPP - Ra - Rh - fFire - E_{LUC}.$$

As a complementary analysis, additional output variables, such as net primary productivity ($NPP = GPP - Ra$), net ecosystem productivity ($NEP = GPP - Ra - Rh$), the different carbon pools (land, litter, soil, stem, root and vegetation), latent heat flux (HFLS) and sensible heat flux (HFSS), were considered.

Parameter Uncertainty Ranges

We have used 126 input parameters (Table A.2) of which 120 are independent, and six parameters are dependent (discussed further below). Each independent parameter is varied within its uncertainty range. Some of these independent parameters have PFT-specific values with individual uncertainty ranges (e.g., *vmax*; Table 3.1). All PFT-specific values of a particular parameter are perturbed such that the new values are scaled proportionally within their respective uncertainty ranges. Proportional scaling also helps avoid inconsistencies which may lead to unrealistic parameter combinations. Treating each PFT separately would increase the number of parameters by a factor of nine and result in a numerically intractable analysis. Proportional scaling across PFTs thus helps reduce the computational expense.

Parameter uncertainty ranges have been assigned based on (1) well-documented values from observations (e.g., $vmax$, from the TRY plant traits database; Kattge et al., 2020); (2) literature survey; (3) our modelling experience and expert advice; and (4) $\pm 10\%$ ranges for parameters that do not have documented uncertainty ranges. A ± 2 K range was used for the lower temperature threshold that is used to estimate cold stress-related leaf loss rate ($lwrthrsh$). The parameter ranges for a few parameters such as upper (tup) and lower ($tlow$) temperature limits for photosynthesis obtained from the literature do not include the default values used in CLASSIC and thus the uncertainty ranges have been modified to include those values.

Some parameters depend on each other. Parameters that must add up to unity such as allocations to leaf, stem and root; and percentages of deforested biomass that is combusted, used in short-term storage as paper and in long-term storage as furniture, have been converted to independent parameters using spherical coordinates (as described in Appendix A.1.2). This conversion results in 124 independent parameters that are used in the GSA method.

3.2.2 Biomes

Our study examines how parameter uncertainties influence the uncertainty of carbon cycle variables and turbulent heat fluxes at grid cells within each of the seven largest biomes worldwide. Our GSA implementation used between 17,168 and 18,704 individual model runs per grid cell (details provided in Section 4.2.3), amounting to over 87,300 CPU hours for all seven grid cells combined. For computational feasibility, a single grid cell was selected from each of the biomes considered, as shown in Figure 4.1. Single grid cells do not fully capture the spatial heterogeneity and diverse ecological dynamics present across the entire biome. More grid cells are desirable, but not practical due to computational expenses. Grid cells were carefully chosen to minimize the influence of land-use changes between 1901 and 2017. The latitude and longitude, soil composition, and PFT types and percentages found at each of these selected grid cells are given in Table A.1.

3.2.3 Global Sensitivity Analysis

GSA quantifies the relationship between variations in input parameters and variations in single or multiple output variables. This quantification is conducted across the entire uncertainty range of multiple input parameters (Saltelli et al., 2004). GSA

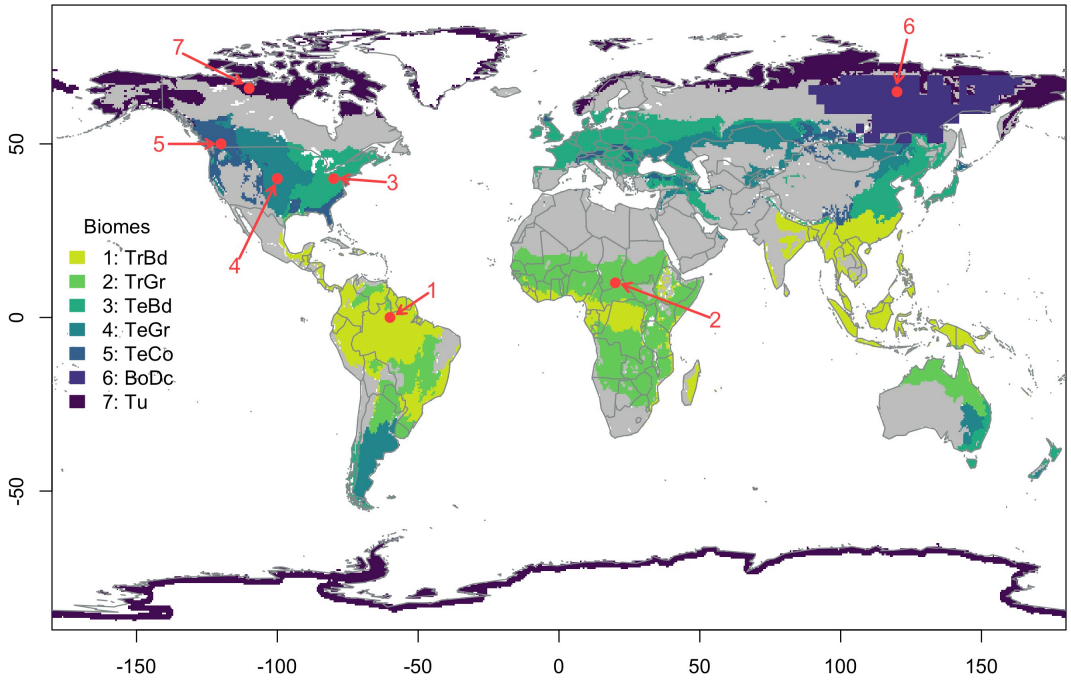

Figure 3.1: Biomes and single grid locations chosen. The biomes are, (1) TrBd: tropical and subtropical moist broadleaf forest, (2) TrGr: tropical and subtropical grasslands, savannas, and shrublands, (3) TeBd: temperate broadleaf and mixed forest, (4) TeGr: temperate grasslands, savannas, and shrublands, (5) TeCo: temperate conifer forest, (6) BoDc: boreal deciduous forests, and (7) Tu: tundra. Biomes that were not chosen due to time constraints are excluded from the analysis and are shaded in grey. In-land areas marked in white represent water bodies, glaciers, or snow-covered mountains.

methods can identify parameters by their influence on the model output variable. Knowing which parameters a model output is most sensitive is important for interpreting the output and guiding future model development. The most influential parameters from GSA can be tuned to optimize model output variables, and must be carefully identified, whereas weakly influential parameters may be disregarded in future model optimization problems. However, tuning parameters based on only one output variable (e.g., NBP) could lead to disruptive effects in other output variables (e.g., sensible heat flux), so GSA should include various interconnected output variables, such as the carbon cycle variables and turbulent heat fluxes.

The number of input parameters considered for GSA is 124. The computational cost of the variance decomposition-based Sobol' analysis increases rapidly with the number of parameters considered and is impractical for all parameters in CLASSIC

to be used in the Sobol' analysis. The first step in GSA is to obtain the top ranked parameters by screening out the non-influential parameters using a qualitative Morris elementary effects method, and the second step is to quantify the uncertainty in the model outputs due to the uncertainties of the top ranked parameters obtained from Morris using the quantitative Sobol' method. We expand the two-step GSA approach used in Chapter 2 by studying the sensitivities of 30-year means and 30-year trends computed over 1988-2017 for all output variables, as the parameters influencing the mean state may differ from those affecting trends.

Morris Elementary Effects Method

According to the widely recognized empirical observation, Pareto's principle, model output uncertainty is generally influenced only by a few parameters' uncertainties (Box & Meyer, 1986). An input parameter is considered influential when variations within its uncertainty range leads to substantial changes in the output, compared to similar variations in other parameters (Wagener & Pianosi, 2019). Screening or qualitative analysis is the technique through which influential parameters can be separated from non-influential ones. The screening test we use in our study is the Morris elementary effects method, initially proposed by Morris (1991) and later refined by Campolongo and Braddock (1999). This test follows a one-at-a-time design, where only one parameter is perturbed between consecutive steps in a random walk through the parameter space. All parameter uncertainty ranges are scaled to a zero to one range thus making the parameter space a unit hypercube. The elementary effects value is given as the ratio of differences of the output values between two consecutive steps in the same random walk to the step size. The model output's sensitivity to the influential parameters is assessed using sensitivity measures like the absolute mean (μ^*) and standard deviation (σ) of the elementary effects values over multiple realizations of the random walk. The Morris elementary effects method is straightforward yet effective in identifying the subset of influential parameters among those considered. The Morris screening test coarsely samples the uncertainty ranges of individual parameters so the sensitivity analysis qualitatively ranks the parameters, but does not provide a quantitative assessment of importance or interactive effects of parameters.

The statistical indices, mean (μ), μ^*, and σ are determined for all input parameters

by (Saltelli et al., 2008):

$$\mu_i = \frac{1}{r}\sum_{j=1}^{r}(EE_i^j), \tag{3.1}$$

$$\mu_i^* = \frac{1}{r}\sum_{j=1}^{r}\left|EE_i^j\right|, \tag{3.2}$$

$$\sigma_i = \sqrt{\frac{1}{r-1}\sum_{j=1}^{r}(EE_i^j - \mu_i)^2}, \tag{3.3}$$

where EE_i^j is the elementary effects value of the i^{th} of n parameters and j^{th} of r realizations. The sensitivity metric used in our study, the Euclidean distance (κ) from the origin to the point (μ_i^*, σ_i) identifies the influential parameters:

$$\kappa = \sqrt{\mu^{*2} + \sigma^2}.$$

Influential parameters will exhibit a higher value of κ, indicating a stronger sensitivity of the output variable to these parameters. To aid in comparison across multiple output variables, we normalized each parameter's value of κ for a given variable by the largest value of κ across all parameters for that variable. This normalization process allows for a consistent evaluation of κ values across different output variables, enabling meaningful comparisons of parameter sensitivities. The κ values are applied for each biome location individually.

Two points within the unit hypercube of parameters are required to determine one parameter's elementary effect value. For n parameters, with n elementary effect values for a single realization, $(n + 1)$ model evaluations are needed. A total of $r \times (n + 1)$ evaluations are needed for r realizations (Saltelli, 2002; Saltelli et al., 2004). We have chosen to use 80 realizations for 124 independent parameters, and a total of $80 \times (124 + 1) = 10,000$ unique runs for each biome location for the Morris screening test. For each output variable and biome location, the top five influential parameters were obtained from the Morris screening test (and will be denoted as the top-ranked subset hereon). The top-ranked subset from all output variables and the two statistical measures (mean and trend) for each biome are combined to form a targeted set. The targeted set of parameters underwent further analysis to assess their individual contributions and interactions using the variance-based Sobol' GSA method for each biome separately. While the screening test reliably identifies the most

influential parameters, the ranking of moderately influential parameters is subject to substantial sampling variability. Based on computational constraints, we have chosen only the five most influential parameters for each output variable for the Sobol' method.

While it is simpler and requires less computational effort to focus on the carbon sink-related parameters alone, such a focused approach could potentially overlook the links between carbon-related variables and other processes, such as turbulent energy fluxes. Mechanisms like stomatal conductance regulate both carbon dioxide uptake and water loss. These mechanisms link the carbon cycle dynamics with the latent and sensible heat fluxes. By broadening the targeted set to include influential parameters from all output variables (Table 4.2), we ensure that our analysis captures the cross-variable links that may otherwise be missed. This approach is critical for avoiding compensating errors, where tuning parameters for one variable (such as NBP) might degrade the optimization of other variables (like latent heat flux). Therefore, obtaining the full targeted set of influential parameters across various variables ensures a more balanced contribution to model optimization.

Though we do not perform any optimization, our study forms the foundation for model optimization, and obtaining the correct targeted set of parameters is important for optimizing different variables. To keep the analysis focused, we have chosen to concentrate on the uncertainty quantification of NBP and its components in this study, thereby focusing on the terrestrial carbon sink while still maintaining a broader context. The other variables will also be considered despite the emphasis on the carbon sink, as they will be used to determine the targeted set for Sobol' analysis.

Sobol' Analysis

The Sobol' method uses variance decomposition to compute the sensitivity measures. Such GSA methods can quantify the relative uncertainty in output variables due to input parameters' uncertainties. The Sobol' method is based on calculations of the variance of the conditional expectation for one or more conditioning parameters. To examine how the output varies with the uncertainty in a single i^{th} input parameter $(Y|x_i)$, we compute the conditional expectation of the output $(E_{x_{\sim i}}(Y|x_i))$, by fixing the i^{th} parameter, and varying all other parameters $(\sim i)$. The conditional expectation's variance $(V_{x_i}[E_{x_{\sim i}}(Y|x_i)])$, measures an output variable's sensitivity to the fixed individual parameter. This approach can be extended to explore sensitivities related

to interactions between parameters by fixing pairs, triplets, and larger combinations of parameters (e.g., Hou et al., 2015; Ricciuto et al., 2018). In our study, we have chosen to use the first-order sensitivity indices (SI) and total-order SIs to understand the individual and interactive influences of the input parameters. The first-order SI that provides individual effects for the i^{th} parameter (SI_{1_i}) is given as (Saltelli et al., 2008):

$$SI_{1_i} = \frac{V_{x_i}[E_{x_{\sim i}}(Y|x_i)]}{V(Y)}, \tag{3.4}$$

where $V(Y)$ is the output variance when all parameters are perturbed. The total-order SI for the i^{th} parameter (S_{tot_i}) that provides all interactive effects is given as (Saltelli et al., 2008):

$$SI_{tot_i} = 1 - \frac{V_{x_i}[E_{x_i}(Y|x_{\sim i})]}{V(Y)}, \tag{3.5}$$

where the output's variance of the conditional expectation when all parameters other than the i^{th} are fixed is given by $V_{x_i}[E_{x_i}(Y|x_{\sim i})]$. By sampling over the i^{th} parameter, we can compute the expectation. The Sobol' indices must be estimated from finite samples of model simulations. Through the use of a bootstrapping method, sampling uncertainties in the index values can also be estimated. If SI_{order_i} is close to zero, the corresponding parameter's influence is negligible. Even if the mean estimate of SI is away from zero, if the confidence interval crosses zero for a parameter, we judge it to not be robustly influential. We have used the Sobol' low discrepancy quasi-random technique to produce the initial matrices required for parameter perturbations. Low discrepancy sequences improve the sampling of the uncertainty space. A simple tutorial example is presented in Appendix A.1.4.

Sobol' is computationally more expensive than Morris. While Morris sparsely samples the high-dimensional parameter space, the variance-based decomposition requires a more extensive sampling of the parameter space. If more parameters are included in the analysis, more perturbation points are required to ensure effective sampling. As an empirical rule of thumb, a total of $N \times (k + 2)$ evaluations are required to compute the first and total-order SIs., where the number of perturbation points per parameter is N and k is the number of parameters in the targeted set (Saltelli et al., 2008). In this study, a targeted set of 13 to 15 parameters and 512 perturbation points were used for the Sobol' analysis for each biome. The total numbers of model evaluations were 7,168 to 8,704 depending on the targeted set of parameters obtained from the Morris elementary effects method for each biome.

Note that Sobol' analysis has been performed only for the targeted set of 13-15 input parameters obtained for each biome and not for the combined parameter pool from all biomes that total to 29 parameters.

Due to an artifact of the estimator used (Appendix A.1.4), Sobol' indices can be negative or greater than one. Additionally, as shown in Section 3.3.3, the confidence intervals (2.5^{th} to 97.5^{th} percentiles) may cross the values zero or/and one. It is also possible that sample values of SI_{tot_i} can be less than SI_{1_i}. The latter case indicate that there are no robust interactions of two or more parameters.

Influence of $vmax$

As mentioned in the Section 4.1, many of the previous GSA studies related to land surface models, have identified $vmax$ as one of the most influential parameters across carbon fluxes, pools and turbulent heat fluxes. A few studies have analysed the net ecosystem productivity (or net ecosystem exchange rate), but not NBP, which has to be simulated for extended time periods. NBP is dependent on the soil carbon stock and disturbances, and requires long evolving climate conditions. To provide a representation of how changes in $vmax$ alone influence NBP over the historical time period (1901-2017), we have assigned $vmax$ to its 25^{th} and 75^{th} percentile values within the uncertainty range, and fixed all other parameters to their default values. NBP simulated with these $vmax$ values were then compared with NBP values when all parameters are set to their default values. This complementary analysis was helpful to investigate the effects of $vmax$ on NBP, and to visualize the differences in the effects among different biome locations.

3.3 Results

3.3.1 Morris Elementary Effects Method

The Morris screening test reveals that more than four-fifths (more than 100/124) of the parameters exhibit negligible influence across biomes and output variables. Analysing individual scatter plots of μ^* against σ, and plots related to κ (not shown), it is evident that among the remaining one-fifth of parameters, only a modest subset, ranging from five to ten show appreciable influence on any output variable for any biome. These influential parameters fall under processes such as photosynthesis,

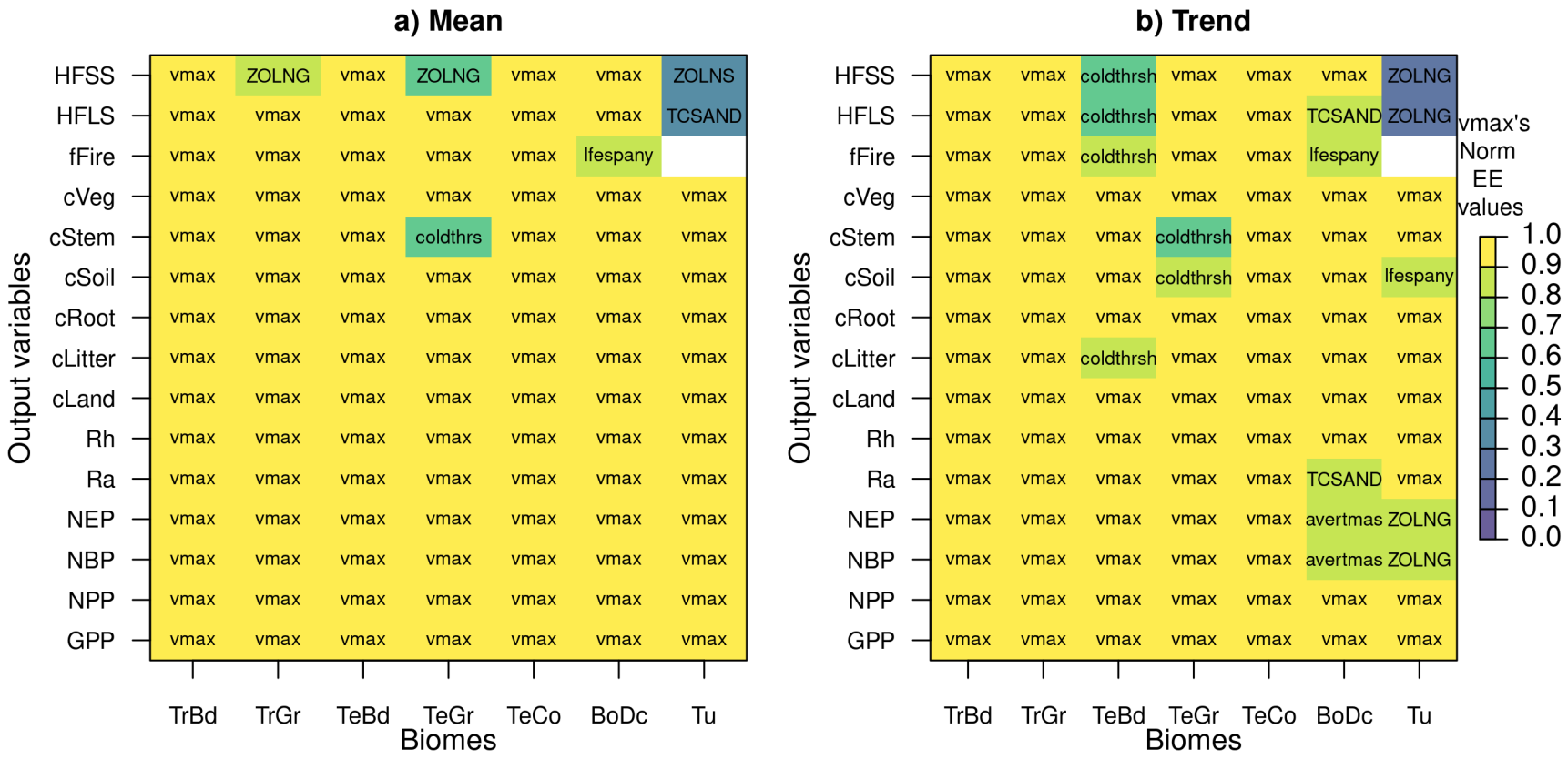

Figure 3.2: Normalized Morris elementary effects distance for *vmax* (as shaded cells), top-ranked parameter (as text) for the seven biomes (on the horizontal axis) and all output variables (on the vertical axis) for the two statistical measures (a) 30- year mean, and (b) 30-year trend. fFire is not simulated for the tundra biome and thus is left blank.

phenology, rooting, autotrophic respiration, physical fluxes, mortality and carbon allocation. The rest of the parameters tend to cluster closely near (μ^*,σ) = (0,0) and are thus screened out by the Morris elementary effects method. The non-influential parameters are from processes such as turnover, heterotrophic respiration, and fire. Fire-related parameters are non-influential in this study as we have chosen specific grid cells, and the fire model within CLASSIC performs reasonably better for large scales. The majority of the parameters related to physical fluxes are non-influential. There could be more parameters within the older physical component of CLASSIC, the CLASS, that we might not have considered in this study.

Figure 3.2 displays the highest ranked parameter for each output variable and biome, for the two statistical measures, mean and trend, as obtained from the normalized Euclidean distances. In addition, the figure also provides the ranking of the photosynthetic parameter $vmax$ relative to the aforementioned top-ranked parameter (as colour gradients). Almost all the carbon variables for the mean state (88/90 combinations of variables and biomes) and a majority for the trend (79/90 combinations) have $vmax$ as the highest-ranked parameter. While $vmax$ appears prominently in the ranking list, other parameters also show some degree of influence for a few of the output variables. In the tundra site, physical parameters such as the natural logarithm of roughness length of soil ($ZOLNG$), thermal conductivity of sand particles ($TCSAND$), natural logarithm of roughness length of snow ($ZOLNS$), and phenology parameter leaf lifespan ($lfespany$) are also influential. For the temperate broadleaf and temperate grassland locations, a phenology parameter, the leaf-fall threshold temperature ($coldthrs$) is the most influential parameter for the trend. For the boreal deciduous site, along with a phenology parameter ($lfespany$) and that related to physical fluxes ($TCSAND$), a rooting parameter, the average root biomass ($avertmas$) is the most influential for a few output variables. The presence of $ZOLNG$ and $ZOLNS$ for the sensible heat flux at the tropical grassland, temperate grassland, and tundra locations is expected, as these locations have short-stature vegetation type, and the roughness length of the ground and snow play an important factor for this output variable. The boreal deciduous and tundra locations chosen for this study have a high percentage of sandy soil (Table A.1), and thus, $TCSAND$ is influential at these locations. For all cases, the relative ranking of $vmax$ is within the top five parameters.

We see a remarkable consistency in the presence of certain parameters across different biomes and output variables which emphasize their role in shaping the model

outputs' sensitivity to these parameters. The 30-year trends can be influenced by different parameters than those for the mean state. The Morris screening test has helped reduce the dimensionality of the parameter search space from 124 to 13-15 for the Sobol' method.

3.3.2 Parametric Uncertainty of Historical NBP

The uncertainty in the 30-year mean NBP strongly depends on parametric uncertainties across biome locations, at the grid cell scale. Figure 3.3 illustrates how uncertainties in the targeted parameters, identified using the Morris method, influence the mean NBP across different biomes. Positive NBP values indicate carbon sinks, while negative values represent carbon sources. Under the default parameter settings (red dot), all biomes except the temperate conifer location function as carbon sinks, though their strengths vary. As we can see, perturbing the targeted parameters within their uncertainty ranges leads to drastic shifts in the 30-year mean NBP values. Some locations, such as tropical broadleaf, temperate broadleaf, and boreal deciduous forests, consistently act as carbon sinks for a broad range within the inter-quartile range (from 2.5^{th} to 97.5^{th} percentile). In contrast, for the other locations, the range of uncertainty spans the boundary between source and sink. These uncertainties hint at the strong influence of parametric uncertainty on carbon dynamics at the grid-cell scale and suggest that some biomes are more susceptible to parametric uncertainty than others.

Sole Influence of *vmax* on NBP

The parameter *vmax* has been found to be influential for the carbon sink for both the mean state and trend across a majority of biome locations, through the Morris method. Figure 3.4 provides a representation of how changes in *vmax* alone influence NBP over the historical time period (1901-2017), for a few biome locations.

In general, higher values in *vmax* lead to higher inter-decadal variability of NBP. For many biome locations, a change to the 25^{th} percentile in *vmax* results in small NBP values with relatively small inter-decadal variability. In contrast, the inter-decadal variability becomes more pronounced for the default and changes to the 75^{th} percentile, characterized by noticeable peaks and troughs. For instance, between 1965 and 1980, the tropical broadleaf location acts as a source of carbon for the changes to the 75^{th} percentile in *vmax* but remains a sink for the default value (Figure 3.4a).

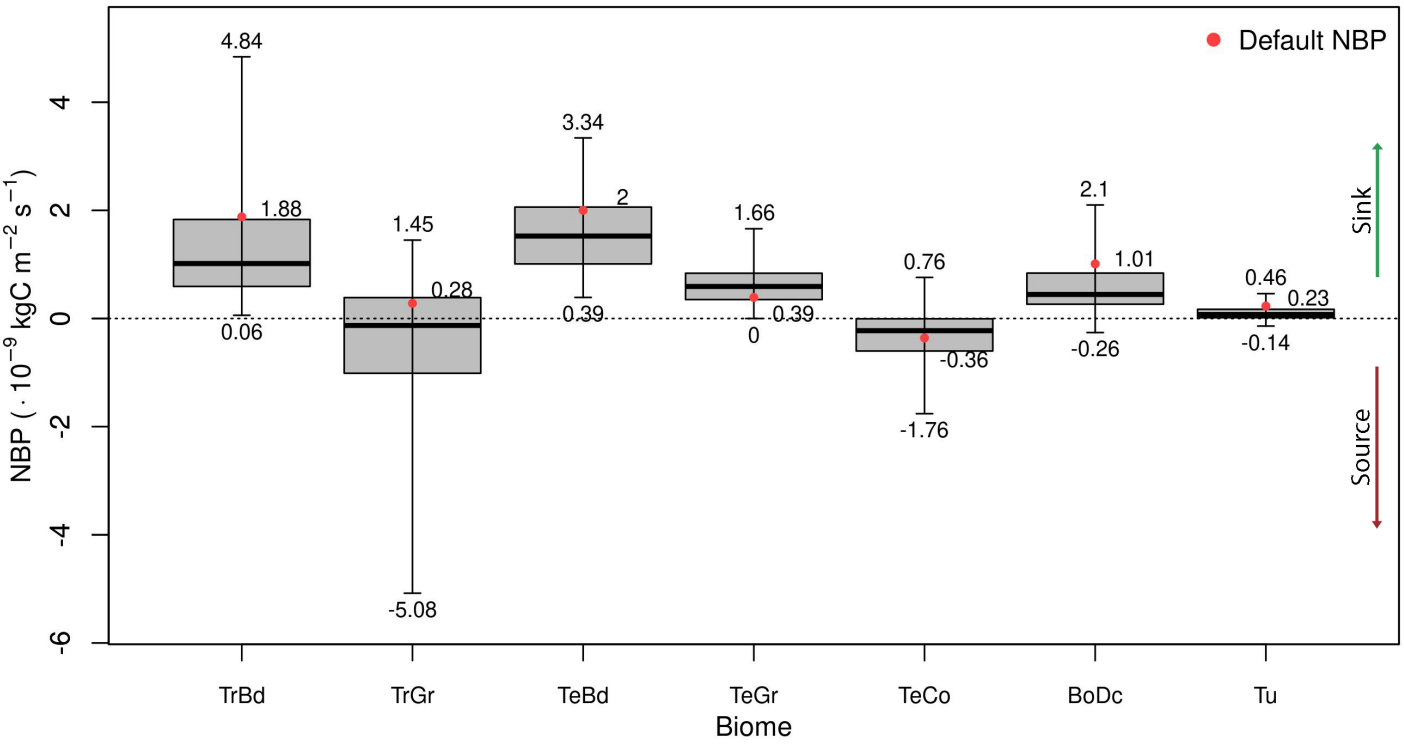

Figure 3.3: Uncertainty of NBP ($\times$ 10^{-9} kgC m^{-2} s^{-1}) for variations in targeted parameters obtained through the Morris method for each biome location, for the 30-year mean (1986-2017). The whiskers enclose the 95^{th} percentiles, while the box encloses the interquartile range. NBP associated with the default parameters is denoted as the red dot.

Similarly, between 1940 and 1970, the tropical grassland location behaves as a strong carbon source under the change to the 25^{th} percentile value in *vmax*, but as a sink for the default and 75^{th} percentile values. These variations indicate that changes in *vmax* not only affect the magnitude of NBP but also influence the timing of transitions between carbon source and sink states. At certain locations, particularly in the tropical broadleaf and temperate conifer biomes, a change to the 75^{th} percentile in *vmax* results in abrupt transitions from sink to source, introducing substantial variability in the carbon balance. This increased variability suggests that increasing *vmax* amplifies the uncertainty in NBP values, both in terms of its mean state and trend. Notably, a higher *vmax* does not always lead to a stronger positive NBP trend over the last three decades (e.g., Figure 3.4c). For situations where all three values produce carbon sinks (e.g., last 30 years in boreal deciduous) or carbon sources (e.g.,

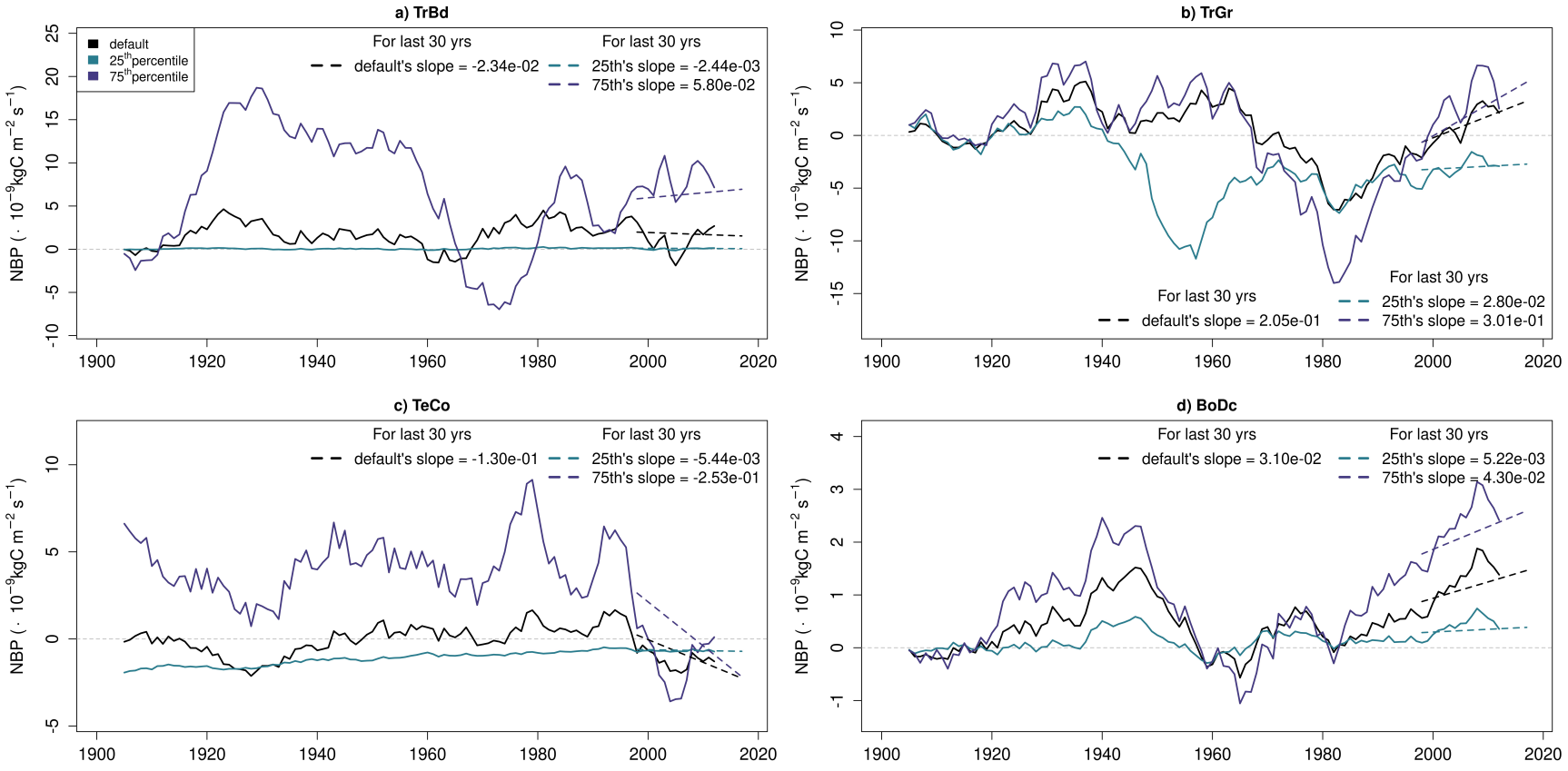

Figure 3.4: The 10-year running mean of NBP (solid lines) due to variations in *vmax* alone, for four biome locations. The trends for the last 30 years (annual means) are denoted as dashed lines.

late 1990s to early 2000s in the temperate coniferous location), the strength of the sink/source varies for different values of $vmax$. The influence of $vmax$ on NBP depends on biome-specific responses, with some locations exhibiting more pronounced inter-decadal fluctuations rather than a consistent enhancement of the strength of NBP.

Over the last 30 years (based on running means), the tropical broadleaf and boreal deciduous biome grid cells consistently act as carbon sinks across all three experimental variations of $vmax$. At the temperate conifer location, although the 30-year mean NBP values are close to zero for all three $vmax$ scenarios, there are distinct variations in NBP over this period, as indicated by the strong trend magnitudes. In contrast, at the tropical grassland location, the 30-year mean NBP values are near zero for higher $vmax$ values but become negative (or a carbon source) under the variation to the 25^{th} percentile. The influence of increasing values of $vmax$ on the trends are strongest for the temperate conifer, and tropical grassland biome locations and relatively weaker for the boreal deciduous location, as shown by the slope of the trend lines. Though we notice that the variations in NBP differ vastly among different biome locations, we have not identified how sensitive the uncertainty of NBP is to $vmax$'s uncertainty. Additionally, the uncertainty of NBP noticed here is only a fraction of that in Figure 3.3, which contains uncertainties due to various influential parameters obtained from the Morris method. The contributions of individual parametric uncertainties to overall parametric uncertainty can be quantified by the Sobol' method.

3.3.3 Sobol' Analysis

The first-order SIs (SI_1) for the 30-year mean NBP for each parameter/biome are shown in Figure 3.5a. Note that the parameters displayed represent a combination of targeted sets from all biomes, and not all parameters are included for each biome, as the parameters screened out differ among locations. Filled symbols represent indices with confidence intervals that do not intersect zero, whereas open symbols represent indices where the confidence intervals do intersect zero. Only those index values with confidence intervals distinctly different from zero are considered robustly influential.

A few parameters stand out with robust influence for a few biome locations, but assigning a clear rank to the influential parameters is not meaningful because of large overlapping confidence intervals. We can also see parameters with SI_1 values close to zero (e.g., for the boreal deciduous location, the photosynthetic parameters kn,

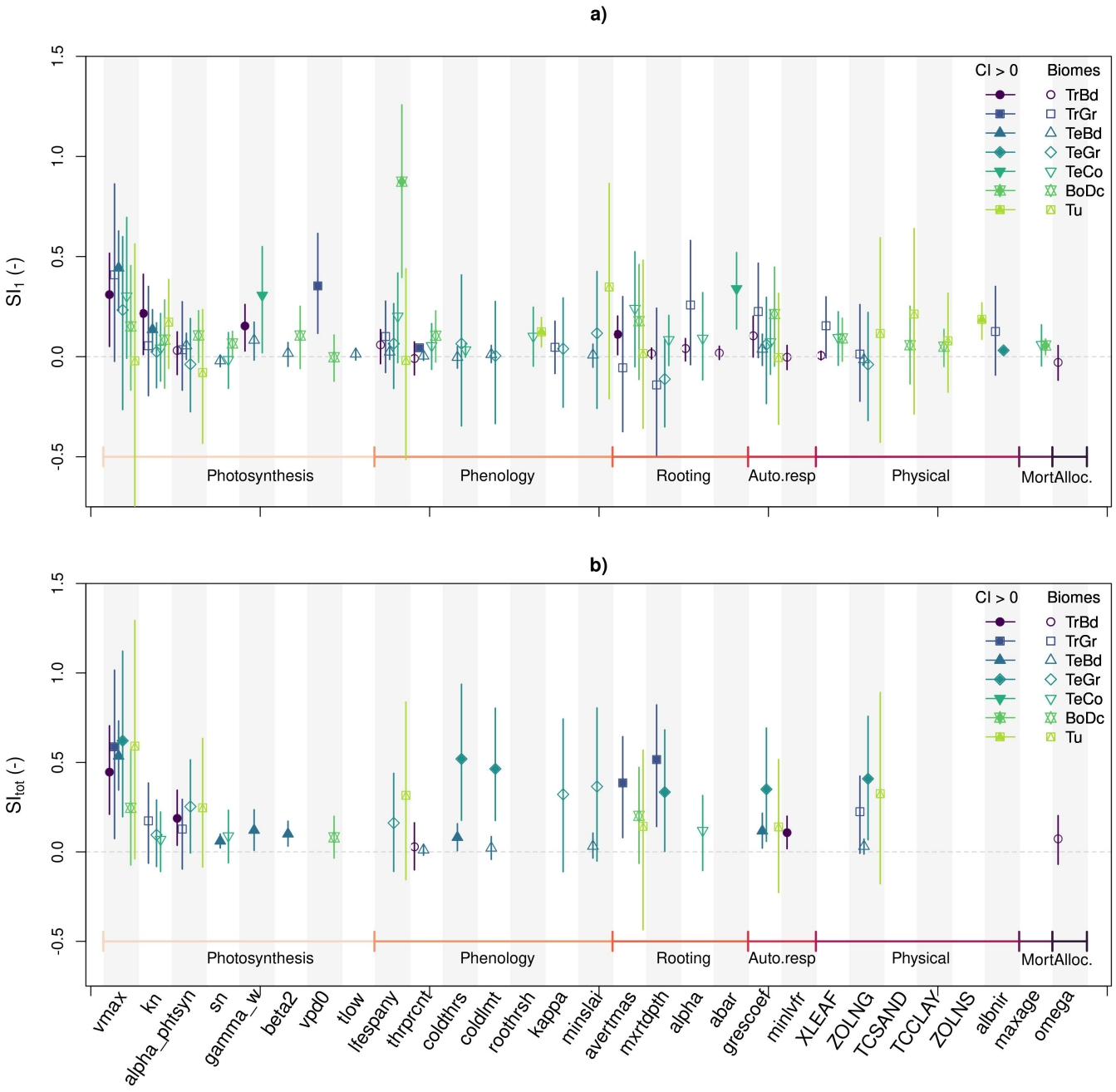

Figure 3.5: First (a) and total-order (b) SIs, and their confidence intervals for NBP for the top-ranked parameters across biomes (open symbols) for the mean state. Filled symbols represent SI values that are robustly different than zero as they have confidence interval ranges not crossing zero. Total-order indices are plotted only where SI_{tot} is greater than SI_1. The parameters are grouped according to the processes.

alpha_phtsyn, the exponent for soil moisture stress (*sn*), the photosynthesis coupling coefficient (*beta*2)). These parameters are weakly influential in the first-order, and if the corresponding SI_{tot_i} is close to zero or if SI_{tot_i} is less than SI_{1_i}, these parameters can be considered non-influential. The mean SI_1 values for a few other parameters are less than zero, but with confidence intervals crossing zero. These parameters are non-influential in the first-order. While the Morris test showed that *vmax* is the most influential parameter for the carbon sink in the boreal deciduous location, SI_1 shows that $lfespany$ has a greater influence. This could be due to the fact that the Morris uses a coarse sampling space, while the Sobol' uses a finer sampling space. In fact, the close κ values of *vmax* and $lfespany$ for the boreal deciduous location supports this finding (not shown).

With broad confidence intervals and a number of non-robust parameter SIs, we are unable to identify the individually most influential parameters based on SI_1, but can group them based on the processes they belong to. Among the photosynthetic parameters, *vmax* and *kn* are influential across a majority of biome locations, with the photosynthesis down regulation parameter with equivalent CO_2 fertilization effect (*gamma_w*) influencing the tropical and temperate broadleaf locations and temperate conifer, and vapour pressure deficit (*vpd*0) influencing the tropical grassland. Phenology parameter $lfespany$ is influential at the boreal deciduous and temperate conifer locations, while minimum storage leaf area index (*minslai*) is influential at grass dominated locations such as the tundra and temperate grassland locations. The influential rooting parameters are *avertmas* (at temperate conifer, boreal deciduous and tropical grassland), the exponential factor for root distribution profile (*alpha*) (at the tropical broadleaf and temperate conifer), and *abar* (at temperate conifer). The autotrophic respiration parameter *grescoef* is influential at the tropical locations and boreal deciduous. Parameters related to physical fluxes $ZOLNG$, $TCSAND$, thermal conductivity of clay particles ($TCCLAY$) and $ZOLNS$ are primarily influential at the tundra location. Additionally, the leaf dimension factor used in calculating the leaf boundary resistance ($XLEAF$) influences the tropical grassland, temperate conifer and boreal deciduous locations, while near infra-red albedo (*albnir*) is influential at the tropical grassland location. Parameters related to mortality and carbon allocation have negligible SI_1 values for the mean state.

Even though some parameters have low SI_1 values, they may be influential due to interactive effects. We identify these interactive effects using the total-order indices. Only those sample estimates of total-order SIs (SI_{tot}) for each parameter/biome for

the 30-year mean NBP where SI_{tot_i} is greater than SI_{1_i} are shown in Figure 3.5b. Fewer SI values are plotted in Figure 3.5b than in Figure 3.5a showing that there is robust evidence of parameter interactions for NBP only for a few input parameters. The photosynthetic parameter *vmax* shows interactive effects among five of seven biome locations. The temperate grassland location has prominent interactive effects for multiple phenology related parameters such as $lfespany$, the required days of sub-threshold temperature to trigger leaf loss (*coldlmt*), $coldthrs$, the exponential parameter for allometric scaling of green leaf biomass (*kappa*) and *minslai*. Similarly, the tropical grassland location has notable interactive effects for the rooting parameters such as *avertmas* and maximum root depth (*mxrtdpth*). There are no robust interactive effects for the phenology related parameters in the tropics, temperate conifers or boreal deciduous locations. Rooting parameters do not have robust interactive effects at the broadleaf locations. Of all the biome locations considered, the temperate conifer location has the weakest interactive effects among all processes, as there are only three parameters where SI_{tot_i} is greater than SI_{1_i}.

The process-based influential parameters obtained from the Sobol' method are included below. These parameters correspond to those obtained from SI_{tot}, and those from SI_1 where there is no robust interactive influence. Photosynthetic parameters from the targeted set are influential for the 30-year mean NBP at all biome locations, and without considering the absolute ranking, *vmax* is among the most influential across all biome locations, *kn* at five locations, *alpha_phtsyn* at four and *gamma_w* at three. Rooting parameters are influential at six locations, except the temperate broadleaf. Of these parameters, *avertmas* is shown to be influential at five locations, along with *mxrtdpth*, *alpha*, and *abar* at one location each. Parameters related to phenology such as $lfespany$, *minslai*, $coldthrs$, *coldlmt*, and *kappa* are influential at four locations. The parameters related to physical fluxes $XLEAF$, $ZOLNG$, $ZOLNS$, $TCSAND$ and *albnir* are influential at locations dominated by grass such as tropical and temperate grasslands, and tundra. The parameter used in the allocation formula (*omega*) is only influential at the tropical broadleaf location through interactive effects. The parameter related to mortality has negligible or no influence on any biome location for the mean state. The influential parameters mentioned are based on the grid cells chosen. Though processes that these parameters belong to might remain the same for other grid cells, the lesser of the most influential parameters obtained from the Morris may vary for other grid cells. A summary of the influential parameters for the 30-year means of NBP, based on the mean SI values,

grouped according to the processes are provided in Table 3.4.

Since *vmax* has shown prominent influence, we illustrate the relationship between the 30-year mean NBP and *vmax* for the seven biome locations chosen, allowing for variations in all parameters in the targeted set within their respective uncertainty ranges (Figure 3.6). The density of points shown in the shaded hexagons represents the conditional distribution of NBP values for different values of *vmax*. Areas with darker shades represent multiple model runs where combinations of NBP and *vmax* are more frequently observed. The solid magenta-coloured line represents the conditional expectation of NBP as *vmax* increases, showing the overall direction and strength of the relationship between NBP and *vmax*. The extent of changes in the conditional expectation for changes in *vmax* determines the conditional variance of NBP as measured by SI_1. The spread of the hexagons around the conditional expectation indicates the variability in NBP due to the simultaneous variation of the other targeted set of parameters in the Sobol' analysis for given values of *vmax*. The blue lines represent the conditional 25^{th} and 75^{th} percentile curves, which can be helpful in identifying the noise in the conditional spread. The simultaneous variation of all parameters in the targeted set may produce outliers with high or low NBP values for a specific value of *vmax* (e.g., the faintest shaded hexagons in Figure 3.6). The spread of the conditional distributions provide insights into the estimates of sampling variability based on bootstrapping. The abundance and spread of isolated regions or hexagons present influence the confidence intervals in Figure 3.5a. Larger deviations of outliers from the conditional spread correspond to even broader confidence intervals. The red floating levers represent the default 30-year mean NBP values obtained when no input parameter is perturbed. A single value of *vmax* does not exist, as each location has multiple PFTs corresponding to multiple *vmax* values.

The response of the 30-year mean NBP to variations in *vmax* reveals distinct biome-specific patterns, emphasizing the complexity of carbon cycle dynamics (Figure 3.6). Biomes such as tropical grassland transition from acting as carbon sources at lower *vmax* values to being near neutral at higher values. The tropical and temperate broadleaf locations, temperate grassland, boreal deciduous, and tundra biomes generally act as carbon sinks across *vmax*'s range. While many of the biome locations are predominantly carbon sinks as *vmax* changes, numerous simulations in the tropical grassland and temperate conifer biomes are carbon sources. The tropical broadleaf location acts as a source of carbon for very few simulations, where *vmax* values are higher. As *vmax* increases, the number of occurrences where the tundra location act

Table 3.4: Influential parameters grouped according to the processes for the 30-year mean NBP, for each biome grid cell.

Biome	**Photo-synthesis**	**Phenology**	**Rooting**	**Auto-trophic respiration**	**Physical**	**Mort-ality**	**Alloc-ation**
TrBd	*vmax*, *alpha_phtsyn*, *kn*, *gamma_w*	-	*avertmas*	*grescoef*	-	-	*omega*
TrGr	*vmax*, *alpha_phtsyn*, *kn*, *vpd*0	-	*avertmas*, *mxrtdpth*, *alpha*	*grescoef*	*XLEAF*, *albnir*, *ZOLNG*	-	-
TeBd	*vmax*, *kn*, *gamma_w*, *beta*2	-	-	*grescoef*	-	-	-
TeGr	*vmax*, *alpha_phtsyn*	*lfespany*, *coldthrs*, *coldlmt*, *kappa*, *minslai*	*mxrtdpth*	*grescoef*	*ZOLNG*	-	-
TeCo	*vmax*, *gamma_w*	*lfespany*	*avertmas*, *abar*	-	-	-	-
BoDc	*vmax*, *alpha_phtsyn*, *beta*2	*lfespany*, *thrprcnt*	*avertmas*	*grescoef*	-	-	-
Tu	*vmax*, *alpha_phtsyn*, *kn*	*lfespany* *minslai*	*avertmas*	*grescoef*	*ZOLNG*, *TCSAND*, *ZOLNS*	-	-

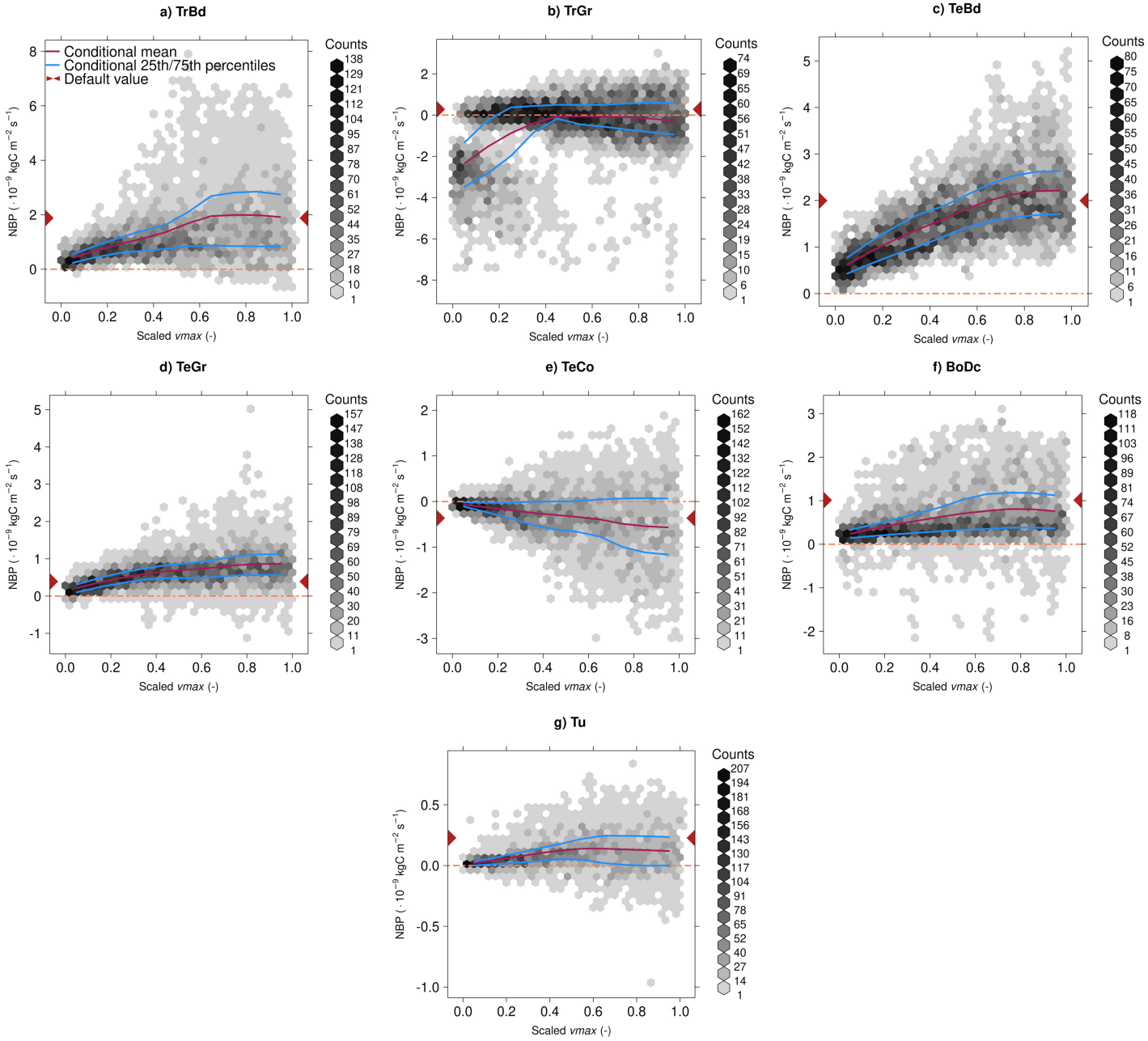

Figure 3.6: Conditional distributional of mean state of NBP ($\times$ 10^{-9} kgC m^{-2} s^{-1}) for all biomes, for changes in *vmax*, along with the conditional expectation (magenta line), the conditional 25^{th} and 75^{th} percentile curves (blue lines), and the default mean NBP value (red arrow heads). Multiple *vmax* values are used for each biome location. PFT-specific *vmax* values are scaled to (0,1) for representation purposes.

as sources of carbon increases. At the boreal deciduous location, there is no clear pattern of how *vmax*'s values cause the biome location to act as a source of carbon.

Most biome locations exhibit an increase of the conditional expectation of NBP as *vmax* increases, indicating the higher values of *vmax* generally enhance the carbon sink or weaken a carbon source. The temperate conifer location is an exception, showing the decrease of NBP as *vmax* increases, which indicates a stronger carbon source. The variance of the conditional expectation for *vmax* is highest for temperate broadleaf biome and decreases sequentially across tropical grassland, tropical broadleaf, temperate conifer, temperate grassland, boreal deciduous, and tundra biomes, as reflected in the reducing SI_1 values (Figure 3.5). While the conditional expectation remains linear for lower *vmax* values, it saturates at higher values, as seen in the tropical broadleaf biome where the conditional expectation increases over the lower three-fifths of the *vmax* range before plateauing. This saturation indicates diminishing direct sensitivity to further increases in *vmax*. For higher *vmax* values, the spread of 30-year mean NBP values from the conditional expectation is greatest for the tropical broadleaf and temperate conifer biomes. An obvious outlier at the tundra location stands out far away from the conditional percentile curves (Figure 3.6g). This outlier, along with the spread of the distribution around the conditional percentile curves, is a good example of how the conditional spread can affect the estimates of the width of the conditional distribution, as seen in Figure 3.5. In comparison, at the temperate broadleaf location, the spread around the conditional expectation (and conditional percentile curves) is less, and the corresponding confidence intervals in $SI_{1_{vmax}}$ is the least among all biome locations.

Figure 3.7a,b shows the absolute first and total-order SI values for *vmax*, for all biome locations and output variables, for the 30-year means. Figure 3.7c shows the corresponding differences between the SI_{tot} and SI_1. As a general pattern for the mean state, the broadleaf locations and temperate conifer biome have higher $SI_{1_{vmax}}$ for the mean gross primary productivity and respiration rate, but lower $SI_{1_{vmax}}$ for NBP and net ecosystem productivity (Figure 3.7a). $SI_{1_{vmax}}$ for the boreal deciduous biome location is lesser than all other biomes for all output variables. The $SI_{tot_{vmax}}$ is greater for the tropical broadleaf biome site compared to the boreal deciduous or tundra locations (Figure 3.7b). We also see that there are small but robust interactive effects for the mean state (Figure 3.7c). There are very few instances where the $SI_{tot_{vmax}}$ is less than $SI_{1_{vmax}}$ (e.g., sensible heat flux for the temperate conifer and tundra biome locations). The interactive effects of *vmax* are lesser for the tropical

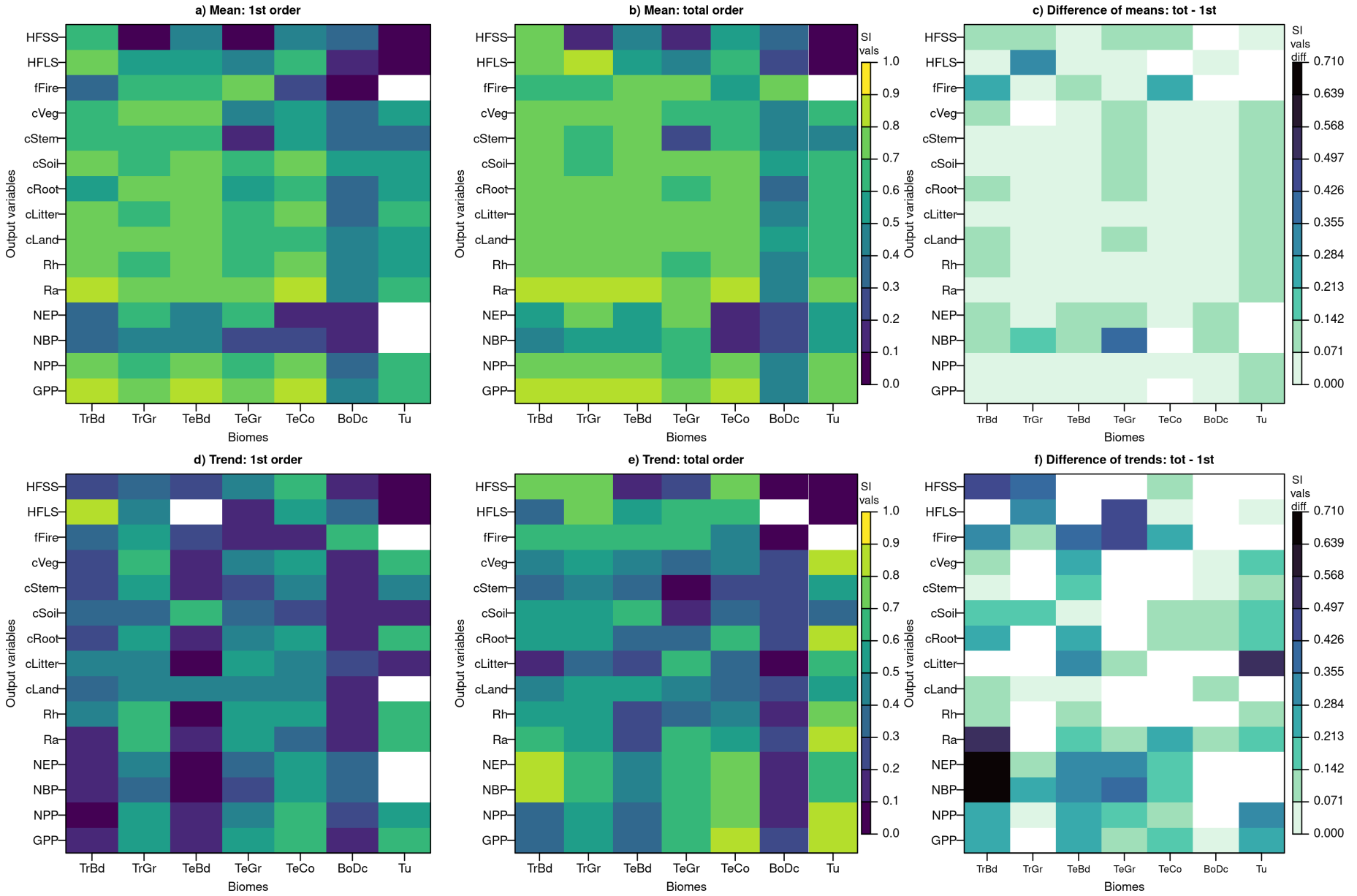

Figure 3.7: Absolute SI values for $vmax$ for all the biomes and output variables. The upper row corresponds to the mean state, and the lower row corresponds to the trends; the left column is the first-order indices, the middle column gives the total-order indices and the right column shows the differences between the corresponding total and first-orders. Empty cells other than tundra-fFire in (a), (d), and (e) represent SI values less than 0. Empty cells other than tundra-fFire in (c) and (f) represent output/biome combinations where $SI_{tot_{vmax}}$ is less than $SI_{1_{vmax}}$.

grassland, temperate broadleaf, temperate conifer and boreal deciduous biome locations than for tropical broadleaf, temperate grassland or tundra locations for a majority of output variables, which denotes that at the former locations, *vmax*'s interactions with other parameters are comparatively lesser.

Figure 3.8a represents the SI_1 and confidence intervals for the 30-year trend of NBP for each parameter/biome. Compared to the mean state (Figure 3.5a), the SI_{1_i} values for the trend are generally smaller for all biome locations except at the boreal deciduous location. Confidence intervals for the trend are generally broad across all parameters, with varying degrees of overlap, and we cannot identify the individual influential parameters in a robust way. The boreal deciduous biome exhibits the highest sampling uncertainty among all locations. Unlike the mean state, photosynthetic parameters have limited first-order influences on the trend across most biomes, except the boreal deciduous biome, where *vmax*, *kn*, *alpha_phtsyn*, *sn*, and *beta*2 are influential. The parameter *vmax* for the temperate conifer biome is uniquely influential, as it is the parameter for this biome for which the confidence intervals of the SI do not overlap those of other parameters. While *vmax* also shows influence at the grasslands and boreal deciduous locations, its confidence intervals overlap with those of other parameters. Additionally, the *vpd*0 for the temperate grassland stands out as a notable photosynthetic influential parameter. The phenology-related parameters $lfespany$ and percentage of maximum leaf area index that can be supported (*thrprcnt*) for the boreal deciduous, *coldthrs* and *coldlmt* for temperate grassland, and *coldlmt* for temperate broadleaf locations are influential. All other rooting and phenology parameters have negligible individual effects across biome locations. For the boreal deciduous location, the autotrophic respiration parameter $grescoef$, parameters related to physical fluxes $XLEAF$, $TCSAND$, and the mortality parameter maximum plant age (*maxage*) are influential among the specific processes. For all other biome locations, these processes have low first-order influence.

The only photosynthetic parameters to have moderate to high interactive influence at any of the biome locations are *vmax*, *kn*, and *alpha_phtsyn* (Figure 3.8b). Out of these parameters, the interactive effects are greatest for *vmax* at all biome locations except at the boreal deciduous location. The parameter *kn* interacts with other parameters in the tropics and *alpha_phtsyn* at topical grassland, temperate broadleaf and tundra locations. Among the parameters related to phenology, *coldthrs* and *minslai* at the temperate broadleaf location show interactive influence. For the temperate grassland location, the parameters are *kappa* and *minslai*, and for the tropical

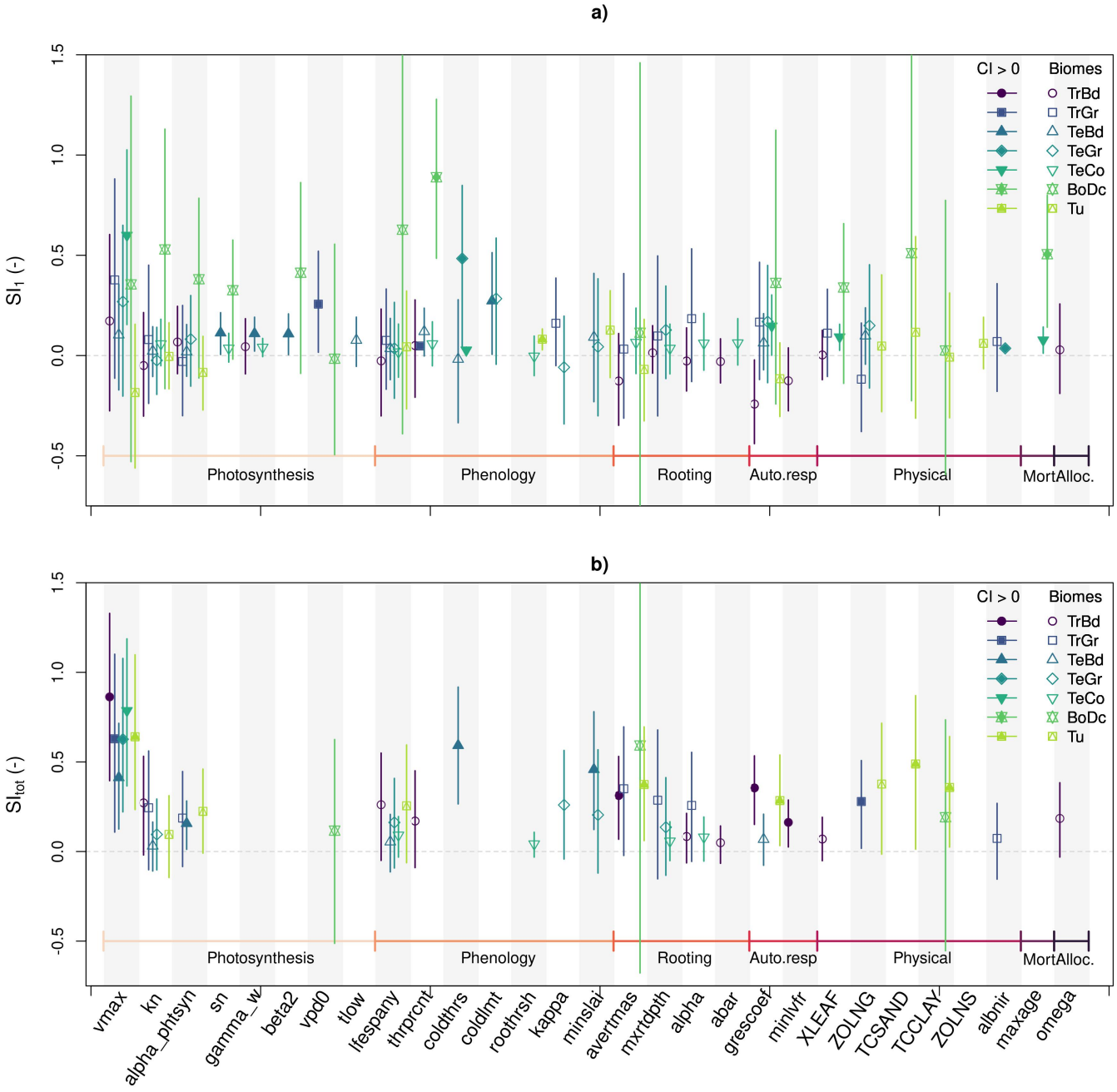

Figure 3.8: First (a) and total-order (b) SIs, and their confidence intervals for NBP for the top-ranked parameters across biomes (open symbols) for the trends. Filled symbols represent higher robustness where confidence interval values are greater than 0. Total-order indices are plotted only where SI_{tot} is greater than SI_1. The parameters are grouped according to the processes.

broadleaf location, they are $lfestapny$ and $thrprcnt$. The parameter $lfespany$ also has interactive effects at the tundra location. The rooting parameter $avertmas$ has interactive effects at the boreal deciduous and tundra locations, $mxrtdpth$ and $alpha$ show influence at the tropical grassland location. The autotrophic respiration parameter $grescoef$ has interactive effects at the tropical broadleaf and tundra locations. Physical parameters such as $ZOLNG$, $TCSAND$ and $TCCLAY$ have interactive effects at the tundra location, while $ZOLNG$ also has interactive effects at the tropical grassland location. All other parameters in the each targeted set have negligible or zero interactive effects across biome locations. A summary of the influential parameters for the 30-year trends of NBP, grouped according to the processes are provided in Table 3.5.

The corresponding conditional distributions in Figure 3.9 illustrate the variation of the 30-year NBP trend across biomes with $vmax$ (not all biomes are shown). Similar to the mean state, we see distinct biome-specific patterns for the 30-year NBP trends to variations in $vmax$. Over the last 30 years, biomes such as the temperate broadleaf, and tropical grassland locations have positive values in a majority of the 30-year trend NBP simulations for changes in $vmax$. The 30-year trends at the boreal deciduous location is positive, but close to zero. At the tundra location, even though there is a comparable spread of positive and negative trends for increasing values of $vmax$, the conditional expectation changes from small negative for smaller values of $vmax$ to small positive for higher values of $vmax$. At the temperate conifer location, the conditional spread of NBP trends is predominantly negative. On the other hand, at the tropical broadleaf location, small negative values and weak positive trends are dominant for the lower half of $vmax$'s range, and small positive values and strong negative trends are dominant for the upper half of $vmax$ values. At the tropical grassland location, isolated negative 30-year NBP trends are present across $vmax$'s uncertainty range.

The 30-year trends of NBP at the tropical broadleaf and temperate conifer locations become more negative for changes in $vmax$. The corresponding NBP trend values at the boreal deciduous location is close to zero. The temperate conifer biome location exhibits the largest variance of the conditional expectations for trends, and is seen as the highest $SI_{1_{vmax}}$ value in Figure 3.8. The spread around the conditional expectation increases for increasing values of $vmax$ for the temperate biome locations and for tundra. While isolated outliers are less prominent compared to the mean state, the spread of model simulations with low counts remains noticeable across

Table 3.5: Influential parameters for the 30-year trends of NBP, grouped according to the processes.

Biome	**Photo-synthesis**	**Phenology**	**Rooting**	**Auto-trophic respiration**	**Physical**	**Mort-ality**	**Alloc-ation**
TrBd	*vmax* *kn*	*lfespany*, *thrprcnt*	*avertmas*	*grescoef*, *minlvfr*	-	-	*omega*
TrGr	*vmax*, *alpha_phtsyn*, *kn*, *vpd*0	*kappa*	*avertmas*, *mxrtdpth*, *alpha*	*grescoef*	*XLEAF*, *ZOLNG*	-	-
TeBd	*vmax*, *alpha_phtsyn*, *sn*, *gamma_w*, *beta*2 *tlow*	*thrprcnt*, *coldthrs*, *coldlmt*, *minslai*	-	*grescoef*	*ZOLNG*	-	-
TeGr	*vmax*	*coldthrs*, *coldlmt*, *kappa*, *minslai*	*mxrtdpth*	*grescoef*	*ZOLNG*	-	
TeCo	*vmax*	-	-	*grescoef*	-	-	-
BoDc	*vmax*, *alpha_phtsyn*, *kn*, *sn*, *beta*2 *vpd*0	*lfespany*, *thrprcnt*	*avertmas*	*grescoef*	*XLEAF*, *TCSAND*, *TCCLAY*	*maxage*	-
Tu	*vmax*, *alpha_phtsyn*, *kn*	*lfespany*, *minslai*	*avertmas*	*grescoef*	*ZOLNG*, *TCSAND*, *ZOLNS*	-	-

biome locations (e.g., tropical grassland and boreal deciduous). The spread is small around the conditional curves at the temperate broadleaf locations for increasing values of $vmax$. This feature corresponds to lesser noise, and is seen as narrower width of confidence interval in Figure 3.8a. On the other hand, at the boreal deciduous location, the spread of the conditional distribution around the conditional curves is broad, denoting that the noise is comparatively larger. As previously discussed, these large conditional spreads lead to sampling uncertainty in the simulated 30-year NBP trends and correspond to the broader confidence intervals observed for the boreal deciduous location in Figure 3.8a.

Analyzing the SI_{vmax} values for 30-year trend values of NBP (Figure 3.7d-f), interactive effects of $vmax$ are evident, as the first-order SI values are smaller than the total-order SI. Extending the analysis to the sensitivity of all output variables to $vmax$, we find that the $SI_{1_{vmax}}$ values for the trends (Figure 3.7d) are comparatively lesser than the corresponding mean state for a majority of output variables, across biome locations. The $SI_{tot_{vmax}}$ values for the trends are also lesser than the mean state for many instances, except for the tundra biome site, where the total-order index is greater for the trends than the mean state for all the carbon variables (Figure 3.7e). For the tropical broadleaf biome, the total-order index for the net ecosystem productivity and NBP are also higher for the trends than the mean state. For many other output variables, especially at the broadleaf locations and tundra location, the evidence of parameter interactions of $vmax$ with other parameters for the trends are stronger than the mean state (as given by the differences). This finding is consistent with the fact that SI_1 values are generally smaller for the trend than for the mean. The upper limit of differences for $SI_{tot_{vmax}} - SI_{1_{vmax}}$ is 0.71 (Figure 3.7f). This range is almost twice as that of the mean state, which is 0.33 (Figure 3.7c), and thus we observe more influential interactions for the trends than for the mean state.

3.4 Discussion and Conclusions

Previous studies of the terrestrial carbon budget have acknowledged that the uncertainty in the carbon sink can be due to the model's structure and/or due to parametric uncertainty (Booth et al., 2012; Dietze, 2017; Fisher et al., 2019; Knorr et al., 2024; Zheng et al., 2018). Our analysis quantifies how the estimated carbon sink's strength is sensitive to parameter uncertainties in terrestrial biosphere models using CLASSIC as an example. This is the first study assessing the sensitivity of the carbon sink to

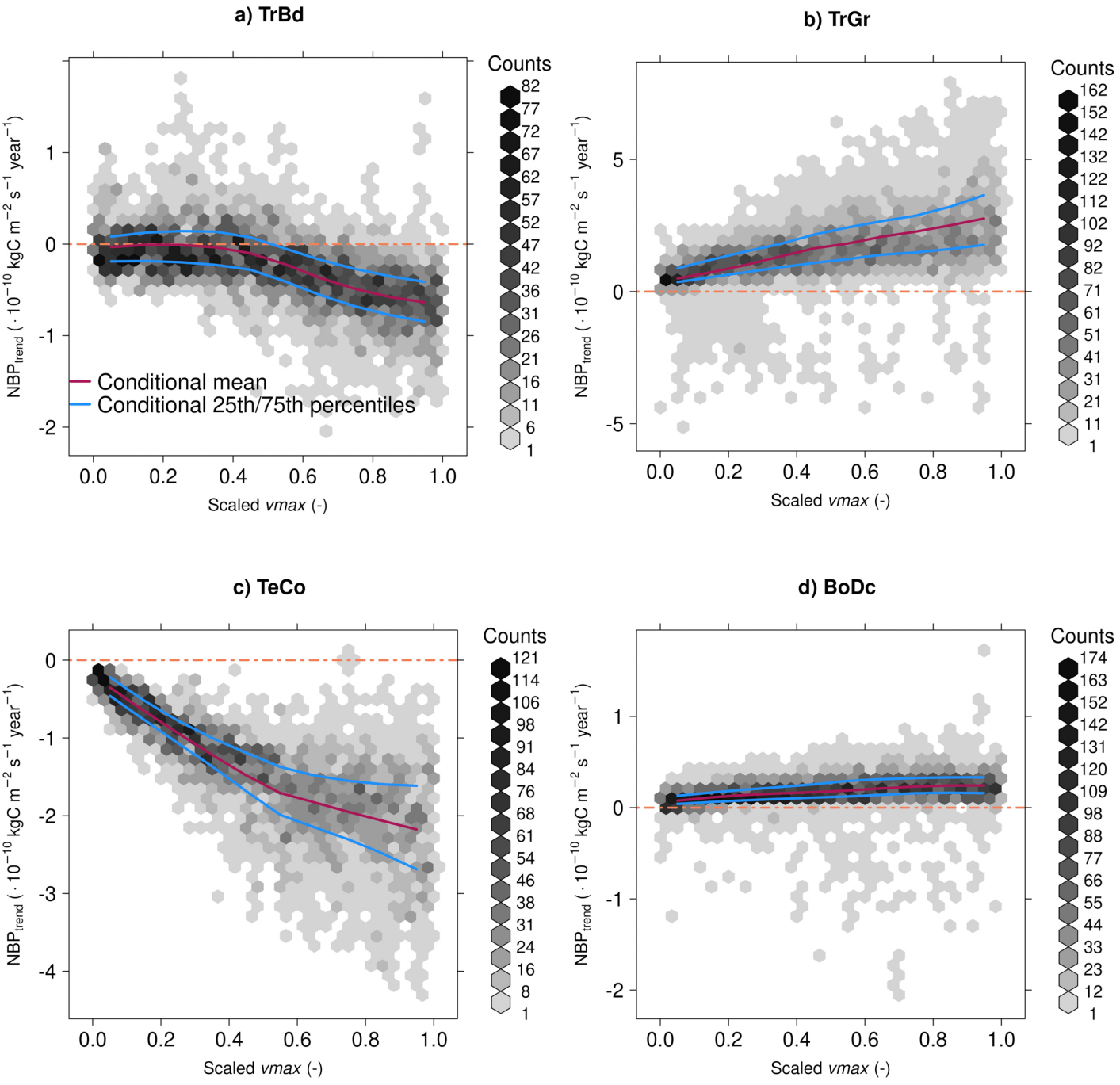

Figure 3.9: Conditional distribution of the 30-year trends of NBP ($\times$ 10^{-10} kgC m^{-2} s^{-1} $year^{-1}$) for four biomes, for changes in $vmax$, along with the conditional expectation (magenta coloured line), the conditional 25^{th} and 75^{th} percentile curves (blue lines), and the default 30-year NBP trend value (red arrow heads).

parameter uncertainties simulated under evolving conditions. We find that the sensitivity of the carbon sink is high, which agrees with previous studies that focused on other flux-components of the carbon balance (Kaminski et al., 2013; Raoult et al., 2024; Xiao et al., 2014; Xing et al., 2023). Using GSA, we have assessed the influential parameters that drive this uncertainty as done by previous studies (Bastrikov et al., 2018; Senapati et al., 2016; Y. Yang et al., 2022; Zhang et al., 2019; Zhu & Zhuang, 2014). But mainly, we have assessed how the uncertainties in parameter values contribute to the uncertainty in the historical carbon sink across individual grid cells for seven biomes.

To investigate the uncertainty in the historical NBP, a different experimental setup is required than those used in previous studies (e.g., Bagnara et al., 2019; J. Li et al., 2016; Y. Li et al., 2022; X. Lu et al., 2013; Ma et al., 2020; Massoud et al., 2019; Ricciuto et al., 2018; Rodriguez & Espíndola, 2024; Q. Yang et al., 2021; Zhu & Zhuang, 2014). Our study quantifies the sensitivity of 30-year mean and trends of NBP under increasing atmospheric [CO_2] and transient environmental conditions for the historical period (1901-2017). The simulation protocol closely follows the TRENDY simulation protocol (Sitch et al., 2024). By simulating output variables over the historical period following a prolonged spin-up, we allow sufficient time for the model to move away from the equilibrium state.

We show that many of the biome locations considered in this study can act as both sources or sinks of carbon within the range of parameter uncertainty. The largest 30-year mean NBP uncertainties are observed at the tropical grassland location and the smallest at the tundra location. The influence of parameters within the targeted set obtained from the Morris method, on the 30-year mean NBP and the 30-year trends varies across biomes. The first takeaway from our analysis is that, out of a very large number of parameters considered for the GSA (124), only a small subset is are found to be influential (18-20) across biome locations, output variables and sensitivity measures. Second, tuning efforts should account for influential parameters from multiple processes rather than focusing solely on maximum carboxylation rate ($vmax$), as establishing a definitive ranking of parameters is challenging due to substantial sampling variation. Third, despite extensive sampling requiring the equivalent of almost 10 CPU years for seven grid cells, the sensitivity indices exhibit broad uncertainty ranges, suggesting that these results should be interpreted with caution.

Previous sensitivity analyses conducted on regional or multi-biome carbon fluxes within land surface models have consistently identified photosynthesis-related param-

eters such as $vmax$, quantum efficiency ($alpha\_phtsyn$), and those governing stomatal conductance, as among the most influential (J. Li et al., 2016; Ma et al., 2020; Massoud et al., 2019; Xing et al., 2023; Zhu & Zhuang, 2014). Similarly, respiration-related parameters, including those affecting autotrophic respiration through the growth respiration coefficient ($grescoef$), and other parameters linked to the ecosystem respiration process, have also been identified to be influential (Massoud et al., 2019; Ricciuto et al., 2018; Zhu & Zhuang, 2014). Added to parameters related to photosynthesis and autotrophic respiration, our study shows that those related to rooting, phenology, physical fluxes, mortality and carbon allocation are also influential for the historical output variables. Parameters related to heterotrophic respiration, turnover, and fire do not have any influence on the carbon cycle variables at any biome location assessed in our study.

While these previous studies provide valuable insights, most have focused on the absolute SI values without incorporating confidence intervals. There are two exceptions among these studies that explicitly accounted for the uncertainty in SI values, but did not include the effects of overlap in confidence intervals across multiple parameters while identifying the most influential parameters (Ricciuto et al., 2018; Xing et al., 2023). In our analysis, we find that sampling uncertainty in SI values, along with overlapping confidence intervals, makes it difficult to identify the most influential parameters with robustness. Although robust rankings of individual parameters cannot be found through our study, clusters of process-related parameters emerge. The exclusion of sampling uncertainty considerations, may have led to the identification of parameters with potentially broader uncertainty as highly influential in some of the previous studies.

Temperature threshold parameters related to phenology ($coldthrs$ and $coldlmt$) influence the carbon sink in biomes with crops and grasslands, such as temperate broadleaf and temperate grassland locations. In contrast, there is no notable sensitivity of NBP to uncertainties in parameters setting upper-temperature ranges for photosynthesis (e.g., tup). Given the rise in global and regional temperatures since the pre-industrial period, the lack of direct influence of temperature parameters (such as those within the hyperbolic tangent ($tanh$) formulation of heterotrophic respiration determination function ($tanhq10$)) on the carbon sink is noteworthy. Rising temperatures could intensify heterotrophic respiration and increase the occurrences of forest fires, resulting in greater CO_2 emissions to the atmosphere. Additionally, prolonged heat stress may contribute to higher plant mortality, further altering the

carbon balance. As these effects become more pronounced, temperature-related parameters may become more influential under high-emission scenarios with extreme warming. In a future study, we will investigate whether this hypothesis holds true for future NBP using CLASSIC as an example of terrestrial biosphere models.

We do observe effects of water stress on the uncertainty of NBP, as a few rooting parameters (e.g., *mxrtdpth*, *avertmas*, *abar*) are found to be particularly influential at the grasslands and temperate conifer biome locations and physical parameter ($TCSAND$) at tundra, which also consists of grasses. The presence of rooting parameters among the influential ones suggests that the roots may be deep-seated at some of these locations. Deeper roots can be advantageous in regions prone to water stress, as the soil moisture increases with soil depth at the chosen grid cells. This finding is consistent with a strong sensitivity of the latent heat flux (HFLS) to rooting parameters across the grassland locations (not shown).

Many parameters from the targeted set obtained from the Morris method for each biome location have robustly greater influence at the first-order level but not at the total-order level (e.g., the mortality parameter *maxage* at boreal deciduous), indicating that these parameters affect the carbon sink individually without robust interactive effects with other parameters. This feature is rarely observed in previous studies that assessed the sensitivity of carbon fluxes through the first and total-order sensitivity indices, but was noticed in the study by Q. Yang et al. (2021) for the net ecosystem exchange simulated at only one of eight ChinaFLUX sites. Conversely, some parameters exhibit low or negligible first-order effects but contribute through their total-order effects (e.g., the autotrophic respiration parameter *grescoef* at tropical broadleaf location), bringing forth their interactive influence. The total-order indices capture the combined individual and interactive effects of a parameter and are shown in many previous studies (e.g., Y. Li et al., 2022; Ma et al., 2020; Pappas et al., 2013; Zhu & Zhuang, 2014, etc.). In general, the strength of interactions is much greater for the trend than the mean state, even though the first-order effects are much weaker. For instance, the interactive effects of *vmax*, reflected by the difference between SI_{tot} and SI_1, are more prominent for the 30-year trends than for the mean state of the carbon sink across various biome locations. However, at the boreal deciduous location, influential parameters primarily exert their effects individually rather than interactively. When selecting parameters for model tuning, it is important to consider those with both first-order and higher-order influences, as the first-order characterizes just the individual effects, whereas the higher-order ef-

fects characterize interactive effects among parameters. A limitation of identifying influential parameters through total-order indices is that it does not specify which parameters interact, but identifies only a single parameter of the set. The Sobol' method, being variance-based, could identify interacting parameters more precisely through the analysis of doublet or triplet interactions, as demonstrated by Hou et al. (2015) and Ricciuto et al. (2018). For instance, Ricciuto et al. (2018) employed a surrogate model to approximate their land surface model, while Hou et al. (2015) utilized the thermodynamic and hydrological modules to simulate fluxes. Such approaches, using emulators or model submodules, are computationally less intensive. However, due to the computational demand of direct model simulation being high (albeit at single points), we limited our analysis to individual and total-order effects through the Sobol' method, leaving the specific interactions involving the most influential parameters to be unclear.

Conducting GSA is a important step for tuning models, and we find that only a limited subset of input parameters (18-20) affect a wide range of output variables. The Morris elementary effects method revealed that while $vmax$ consistently ranks among the most influential parameters, several other parameters also exert notable influence on specific output variables. Through the Sobol' method we notice that not all parameters from the targeted set obtained from Morris are influential. Sobol' analysis refines this selection by quantifying the most influential parameters for each biome's 30-year mean and trend. Our analysis identifies influential processes and sets of associated parameters for both the 30-year means and trends. Tuning can be performed using the targeted influential parameters identified for individual biomes (Bagnara et al., 2019; Bastrikov et al., 2018; Hou et al., 2015) or through a combined parameter pool for global applications. It is important to clearly define the tuning objective; whether it is to optimize for trends, the mean state, or another measure. Using the parameter set derived for the mean state to tune for trends may yield less effective results. Additionally, prioritizing improved trend predictions could lead to increased errors in the mean state, pointing out potential trade-offs in the tuning process. Currently, the combined parameter pool identified through the Morris screening test across all biomes is being used in a machine learning algorithm study aimed at optimizing the output variables from CLASSIC by one of the co-authors.

Tables 3.4 and 3.5 can be helpful in identifying geographic patterns in the influence of few parameters (e.g., $lfespany$ at temperate grassland, temperate conifer, boreal deciduous and tundra locations for the mean state; or the fact that no interactive

effects are noticed for the rooting parameters at the broadleaf locations). A detailed geography-based analysis of why certain parameters are influential in certain biomes is outside of the scope of the present study but is worth future consideration.

The identification of the most influential parameters for the uncertainty of carbon sink will help model development and future optimization studies. We encourage other terrestrial biosphere modelling groups to conduct formal GSA studies to better quantify parameter-induced uncertainties in global NBP estimates, and identify the most influential parameters that could be used in optimization problems. This can be achieved by using emulators (e.g., Ricciuto et al., 2018), adjoint models (e.g., Zhu & Zhuang, 2014) or model sub-modules (e.g., Hou et al., 2015). For those with extensive computational resources, increasing the number of sampled points within parameter uncertainty ranges could further improve the robustness of GSA studies. By identifying the robust effects of influential parameter uncertainties on global carbon sink uncertainties, and tuning them, the carbon sink estimates can be improved. This improvement will further aid in providing better future Global Carbon Budget assessments.

Our results also forms the basis for Chapter 4 that aims to identify the influential parameters for the carbon cycle variables under future climatic conditions. In this chapter, CLASSIC will be forced using the meteorological data from Canadian Earth System Model version 5 (CanESM5) using the Inter-Sectoral Impact Model Intercomparison Project (ISIMIP3b; Lange & Büchner, 2021) simulation protocol. Knowing the most influential model parameters is important for interpreting its outputs, guiding future model development, and aiding in the preparation of reports for policy makers. Identifying the most influential parameter(s) will also enhance optimization efficiency. Our study acts as a stepping stone for future model development and optimization endeavours.

Chapter 4

Global Sensitivity Analysis of the Future Land Carbon Sink

The terrestrial biosphere absorbs more CO_2 than it emits, slowing the accumulation of atmospheric CO_2. However, Earth system models differ in their Net Biome Productivity (NBP) projections, with inter-model ranges of 2 to 7 PgC yr^{-1} by the late 21^{st} century under a fossil-fuel-intensive scenario. We notice that the uncertainty in NBP simulated by the Canadian Land Surface Scheme Including Biogeochemical Cycles (CLASSIC) model is vastly impacted by parameter uncertainty. To address this uncertainty, we conduct a global sensitivity analysis (GSA) for seven grid cells across different biomes. Results of the preliminary screening test show that only 11-15 of 124 input parameters drive the output uncertainty at each location. Among them, the maximum carboxylation rate ($vmax$) consistently influences multiple output variables. Through the secondary quantitative test, we notice that $vmax$'s impact on NBP declines over time, but other photosynthetic and rooting parameters become more influential. In some locations, higher $vmax$ values reduce NBP, as increased ecosystem respiration and wildfire emissions outweigh gross primary productivity. Despite using approximately 15 CPU years of computational effort, the sampling uncertainty among the 11-15 parameters is broad. Ranking the parameters based on robustness is difficult. Expanding the analysis to an additional metric, we find that the same parameters that drive the uncertainty of the projected future NBP also drive the uncertainty of the change from the late historical to late future NBP. These results indicate that future optimization efforts related to NBP must consider multiple parameters rather than focusing solely on $vmax$. By identifying influential parameters and processes, this study enhances our understanding of parametric uncertainty in carbon sink projections and defines

a low-dimensional space of influential parameters, aiding future model refinement.

The contents of this Chapter have been submitted to Atmosphere-Ocean for peer review as "Global Sensitivity Analysis of the Future Land Carbon Sink".

4.1 Introduction

Currently, the terrestrial biosphere absorbs approximately 30% of anthropogenic CO_2 emissions (Friedlingstein et al., 2024). While the absolute uptake of carbon projected by Earth system models is set to increase by the end of the 21^{st} century, the uptake relative to emissions is projected to decrease (Canadell et al., 2023). However, inter-model differences are large, ranging from approximately 2 to 7 PgC yr^{-1} by the end of the 21^{st} century for a fossil-fuel intensive scenario (SSP5-8.5; Kriegler et al., 2017). Longer-term simulations project that the terrestrial biosphere will switch from a carbon sink to either a neutral state or a carbon source by the year 2300 (Koven et al., 2021). Here as well, the inter-model differences remain substantial, ranging from -7 to 0 PgC yr^{-1}. The large inter-model differences may be due to both structural and parametric uncertainties (Booth et al., 2012; Dietze, 2017; Fisher et al., 2019; Knorr et al., 2024). In the process of adding new parameters and/or allowing various existing ones to interact, output uncertainties due to parametric uncertainties increase (Gier et al., 2024; Green et al., 2019; Varney et al., 2024). Uncertainties in the output variables can be reduced by tuning the input parameters of a model ((Bastrikov et al., 2018; Hou et al., 2015; J. Li et al., 2016; Ma et al., 2020; McNeall et al., 2023; "Parameter optimization for global soil carbon simulations: Not a simple problem", n.d.; Rodriguez & Espíndola, 2024; Xing et al., 2023; Zhu & Zhuang, 2014)). Tuning all the input parameters for a given model is computationally prohibitive. In these previous studies, it has been found that tuning a few influential parameters by constraining them using global Earth observations increases the model's accuracy in simulating the output variables. Global sensitivity analysis (GSA) can shed light on the fraction of uncertainty in the output variables corresponding to uncertainties in input parameters (Saltelli et al., 2004). GSA methods can identify the most influential parameters for any given output variable, thereby quantifying the uncertainties in the output variable, and reducing the dimensionality for optimization.

The sensitivity of the historical terrestrial carbon sink to parameter uncertainties was studied for the first time for any land surface model in Chapter 3. We conducted a GSA for the historical carbon sink simulated by the Canadian Land Surface Scheme

Including Biogeochemical Cycles (CLASSIC) model (Melton et al., 2020) forced with reanalysis data. The CLASSIC model is an active member of the model ensemble used for estimating the global carbon sink in the annual publication of the Global Carbon Budget assessments (e.g., Friedlingstein et al., 2023, 2024).

As mentioned above, there are substantial uncertainties present in the projected carbon sink values for the years 2100 (Canadell et al., 2023) and 2300 (Koven et al., 2021). To the best of our knowledge, no terrestrial biosphere modelling group has quantified the effects of input parameter uncertainties on the uncertainties of the projected carbon cycle variables. It remains unclear how the sensitivity of output variables to parameter uncertainty changes with changing climatic conditions in the future.

To address this research gap, for the first time we conduct a GSA for the projected output variables simulated by a terrestrial biosphere model, in the context of the CLASSIC model. The previous version of CLASSIC, CLASS-CTEM serves as the land surface component of the Canadian Earth System Model (CanESM; Swart et al., 2019), which participated in the Coupled Model Intercomparison Project Phase 6 (CMIP6). For this analysis, we forced the CLASSIC model with meteorological data obtained from CanESM version 5 (CanESM5).

The Methods section provides an overview of the CLASSIC model, the experimental setup, the selected output variables, the input parameters along with their uncertainty ranges, the chosen biome grid cells, and the GSA techniques employed. The Results section presents findings from the GSA methods, and the overall uncertainty in NBP attributed to parametric uncertainty. The Discussion section covers insights gained from this analysis, comparison between the results from the previous historical GSA and the present study, limitations related to sampling uncertainty and parameter interactions, the implications for parameter tuning, and the relevance of GSA to the terrestrial biosphere modelling community.

4.2 Methods

4.2.1 CLASSIC

In this study, we have run the CLASSIC model in the offline mode. Physical fluxes for the vegetation, soil, and snow are simulated by the CLASSIC model's component, the Canadian Land Surface Scheme (CLASS; Verseghy, 2017). All other biogeochemical

vegetation processes are simulated by the other component, the Canadian Terrestrial Ecosystem Model (CTEM; Melton & Arora, 2016), which consists of individual processes such as photosynthesis, phenology, and dynamic root distribution. (Arora & Boer, 2003, 2005; Melton et al., 2015). The model version used in this study simulates nine plant functional types (PFTs), as in Chapter 3.

Experimental Design

The model simulations were performed for three different settings: spinup, historical, and SSP5-8.5 future scenario. The pre-industrial forcing from 1601-1850 was repeated once to produce 500 years of spinup. During spin-up, the CO_2 concentration ($[CO_2]$), land cover, population density and lightning strike rate were fixed to constant values from 1850. The transient historical time period was simulated for 165 years from 1850-2014 and the transient future period was simulated for 86 years from 2015-2100, using time-varying values for all inputs. To reduce computational costs, the nitrogen cycle, which requires a longer spin-up (Seiler et al., 2024), is deactivated throughout the study. Similarly, the methane cycle and state variables for moss and peat are excluded from our experimental design, as these components increase the number of model runs for the GSA, and are not consistently present across all biomes. We prescribed the fractional PFT per grid cell.

We simulated the CLASSIC model using CanESM5's bias-adjusted meteorological forcing, provided by the third phase (3b) of the Inter-Sectoral Impact Model Intercomparison Project (ISIMIP; Lange & Büchner, 2021). Previous work by Seiler et al. (2024) demonstrated that using bias-adjusted CanESM5 data improved the performance of various ecosystem variables simulated by the CLASSIC model compared to simulations using raw CanESM5 data. The land cover was derived by Wang et al., 2010, from the European Space Agency Climate Change Initiative (ESA-CCI) (CCI, 2018) adjusted with CMIP6 crop area (Land-Use Harmonization (LUH) project) (Chini et al., 2021; Hurtt et al., 2017). Population density was taken from ISIMIP2b: History Database of the Global Environment (HYDE version 3.2) (Jones & O'Neill, 2016; Klein Goldewijk et al., 2017). The $[CO_2]$ data were obtained from Meinshausen et al. (2020, 2016). The lightning strike rate was from Lange and Büchner (2021). We have summarized the modelling protocol in Table 4.1.

Table 4.1: Summary of the experimental design used in Chapter 4.

Forcing Type	**Forcing based on**	**Spin-up** (500 years)	**Historical** (165 years)	**Future** (86 years)
CO_2	CMIP6	1850 (284.32 ppm)	1850-2014 (284.32-397.55 ppm)	2015-2100 (399.9-1135 ppm)
Meteorology	ISIMIP3b	2×(1601-1850)	1850-2014	2015-2100
Land cover	ESA-CCI + LUH project	1850	1850-2014	2015-2100
Population density	ISIMIP2b: HYDE-v3.2	1850	1850-2014	2015-2100
Lightning strike rate	ISIMIP3b	1850	1850-2014	2015-2100

Output Variables

We examined a comprehensive set of simulated variables (Table 4.2) to identify the most influential parameters. The primary analysis focused on net biome productivity (NBP), which integrates multiple carbon fluxes, including gross primary productivity (GPP), ecosystem respiration terms (autotrophic respiration (Ra) and heterotrophic respiration (Rh)), and disturbance-related emission terms (CO_2 emissions due to forest fires ($fFire$) and land-use change (E_{LUC})). NBP is expressed as:

$$NBP = GPP - Ra - Rh - fFire - E_{LUC}.$$

While our study focuses on NBP, we also assess additional variables, such as net primary productivity ($NPP = GPP - Ra$), net ecosystem productivity ($NEP = GPP - Ra - Rh$), carbon pools (land, litter, soil, stem, root, and vegetation), as well as latent heat flux ($HFLS$) and sensible heat flux ($HFSS$). The processes within the terrestrial carbon cycle is coupled, and thus, we have used a broad range of variables. The output variables considered for the GSA are annual mean values. Identifying influential parameters across these outputs not only enhances our understanding of the terrestrial carbon cycle and its uncertainties but also aids model development by helping us choose parameters important for tuning.

Table 4.2: Annual output variables used.

Short name	**Long name**	**Units**
GPP	Gross primary productivity	kgC m^{-2} s^{-1}
Ra	Autotrophic respiration rate	kgC m^{-2} s^{-1}
Rh	Heterotrophic respiration rate	kgC m^{-2} s^{-1}
fFire	CO_2 emissions from wildfire	kgC m^{-2} s^{-1}
NPP	Net primary productivity	kgC m^{-2} s^{-1}
NEP	Net ecosystem productivity	kgC m^{-2} s^{-1}
NBP	Net biome productivity	kgC m^{-2} s^{-1}
cLand	Land carbon pool	kgC m^{-2}
cLitter	Litter carbon pool	kgC m^{-2}
cRoot	Root carbon pool	kgC m^{-2}
cSoil	Soil carbon pool	kgC m^{-2}
cStem	Stem carbon pool	kgC m^{-2}
cVeg	Vegetation carbon pool	kgC m^{-2}
HFLS	Latent heat flux	W m^{-2}
HFSS	Sensible heat flux	W m^{-2}

Parameter Uncertainty

This study considered 126 input parameters (Table A.2). Six of these parameters are dependent on each other. Here, parameter triplets of a kind adding to one, such as the percentage of disturbed biomass that is used in short-term storage as paper (*paper*), in long-term storage as furniture ($furniture$), and that is combusted (*combust*); and carbon allocations to stem (*epsilons*), root (*epsilonr*) and leaves (*epsilonl*), have been converted to independent parameters through the spherical coordinates conversion technique (as described in Appendix A.1.2). After conversion, we have 124 independent parameters. Since we consider different PFTs, some parameters have different PFT-specific values with different uncertainty ranges (e.g., the mean root distribution profile, *abar* in Table A.1). The perturbations are done in a way that the parameter sampling is such for each sample, the same quantile is drawn for each PFT, relative to the respective uncertainty ranges. That is, the parameters are varied proportionally among all PFTs. The number of parameters would increase by a factor of nine if each PFT-specific value is considered as an individual parameter. Consequently, the computational expense for the GSA would increase ninefold. As explained in Section 4.2.3, performing GSA for the whole model is computationally expensive. As discussed later, such an increase in computational effort would render the analysis intractable.

The four ways by which we obtain the parameter uncertainty ranges are through (1) well-documented values from observations; (2) literature review; (3) expert advice and our modelling experience; and (4) ±10% ranges for parameters that do not fall under the above. For one parameter with units in Kelvin (the lower temperature threshold that is used to estimate cold stress-related leaf loss rate; *lwrthrsh*), we use a ±2 K uncertainty range. In some instances, the CLASSIC model's default parameter value lies outside the uncertainty ranges obtained from literature. In such cases we have extended the uncertainty range to the default values.

4.2.2 Biomes

We use the same seven grid cell locations as in Chapter 3. These are points chosen from seven different biomes (Figure 4.1). Though these single points are biome-specific, they do not represent the entire biome. The diverse ecological dynamics and spatial heterogeneity present across the entire biome cannot be captured by a single grid location. We have chosen only seven grid locations, as the GSA, including the qualitative and quantitative runs, require around 120,000 CPU hours for just seven grid cells. The grid-cells' latitude-longitude locations are given in Table A.1.

4.2.3 Global Sensitivity Analysis

Uncertainty of output variables due to the variations in input parameters within their uncertainty ranges can be quantified using GSA (Saltelli et al., 2004). When variations within an input parameter's uncertainty range lead to substantial changes in the output, compared to similar variations in other parameters, that parameter is considered influential (Wagener & Pianosi, 2019). Influential parameters can be identified through GSA methods. Identifying the most influential parameters helps interpret the model output and guide future model development efforts. The output variables can be optimized by tuning the most influential parameters. Parameters with weak or no influence need not be considered for the future tuning purposes. However, tuning parameters based on only one output variable (e.g., NBP) could lead to disruptive effects in other output variables (e.g., sensible heat flux), so GSA should include various interconnected output variables, such as the carbon cycle variables and turbulent heat fluxes.

The computational expense of the variance-decomposition based quantitative method increases rapidly for larger number of input parameters. It is therefore impractical to

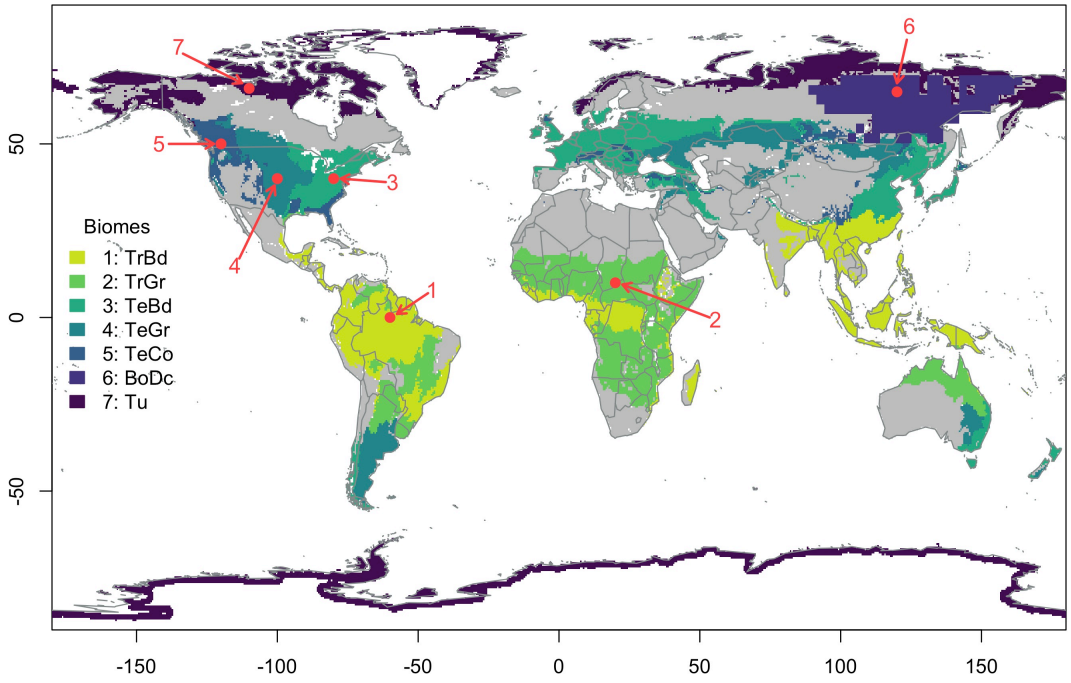

Figure 4.1: Single grid cell locations for each biome. The biomes are, (1) TrBd: tropical and subtropical moist broadleaf forest, (2) TrGr: tropical and subtropical grasslands, savannas, and shrublands, (3) TeBd: temperate broadleaf and mixed forest, (4) TeGr: temperate grasslands, savannas, and shrublands, (5) TeCo: temperate conifer forest, (6) BoDc: boreal deciduous forests, and (7) Tu: tundra. Non-ocean areas in white are glaciers, snow-covered mountains, or lakes. Biomes in grey were not considered due to time constraints and are excluded from the study.

apply the quantitative method to all 124 input parameters of the CLASSIC model. We follow the two-step GSA approach used in Chapters 2 and 3. The first step is to qualitatively screen out non-influential parameters and obtain the top-ranked parameters through the Morris elementary effects method. The second step is to quantify the model outputs' uncertainties due to the top-ranked parameters' uncertainties through the variance-decomposition based Sobol' analysis. We compute the sensitivities of the 20-year mean of the annual values of the future time period from 2081-2100; and the difference between this projected 20-year mean and the 20-year mean of the annual values of the historical time period from 1995-2014, which we will denote as the projected change in 20-year means. The projected change in 20-year means is analogous to the trend over this time period.

Morris Elementary Effects Method

The empirical observation that the input parameter uncertainties of only a few parameters influence the model output's variability is known as Pareto's principle (Box & Meyer, 1986). Qualitative analysis such as the Morris method can screen out the non-influential parameters from influential parameters (Campolongo & Braddock, 1999; Morris, 1991), and has been demonstrated in Chapters 2 and 3. This method can effectively identify the subset of influential parameters among all the parameters. Even though the screening test qualitatively ranks the input parameters, it fails to give a quantitative assessment of individual parameter importance or to what extent these parameters interact with each other.

All parameter uncertainty ranges are scaled from zero to one, thus making the parameter space a unit hypercube. The benefit of the rescaling is that a single step has the same size for all parameters, so the elementary effects are directly comparable. The elementary effects value is given as the ratio of differences of the output values between two consecutive steps in the same random walk to the step size. The model output's sensitivity to parameters is assessed using sensitivity measures like the mean (μ), absolute mean (μ^*) and standard deviation (σ) of the elementary effects values.

Sampling of the uncertainty ranges of all parameters is done by a one-at-a-time design with multiple realizations. For each realization within the screening test, a random walk is performed through the uncertainty space. Here, one parameter is perturbed between successive steps until all parameters have been perturbed. Multiple realizations help in a better sampling of the volume of the parameter uncertainty space. The sensitivity measures can be determined for all parameters by (Saltelli et al., 2008):

$$\mu_i = \frac{1}{r}\sum_{j=1}^{r}(EE_i^j), \tag{4.1}$$

$$\mu_i^* = \frac{1}{r}\sum_{j=1}^{r}\left|EE_i^j\right|, \tag{4.2}$$

$$\sigma_i = \sqrt{\frac{1}{r-1}\sum_{j=1}^{r}(EE_i^j - \mu_i)^2}, \tag{4.3}$$

where the elementary effects is given by EE_i^j, for the j^{th} out of r realizations and i^{th}

out of n parameters. The sensitivity metric, the Euclidean distance (κ)

$$\kappa = \sqrt{\mu^{*2} + \sigma^2},$$

is the distance from the origin (0,0) to the point (μ_i^*, σ_i). We can identify the parameters to be included in Sobol' based on the the values of κ. These κ values are calculated separately for each biome location.

Higher values of κ denote higher influence of parameters on the output variable. To facilitate comparisons of parameter sensitivities across multiple output variables, each parameter's elementary effect distance for a given variable was normalized by dividing it by the elementary effect distance of the highest-ranked parameter for that variable.

To calculate a parameter's elementary effects value, two points are required within the unit hypercube. The number of model evaluations for n parameters and n elementary effects values is $(n + 1)$. For r realizations, we require a total of $r \times (n + 1)$ evaluations. The total number of parameters is 124 and we have chosen r to be 80, which gives us a total of $80 \times (124 + 1) = 10,000$ unique runs. The seven biome locations have 10,000 unique runs each for the Morris screening test. We obtain the top five parameters from the Morris method for each output variable and biome location. This subset of five parameters will be denoted as the top-ranked subset. Combining the top-ranked parameters for all the output variables, we arrive at the set of parameters that will be targeted for quantification through the Sobol' analysis for each biome location and will be called the targeted set of parameters. We can rely on the Morris method to identify targeted parameters. But, the parameters with moderate κ values within the targeted set can have substantial sampling variability. Due to computational expense of the Sobol' analysis, we chose to use only the top five parameters selected for each output variable.

Focusing solely on carbon sink-related parameters is simpler and less computationally demanding than using multiple output variables. However, this narrow approach risks overlooking critical connections between carbon-related variables and other processes, such as turbulent energy fluxes. For instance, stomatal conductance influences both carbon dioxide uptake and water loss, linking carbon cycle dynamics to latent and sensible heat fluxes (Melton et al., 2020). Expanding the scope to include the top-five parameters across all output variables (Table 4.2) ensures that the analysis captures these interconnections. This comprehensive approach is essential to prevent

compensating errors if using these results for a parameter tuning exercise, as mentioned earlier. By identifying the complete set of top-five parameters across multiple variables, this strategy supports a more balanced and effective model optimization.

Although this study does not involve optimization, it lays the groundwork for future model optimization efforts, emphasizing the importance of accurately identifying the targeted set of parameters for optimizing various variables. To maintain a clear focus, we concentrate on quantifying the uncertainty of NBP and its components, thereby centering our analysis on the terrestrial carbon sink within a broader context.

Sobol' Analysis

The Sobol' analysis applies variance decomposition to calculate sensitivity measures, making it a powerful tool for quantifying the proportion of uncertainty in output variables attributable to uncertainties in input parameters. This method evaluates the variance of the conditional expectation for one or more conditioning parameters. To investigate how the output responds to uncertainty in a single i^{th} input parameter $(Y|x_i)$, the conditional expectation of the output $(E_{x_{\sim i}}(Y|x_i))$ is calculated by fixing the i^{th} parameter while allowing all other parameters $(\sim i)$ to vary. The variance of this conditional expectation $(V_{x_i}[E_{x_{\sim i}}(Y|x_i)])$ represents the sensitivity of the output variable to the fixed parameter. This technique can also be extended to examine sensitivities arising from interactions between parameters by fixing pairs, triplets, or larger combinations (e.g., Hou et al., 2015; Ricciuto et al., 2018). In this study, we utilize first-order sensitivity indices (SIs) and total-order SIs to assess the individual and interactive effects of input parameters. The first-order SI, which captures the individual contribution of the i^{th} parameter (SI_{1_i}), is defined as (Saltelli et al., 2008):

$$SI_{1_i} = \frac{V_{x_i}[E_{x_{\sim i}}(Y|x_i)]}{V(Y)}, \tag{4.4}$$

where the output variance $(V(Y))$ is obtained when all parameters are perturbed. The interactive effects of the i^{th} parameter with all other parameters is given by the total-order SI (SI_{tot_i}) and is given as (Saltelli et al., 2008):

$$SI_{tot_i} = 1 - \frac{V_{x_i}[E_{x_i}(Y|x_{\sim i})]}{V(Y)}, \tag{4.5}$$

where the variance of the conditional expectation, when all parameters except the i^{th} are fixed, is expressed as $V_{x_i}[E_{x_i}(Y|x_{\sim i})]$. Sampling over the i^{th} parameter enables the calculation of this expectation. Estimating the Sobol' indices relies on finite samples from model simulations. A bootstrapping method has been employed to estimate sampling uncertainties in the index values. The bootstrapping method provides the confidence interval (ranging from the 2.5^{th} to 97.5^{th} percentiles). If SI_{order_i} is nearly zero, the corresponding parameter's influence is considered negligible. However, even if the best estimate of SI is non-zero, and if its confidence interval includes zero, a parameter is deemed to be not robustly influential. In this study, the Sobol' low-discrepancy quasi-random technique was used to generate the initial matrices required for parameter perturbations. This technique enhances the sampling of the uncertainty space by utilizing low-discrepancy sequences.

The Sobol' analysis is computationally more intensive than the Morris method. While Morris employs sparse sampling of the high-dimensional parameter space, variance-based decomposition requires denser sampling. Increasing the number of parameters in the analysis necessitates more perturbation points for effective sampling. As a general guideline, calculating the first and total-order SIs requires a total of $N \times (k+2)$ evaluations, where N represents the number of perturbation points per parameter, and k denotes the number of parameters in the targeted set (Saltelli et al., 2008). For this study, a targeted set of 11 to 15 parameters with 512 perturbation points was used for the Sobol' analysis for each biome, resulting in 6,656 to 8,704 model evaluations depending on the biome-specific targeted parameters derived from the Morris elementary effects method. It is important to note that the Sobol' analysis was conducted only for the biome-specific targeted sets of 11-15 input parameters and not for the combined parameter pool of 30 parameters spanning all biomes.

An artifact of the estimator used (as detailed in the Appendix A.1.4) can result in Sobol' indices being negative or exceeding one. Furthermore, the confidence intervals might cross zero and/or one. There may also be instances where best estimate values of SI_{tot_i} are lower than SI_{1_i} suggesting an absence of robust interactions among the ith parameter and other parameters.

4.3 Results

4.3.1 Morris Elementary Effects Method

We find that over 80% of the parameters (more than 100 out of 124) have negligible influence across biomes, output variables, and the two statistical measures (projected 20-year means and projected change in 20-year means). Only a small subset, typically five to ten, have any influence on any given output variable for any biome location. The targeted set of parameters are inclusive of most processes. Notably, only fire-related parameters are found to be non-influential. The absence of fire-related parameters may be because the fire module within CLASSIC performs better for larger spatial scales that for a grid cell.

The top-ranked parameters from the Morris results were combined across all output variables and the two statistical measures. By doing so, we reduce the number of parameters used in Sobol' from 124 to 11-15 for each biome location. An analysis of the parameter with the highest κ value for each output variable and biome, along with the relative position of $vmax$ compared to the top-ranked parameter was conducted (not shown). This analysis revealed that $vmax$ is the parameter with the highest influence for a majority of the carbon variables for future 20-year mean (81 out of 91 variable-biome combinations) and projected change in 20-year means (70 out of 91 combinations). Across all cases, $vmax$ consistently ranks among the top five parameters.

In addition to $vmax$, a few parameters are consistently present across different biomes and output variables (e.g., the mean root distribution profile ($abar$), the maximum rooting depth ($mxrtdpth$), leaf lifespan ($lfespany$)). While these parameters reoccur for both the statistical measures, there are a few parameters that occur only for the projected means, but not for the projected change in 20-year means or vice-versa (e.g., kn). The Morris screening test has effectively reduced the dimensionality of the parameter space, making it more manageable for subsequent Sobol' analysis. The targeted sets of 11-15 parameters used in the Sobol' analysis dominate the uncertainty in any of the output variables. The following Subsection depicts the uncertainty of NBP due to the targeted parameters for each biome location.

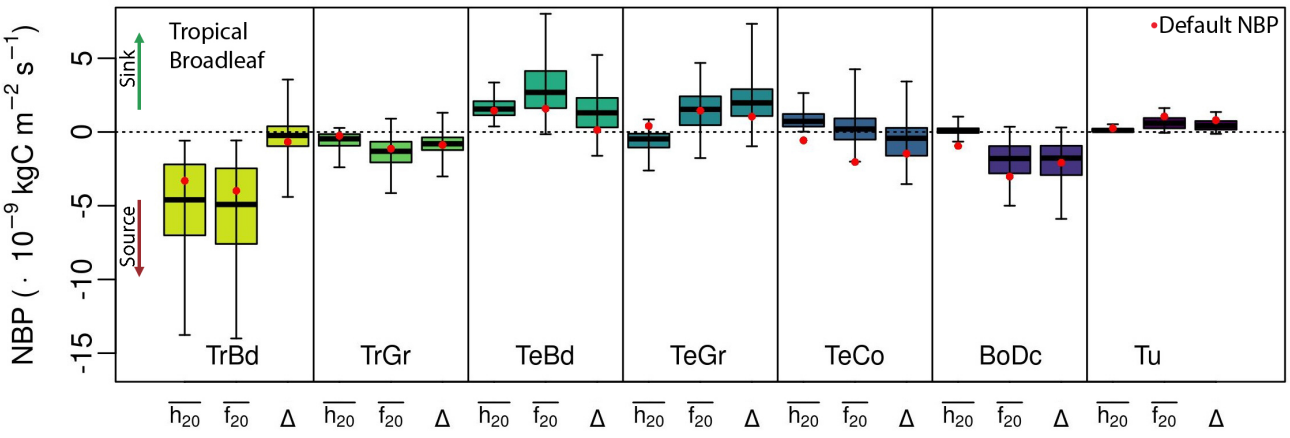

Figure 4.2: Uncertainty of NBP due to variations in targeted parameters for each biome location, for the historical means (1995-2014) ($\overline{h_{20}}$), projected means (2081-2100) ($\overline{f_{20}}$), and projected change in 20-year means (Δ). The whiskers enclose the 95^{th} percentiles, while the box encloses the interquartile range. NBP associated with the default parameters is denoted as the red dot.

4.3.2 Parametric Uncertainty of NBP

Figure 4.2 depicts the uncertainty of NBP for the 20-year historical means ($\overline{h_{20}}$), projected 20-year means ($\overline{f_{20}}$), and projected change in 20-year means (Δ) due to variations in targeted parameters for each biome location. Here, positive NBP values indicate sinks of atmospheric carbon, and negative values indicate sources of carbon. While some biomes remain either a sink (e.g., tropical broadleaf) or source (e.g., temperate broadleaf) regardless of the choice of parameters, other biomes switch signs (e.g., temperate grassland and boreal deciduous). This ambiguity arises because of strong parametric uncertainties of NBP. In most cases, the default NBP values (red dots) fall within the 95^{th} percentile values. Prominent changes in the median NBP are seen at the temperate broadleaf, temperate grassland and boreal deciduous locations, as we move from the recent past to the end of the 21^{st} century. The uncertainty ranges of NBP for the three situations are greatest at the tropical broadleaf location, and the least at the tundra location. The uncertainty at the tundra location does not account for the release of carbon through thawing of permafrost, as this process is not fully accounted for in the model version we have used. The uncertainty of the NBP values increases as we progress from the 20-year historical means to the projected 20-year means. This increase in uncertainty is because the system has a longer time to allow for the manifestation of the parameter uncertainties onto the

output variable. It is important to understand if there are specific parameters, or a parameter subset, which dominates the variance of the parametric uncertainty. Thus, a deeper investigation of parametric uncertainties is needed, and we use the Sobol' analysis to identify which parameters exert the greatest influence among all influential parameters.

4.3.3 Sobol' Analysis

Figure 4.3a displays the first-order sensitivity indices (SI_1) for the projected 20-year mean NBP for each parameter and biome. The displayed parameters represent a compilation of influential parameters identified by the Morris method across all biomes and output variables. While filled symbols denote indices with confidence intervals that do not overlap zero, open symbols represent indices where the confidence intervals do overlap zero. Only indices with confidence intervals clearly distinct from zero are regarded as robustly influential.

The influential parameters vary for different biome locations. Certain parameters are robustly influential at specific biome locations (e.g., upper temperature limit for photosynthesis (*tup*) at tropical grassland, *abar* at temperate broadleaf, and quantum efficiency (*alpha_phtsyn*) at tundra). In contrast, others show non-robust SI_1, as seen with the photosynthetic parameters *vmax*, canopy light extinction coefficient (*kn*), and *alpha_phtsyn* at the tropical broadleaf location, which exhibit broad confidence ranges extending beyond zero and one. Across all biome locations (excluding tropical broadleaf), parameters related to photosynthesis (e.g., *vmax*, *kn*, *alpha_phtsyn*) and rooting (e.g., *abar*) are the most recurrent influential parameters. Parameters related to phenology (e.g., *lfespany*) and autotrophic respiration (e.g., growth respiration coefficient, *grescoef*) are less recurrent, while all other parameters have negligible or no first-order influence. At the temperate grassland location, the presence of phenology parameters leaf-fall threshold temperature (*coldthrs*) and the required days of sub-threshold temperature to trigger leaf loss (*coldlmt*) indicate that the uncertainty of the carbon sink at this biome location is affected by cold temperatures. The individual effects of *vmax* are less than 25% for a majority of the biome locations, while that of *abar* for a few biome locations is greater than 25%, where the percentage values relate to the variances. The influential parameters grouped by the processes for the projected 20-year NBP mean are summarized in Table 4.3.

Interactive effects are seen for some of the parameters that have first-order

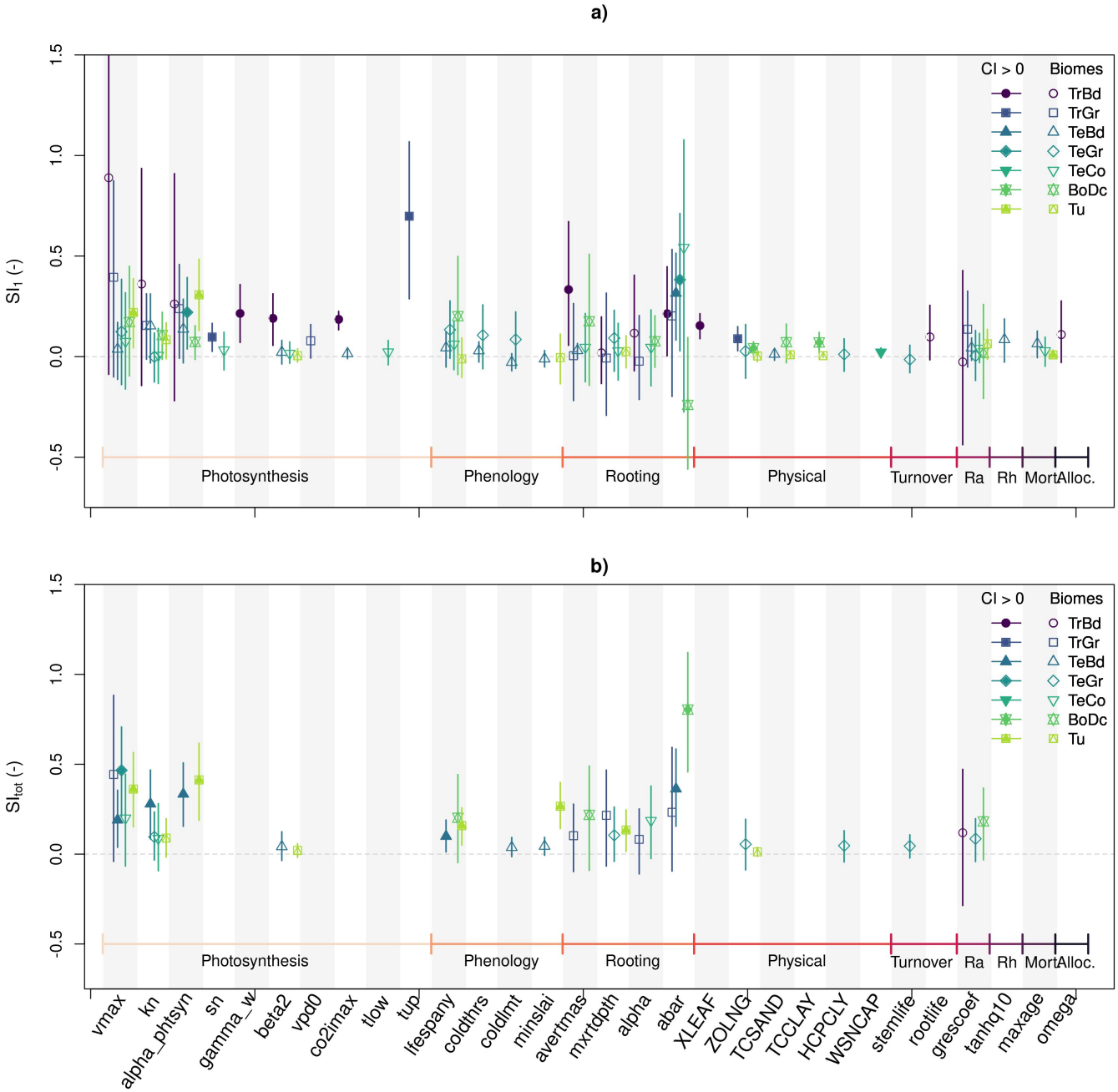

Figure 4.3: (a) First and (b) total-order SIs, and their confidence intervals for the top-ranked parameters across biomes (open symbols) for the projected 20-year mean NBP. Filled symbols represent robust SIs. Total order indices are plotted only where SI_{tot} greater than SI_1. The parameters are grouped according to the processes.

Table 4.3: The projected 20-year NBP mean's influential parameters grouped according to the processes, for each biome grid cell. The asterisk denotes parameters influential through robust interactive effects. Influential parameters for tropical broadleaf location are denoted as NA, as the confidence intervals are broad and overlap for various parameters.

Biome	**Photo-synthesis**	**Phenology**	**Rooting**	**Physical fluxes**	**Turnover**	**Auto-trophic respiration**	**Hetero-trophic respiration**	**Mort-ality**	**Alloc-ation**
TrBd	NA	-	NA	NA	NA	-	-	-	NA
TrGr	tup, $vmax$, $alpha\_phtsyn$, kn, sn, $vpd0$	-	$abar^*$, $mxrtdpth^*$, $avertmas^*$, $alpha^*$	$ZOLNG$	-	$grescoef$	-	-	-
TeBd	kn^*, $alpha\_phtsyn^*$, $vmax^*$	$lfespany^*$	$abar^*$	-	-	$grescoef$	$tanhq10$	$maxage$	-
TeGr	$vmax^*$, $alpha\_phtsyn$, kn	$lfespany$, $coldthrs$, $coldlmt$	$abar$, $mxrtdpth^*$, $avertmas^*$	-	-	$grescoef^*$	-	-	-
TeCo	$vmax^*$	-	$abar$, $alpha^*$	-	-	-	-	-	-
BoDc	$vmax$, $alpha\_phtsyn$, kn	$lfespany^*$	$abar^*$, $avertmas^*$	-	-	$grescoef$	-	-	-
Tu	$vmax^*$, $alpha\_phtsyn^*$, kn^*	$lfespany^*$ $minslai^*$	$mxrtdpth^*$	-	-	$grescoef$	-	-	-

influence, and for a few that do not have any first-order influence (Figure 4.3b). At the tropical broadleaf location, of all the parameters, only *grescoef* has an interactive effect. On the other hand, at the tundra location, multiple parameters from photosynthesis, phenology and rooting processes have interactive effects. The photosynthetic parameters have interactive effects at five locations for *vmax*, four locations for *kn*, and tropical broadleaf and tundra locations for *alpha_phtsyn*. The parameters that show robust interactive effects are denoted with an asterisk in Table 4.3. Although we have identified parameters with interactive effects, it is difficult to determine which two or more parameters interact. The interacting parameters could be shown by second- or third-order indices, but the computational cost of required for calculating these is too high.

Figure 4.3a indicates that *vmax* is among the five most influential parameters for four out of seven biome locations. To further explore this influence, we present the relationship between the projected 20-year NBP mean and *vmax* across the biome locations, with all parameters in the targeted set varied within their respective uncertainty ranges (Figure 4.4). The shaded hexagons in the figure show the conditional distribution of NBP values for different *vmax* values, where darker shades indicate regions with a higher density of model simulations. The solid magenta line represents the conditional expectation of NBP as a function of *vmax*, providing insight into the overall trend and strength of their relationship. The extent to which the conditional expectation changes with *vmax* corresponds to the conditional variance of NBP, as quantified by SI_1 in Figure 4.3a. The spread of hexagons around the conditional expectation reflects the uncertainty of NBP caused by the simultaneous variation of other parameters in the targeted set for given *vmax* values. The blue lines mark the 25^{th} and 75^{th} percentile curves of the conditional distribution. Some extreme NBP values may arise due to particular parameter combinations, as indicated by the faintest shaded hexagons. This conditional spread helps understand the sampling variability through bootstrapping, which is reflected in the confidence intervals of Figure 4.3a. Longer tails of the conditional distribution result in broader confidence intervals. The red arrows in the figure correspond to the default 20-year mean NBP values obtained when no input parameters are perturbed (red dots in Figure 4.2). The horizontal axis denotes scaled *vmax*, which corresponds to a different range of dimensional values of this parameter for each PFT.

The response of the projected 20-year NBP mean to variations in *vmax* exhibits distinct biome-specific patterns (Figure 4.4). Biomes such as tropical broadleaf, trop-

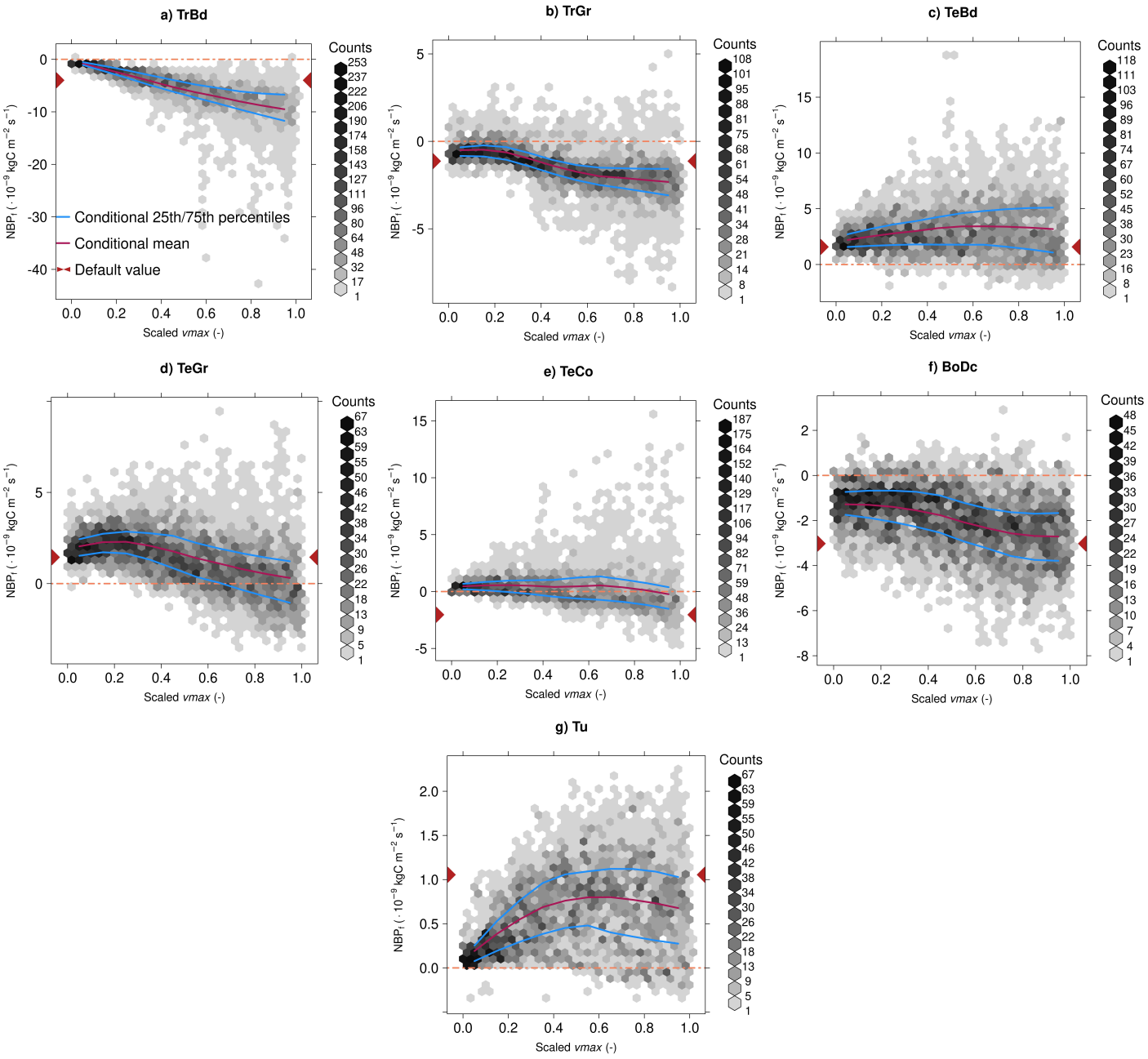

Figure 4.4: Conditional distributional of projected 20-year NBP mean for all biomes, for changes in $vmax$, along with the conditional mean (magenta coloured line), and conditional 25^{th} and 75^{th} percentile curves (blue lines).

ical grassland, and boreal deciduous predominantly act as carbon sources across the uncertainty range of $vmax$, whereas temperate broadleaf, temperate grassland, temperate conifer, and tundra act as carbon sinks. Among all biome locations, tropical broadleaf is the only location close to being consistently a source. Both sources and sinks are simulated at all other locations.

The conditional expectation of NBP differs among biome locations. For all the three temperate locations, there are very small changes to the conditional expectation of NBP for larger values of $vmax$. The conditional expectation follows a sigmoidal curve for the tropical grassland, temperate grassland and boreal deciduous locations, and becomes increasingly negative for the tropical broadleaf location. The strongest variance of the conditional expectation occurs at the tropical broadleaf location. The associated conditional spread is broad at this location, and can be seen as a broad confidence interval in Figure 4.3a. On the other hand, at the temperate broadleaf location, even though the variance of the conditional expectation is the least among all biome locations, the conditional spread is the narrowest, denoting the smallest SI_1 value and narrowest confidence interval range in Figure 4.3.

At the tropical broadleaf, tropical grassland, temperate grassland, and boreal deciduous locations, NBP decreases for larger values of $vmax$. To investigate this further, we assess the gross primary productivity (GPP; 10^{-8} kgC m^{-2} s^{-1}), autotrophic respiration (Ra; 10^{-8} kgC m^{-2} s^{-1}), heterotrophic respiration (Rh; 10^{-8} kgC m^{-2} s^{-1}), and CO_2 emissions due to forest fire ($fFire$; 10^{-9} kgC m^{-2} s^{-1}) for an example biome location, the tropical broadleaf (Figure 4.5). We notice that the four fluxes increase for larger $vmax$ values. As GPP increases, the amount of biomass in the location increases. This increase in biomass increases the autotrophic respiration rate through the live components (e.g., stem, root and leaves) and heterotrophic respiration rate through the dead components (e.g., bark, litter). The indirect effects of less precipitation (Figure A.2a), high temperature (Figure A.2b), and the availability of fuel in terms of biomass, are felt by the fire module, thereby increasing $fFire$ as well. From these four components, we observe that the conditional mean's value of the projected 20-year NBP mean value e.g., at the 0.1^{th} quantile of $vmax$'s uncertainty ranges is -1.35 $\times$ 10^{-9} kgC m^{-2} s^{-1} and -9.104 $\times$ 10^{-9} kgC m^{-2} s^{-1} for the 0.9^{th} quantile of $vmax$'s uncertainty ranges. The reduction in NBP for bigger $vmax$ values is due to a higher release of CO_2 into the atmosphere through ecosystem respiration and wildfires. A similar comparison for the historical NBP and its components when the CLASSIC model is forced with reanalysis and with CanESM5 data is provided

in Appendix A.2.1. From Figures 4.3a and 4.4 it is clear that *vmax*'s influence is lesser for the projected 20-year mean NBP. Other parameters for example, *tup* for the tropical grassland, *abar* for temperate broadleaf and *alpha_phtsyn* for the tundra locations have strong individual influence (Figure 4.3a). Figure 4.6 shows the conditional distribution for these most influential parameters for individual biomes. When comparing Figure 4.6 with Figure 4.4, there is a clear dependence of the conditional expectation on the parameter value. Although the dependence of the conditional expectations for *vmax* and *tup* look like they are of the same magnitude, the variance is larger for *tup*. This feature is seen as bigger $SI_{1_{tup}}$ for the tropical grassland location in Figure 4.3a. The conditional spread is also relatively narrow for *tup*, as shown by a comparatively less broad confidence interval in Figure 4.3a.

The first and total-order SI and confidence intervals for the difference between the projected 20-year (2081-2100) mean NBP and 20-year historical (1995-2014) mean NBP are presented in Figure 4.7 for each parameter/biome. The best estimates of the SI values of the projected change in 20-year means are similar to those of the projected 20-year means (Figure 4.3) for all biome locations except the tropical broadleaf location for both the first and total orders. This similarity implies that the influential parameters for the two statistical measures do not differ much (described further in the Discussion and Conclusions section). The overlap in broad confidence intervals of SI_1 is the greatest at the tropical grassland location across all parameters. Robust ranking of the parameters cannot be assigned due to the overlap.

Additionally, the confidence intervals of SI_1 for the mean root distribution profile (*abar*) are broader across all biome locations for the projected change in the 20-year NBP mean, indicating that this rooting parameter is highly non-robust for this statistical measure. The only major difference in total-order SI (Figure 4.7b) is that *abar*'s interactive influence reduces at the tundra location. The conditional distribution of the projected change in 20-year means to changes in *vmax* (not shown) indicates a similar story. There are no substantial differences between the conditional distributions of the projected 20-year NBP mean and the projected change in 20-year means. Table 4.4 provides a summary of the influential parameters for the projected change in 20-year means for all biome locations except the tropical broadleaf due to broad overlapping confidence intervals. We can see modest differences in the influential parameters from those in Table 4.3.

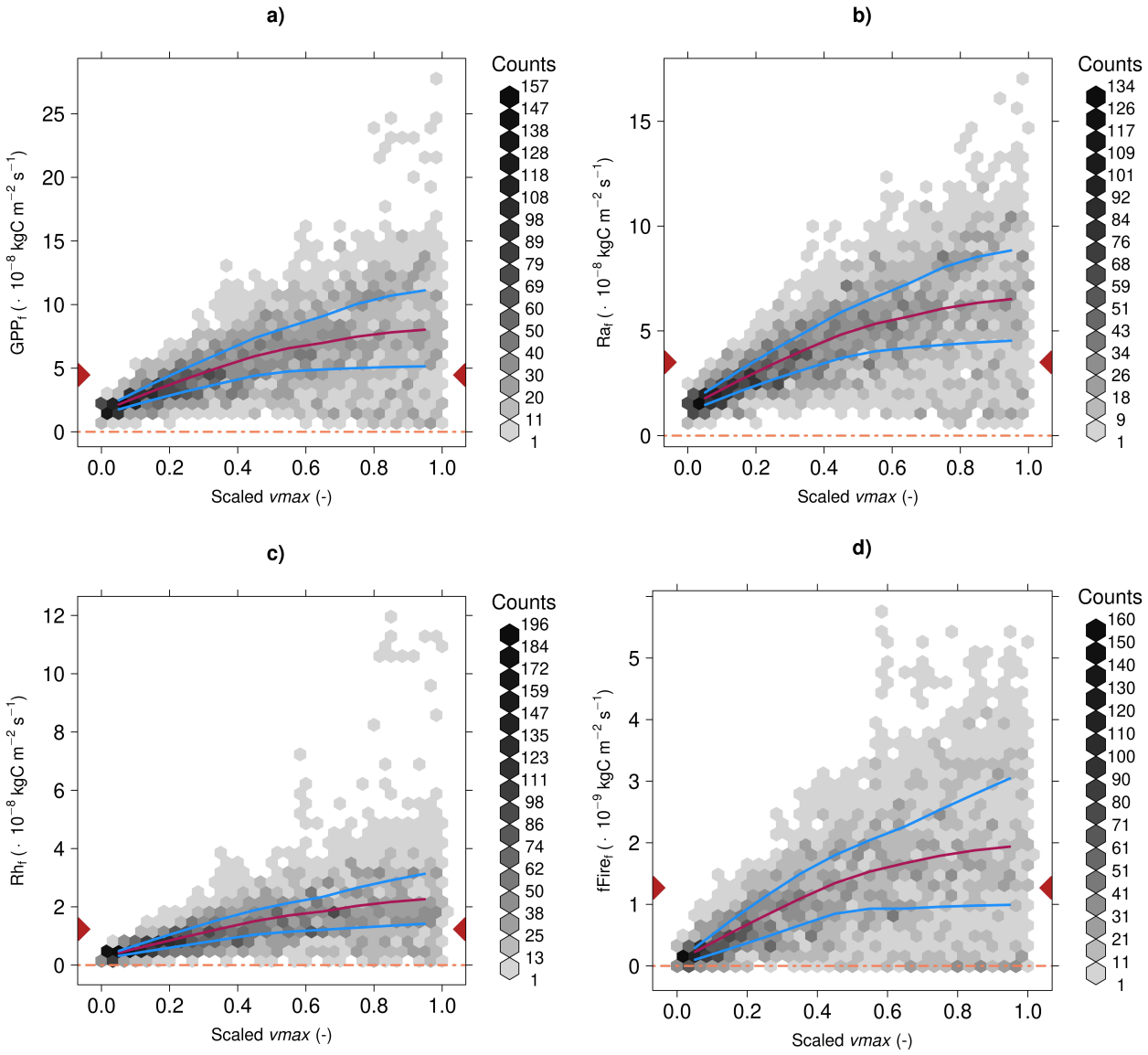

Figure 4.5: Similar to Figure 4.4, but for the four components of NBP (a) GPP (10^{-8} kgC m^{-2} s^{-1}), (b) Ra (10^{-8} kgC m^{-2} s^{-1}), (c) Rh (10^{-8} kgC m^{-2} s^{-1}), and (d) $fFire$ (10^{-9} kgC m^{-2} s^{-1}) , simulated at the tropical broadleaf location.

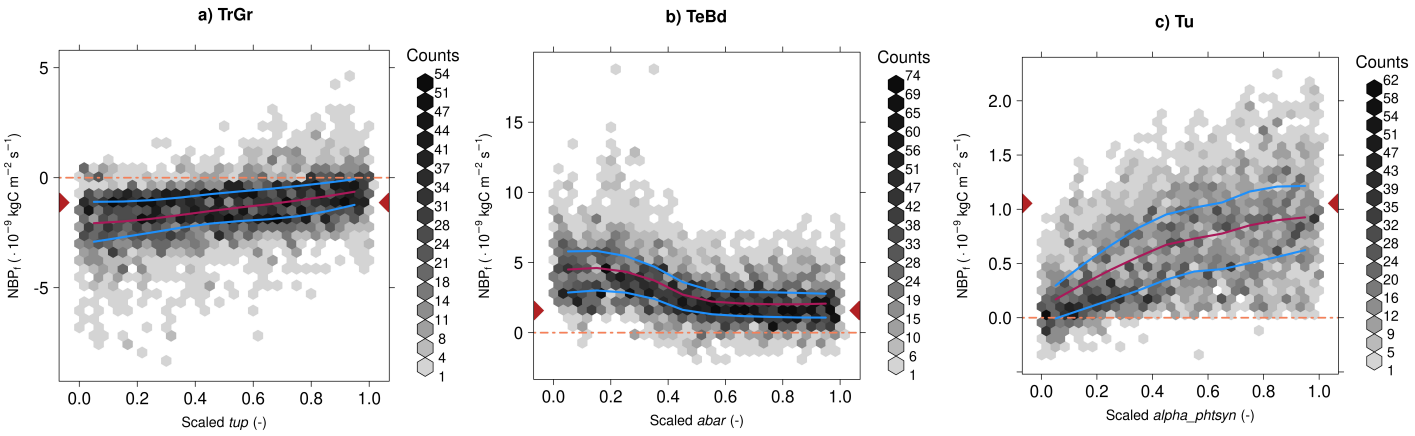

Figure 4.6: Similar to Figure 4.4, but for the changes in most influential parameters for three biome locations (a) tropical grassland; *tup*, (b) temperate broadleaf; *abar*, and (c) tundra; *alpha_phtsyn*. Multiple parameter values are used for each biome location. PFT-specific parameter values are scaled to (0,1) for representation purposes.

4.4 Discussion and Conclusions

In this study, we address the extent to which parameter uncertainties influence the future carbon sink projections in terrestrial biosphere models, in the context of the CLASSIC model. Additionally, we compare parameters driving the uncertainties of the projected change in means of the carbon sink from the historical to future periods. The projected change in carbon sink shows substantial parametric uncertainty across individual grid cells for seven different biomes (e.g., default value of -2 μgC m^{-2} s^{-1} for the projected change in 20-year NBP mean with uncertainties ranging from -6 to 0 μgC m^{-2} s^{-1} at the boreal deciduous location). One way to reduce uncertainties in the carbon sink is by tuning the influential parameters, which can be identified by GSA as shown in our study.

The Morris screening results for the projected 20-year mean NBP and the projected change in 20-year means closely resemble those from Chapter 3. In the previous study, the CLASSIC model was driven by reanalysis data (CRUJRAv2; Harris, 2019; Kobayashi et al., 2015) and used the 30-year historical NBP mean and trend as statistical measures for the GSA. While the targeted parameters used in Sobol' for each biome location differs slightly between the previous and present studies, the total number of parameters within the targeted-set across all biomes is comparable

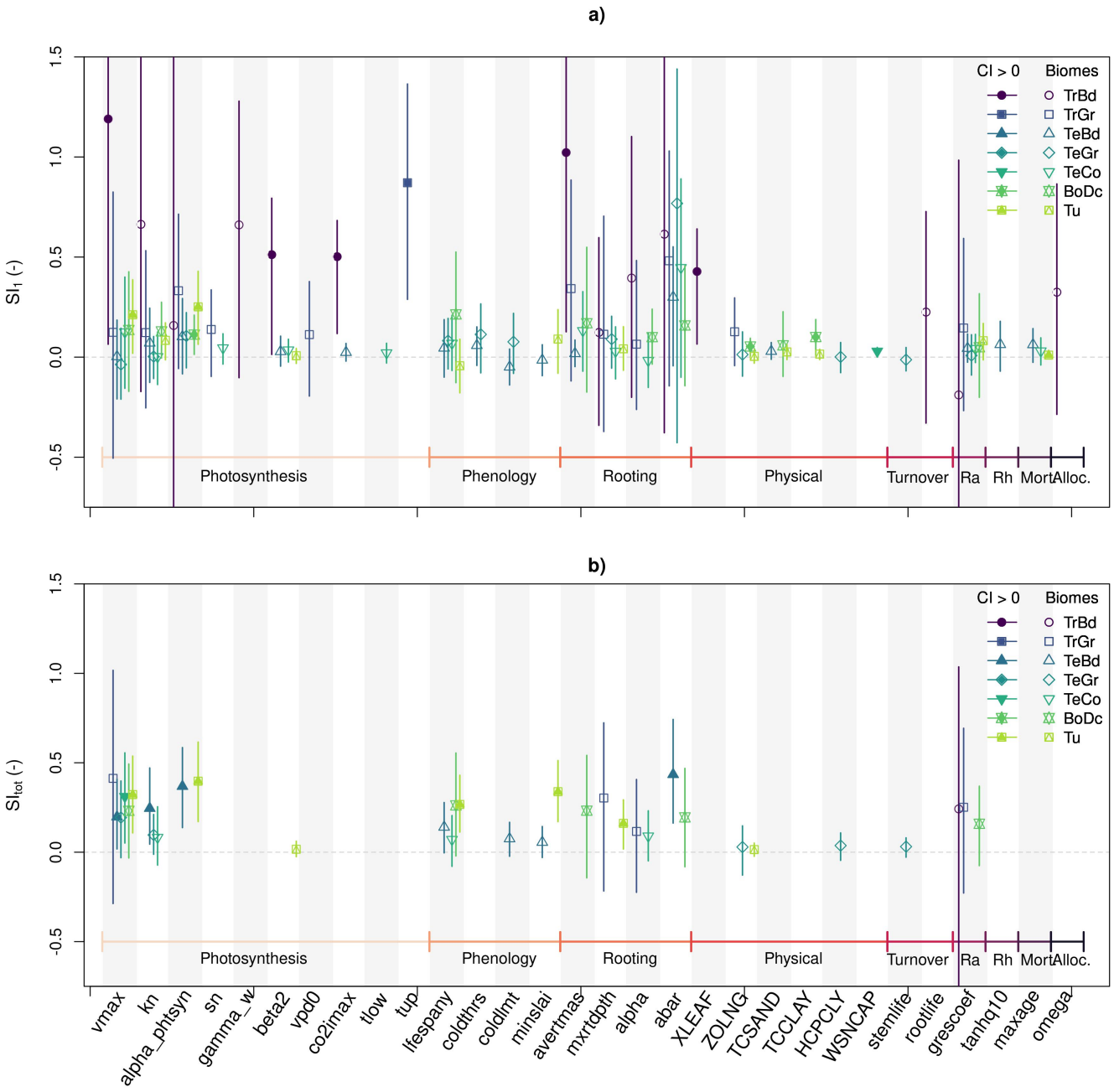

Figure 4.7: (a) First and (b) total-order SIs, and their confidence intervals for the top-ranked parameters across biomes (open symbols) for the projected change in 20-year means. Filled symbols represent robust SIs. Total order indices are plotted only where SI_{tot} greater than SI_1. The parameters are grouped according to the processes.

Table 4.4: The influential parameters grouped according to the processes, for the projected change in 20-year means, for each biome grid cell. The asterisk denotes parameters influential through robust interactive effects. Influential parameters for tropical broadleaf location are denoted as NA, as the confidence intervals are broad and overlap for various parameters.

Biome	**Photosynthesis**	**Phenology**	**Rooting**	**Physical fluxes**	**Turnover**	**Autotrophic respiration**	**Heterotrophic respiration**	**Mortality**	**Allocation**
TrBd	NA	-	NA	NA	NA	NA	-	-	NA
TrGr	$vmax^*$, $alpha\_phtsyn$, kn, $vpd0$, tup, sn^*	-	$abar$, $mxrtdpth^*$, $avertmas^*$, $alpha$	$ZOLNG$	-	$grescoef$	-	-	-
TeBd	$vmax^*$, kn^*, $alpha\_phtsyn^*$, $beta2^*$	$coldthrs^*$	$abar$, $avertmas^*$	-	-	-	$tanhq10$	$maxage$	-
TeGr	$alpha\_phtsyn$, kn^*	$lfespany$, $coldthrs$, $coldlmt^*$	$abar$, $mxrtdpth$	-	-	-	-	-	-
TeCo	$vmax$, $tlow^*$, sn^*	$lfespany$	$abar$, $avertmas$, $alpha^*$	-	-	-	-	$maxage$	-
BoDc	$vmax^*$, $alpha\_phtsyn$, kn	$lfespany^*$	$abar^*$, $avertmas$, $alpha$	$TCCLAY^*$, $TCSAND$ $ZOLNG$	-	$grescoef^*$	-	-	-
Tu	$vmax^*$, $alpha\_phtsyn^*$, kn^*	$lfespany^*$, $minslai$	-	$ZOLNG^*$	-	$grescoef$	-	-	-

(30 in the present study vs. 29 previously). Parameters related to the processes heterotrophic respiration and turnover were not influential through either of the two-steps in GSA in the previous study, but are influential in the present study due to the driving climate at the specific grid cells.

Photosynthetic and rooting parameters identified as influential in the earlier study through the Sobol' analysis remain influential for both the future projections and projected changes in 20-year means. However, certain parameters such as the exponential parameter for allometric scaling of green leaf biomass ($kappa$) and the percentage of maximum leaf area index that can be supported ($thrprcnt$), the near infra-red albedo ($albnir$) and natural logarithm of roughness length of snow ($ZOLNS$), and the minimum live wood fraction ($minlvfr$) lose their influence when simulations are forced by CanESM5 instead of CRUJRAv2. In the present study, new influential parameters emerge for the projected conditions, including the photosynthetic parameters maximum intercellular [CO_2] ($co2imax$) and tup, the parameter which consists of the constants used in the hyperbolic tangent ($tanh$) formulation of heterotrophic respiration determination function ($tanhq10$), and the turnover timescale for root ($rootlife$). A majority of the parameters mentioned in this paragraph that were not included in the targeted set for Sobol' in the corresponding study, have very small Euclidean distances (κ). These small κ valued parameters do not appear within the top 15 parameters for individual output variables, and are unlikely to appear as a result of sampling variability.

In Chapter 3 we observed that temperature-related parameters influencing heat-induced mortality and heterotrophic respiration, such as tup and those within $tanhq10$, were non-influential for the historical carbon sink across all biome locations. However, in the present study, which examines the future carbon sink, both tup and $tanhq10$ emerge as influential based on the Sobol' results. Specifically, tup is influential for the gross primary productivity at the tropical grassland biome (not shown) and strongly influences the uncertainty in NBP. Similarly, $tanhq10$ is influential for the litter carbon pool at the temperate broadleaf location (not shown). These results show that the uncertainties in these parameters are important from the point of view of the overall parametric uncertainty. The parameter $tanhq10$'s influence is less than 20% of the whole variance for the two statistical measures, while that of tup is greater than 50%, although with a broad confidence interval.

The subset of the highest-ranked influential parameters identified using the Sobol' analysis remains consistent for both the projected 20-year NBP mean and the pro-

jected change in 20-year means. This consistency could be a consequence of the variance of the projected values resulting from parameter variations being substantially larger than the historical values. Or in other words, the variations in the projected change are being driven by variations in the projected 20-year NBP mean with little influence from variations in the 20-year historical means. This finding indicates that the sensitivity of the late historical mean may not be relevant if we are interested in the sensitivity of the mean NBP at the end of the century. The selection of an appropriate measure should be chosen by the specific research question being addressed, as different measures may capture distinct aspects of variability in the output variable as shown in Chapter 3. The consistency in the subset of highest-ranked influential parameters varies if a different future time period, rather than when 2081-2100 is used (as noted below). It may also vary if a different SSP scenario is used (experiments not conducted). We noticed that the inter-decadal variability in the evolution of NBP for the SSP5-8.5 scenario was high at each biome location (Figure A.6). In these time series evolutions, the NBP values switched signs, even for the default state where no parameters were perturbed. A comparison of SI values of the projected changes in 20-year NBP means for the late historical (1995-2014) and early future (2015-2034) time periods are provided in the Appendix . The Zenodo link provided in Section A.4 contains a comparison of SI values (Similar to Figure 4.3) for projected 10- and 20-year NBP means of different time periods. Interested readers are suggested to have a look at the figures in the Zenodo repository.

We find that the sensitivity of NBP to most influential parameters varies between the historical period (not shown) and the future period. Notably, the influence of certain parameters, such as the $vmax$, is projected to decrease from the recent past to the late 21st century. The best estimate values of the total-order effect of $vmax$ ($SI_{tot_{vmax}}$) that accounts for both individual and interactive effects, exceeded 50% for historical NBP across most biome locations. However, this influence was comparatively lower for the projected 20-year NBP mean, as shown in Section 4.3.3 . This decline in $vmax$'s influence aligns with findings from Canadell et al. (2023), which show that the terrestrial biosphere's capacity to absorb anthropogenic CO_2 emissions is expected to weaken over time in the future. The reduction in sensitivity of NBP to $vmax$ indicates that as atmospheric [CO_2] rises, the carbon cycle processes become increasingly constrained by factors other than the photosynthetic capacity (e.g., rooting processes). This change in influential processes has implications for future land carbon sink projections, leading to a reduced ability of terrestrial ecosystems to miti-

gate rising atmospheric [CO_2]. The study by Seiler et al. (2024) separates the effects of rising [CO_2] from those of climate change, showing that increasing temperatures reduce NBP while elevated [CO_2] counteracts this decline. The identification of *tup* as an influential parameter in our study supports their conclusion that temperature is one of the key influences on the changes in the terrestrial carbon balance. However, since *tup* is influential only at the tropical broadleaf location, processes such as rooting, represented by the mean rooting profile (*abar*), plays a more dominant role in influencing NBP at the other biome locations. At these locations, the land and soil carbon pools are the most sensitive to uncertainties in *abar* (not shown), implying that the respiration through deep-rooted vegetation eventually affects NBP and its uncertainty.

The parameter *vmax* turns out not to be particularly influential for many biome locations for the projected NBP mean or the projected changes in NBP through the first-order Sobol' effects. Many previous studies where the land surface model was forced using available observational meteorological data instead of reanalysis or model output data have identified *vmax* to be among the most influential parameters for various carbon cycle variables (J. Li et al., 2016; Ma et al., 2020; Rodriguez & Espíndola, 2024; Xing et al., 2023; Zhu & Zhuang, 2014). These studies have also performed model optimization related to the components of NBP by tuning *vmax* as one of the parameters. Due to its reducing influence over time, when performing tuning experiments for the projected carbon sink, *vmax* should be used with multiple parameters. Our results support previous finding that tuning cannot rely on *vmax* alone, irrespective of the output variable considered.

A further analysis similar to Figure 4.5 was performed for the historical NBP (Supplemental document). The components of NBP, when the CLASSIC model is simulated with reanalysis data (Chapter 3) and with CanESM5 data, were compared. From this analysis, we find that the same location (e.g., tropical broadleaf) acts as a source or sink of carbon depending on the forcing used. The finding indicates that the uncertainty of the carbon sink is also influenced by uncertainty in the forcing, beyond parameter or model uncertainty. Thus, the uncertainty in NBP cannot be addressed solely through tuning the influential parameters.

We varied all parameters proportionally among the PFTs. By doing so, we have reduced the number of parameters by a factor of nine. By not including the nitrogen and methane cycles, or the state variables for moss and peat, we have reduced the total number of input parameters to 124. Additionally, by not including the nitrogen cycle,

we have also reduced the spin-up time from many thousand years (Seiler et al., 2024) to 500 years for each run. Excluding the conditions mentioned, the computational expense for the GSA study still required around 120,000 CPU hours or approximately 15 CPU years to simulate the Morris and Sobol' runs for just seven grid cells. Even after using 15 CPU years, the confidence intervals are broad for the sensitivity of NBP to the influential parameters. Performing global runs with the whole model will be computationally prohibitive owing to the number of terrestrial grid cells that have to be considered, and is likely out of scope for any study for the foreseeable future.

Though the computational expense will be substantial, identifying the influential parameters for the projected global terrestrial carbon sink will be useful for refining the terrestrial biosphere model(s). We encourage future studies to use emulators for the terrestrial biosphere model(s) instead of using the whole model within the GSA. Emulators are less complex and have comparatively lesser computational demand, as they are statistical proxies of the model. These proxy models have been successfully used in previous GSA and optimization studies for small-scale studies (Baker et al., 2022; Gao, Avramov, Saikawa, & Schlosser, 2021; McNeall et al., 2023, 2020; Petropoulos et al., 2014).

This current study presents the first GSA of projected future carbon cycle variables simulated by a terrestrial biosphere model, the CLASSIC model. The GSA is an essential step for model parameter calibration, and our findings show that only a small subset of input parameters (11-15) influence the projected future 20-year means and projected changes in 20-year means of output variables. The Morris elementary effects method consistently identified the maximum carboxylation rate ($vmax$) among the top five parameters across different biome locations, output variables, and the two statistical measures considered. The Sobol' analysis revealed that not all parameters obtained through Morris remain influential. We notice that $vmax$'s influence on the uncertainty of NBP reduces, and that of the mean rooting profile ($abar$) increases by the end of the 21^{st} century. Additionally, even after substantial computational usage of approximately 15 CPU years, robust ranking of the influential parameters is difficult due to overlapping confidence intervals. Given these results, future model optimization efforts should use multiple parameters including $vmax$ to reduce the uncertainty in projected carbon sinks. The subset of influential parameters obtained through the GSA depends on the statistical measure used (e.g., mean vs. trends as shown in Chapter 3), but we notice that the influence of parameters do not vary much between the projected mean and the projected change in 20-year means in the

present study. This similarity is likely driven by the substantially larger variance in the future period resulting from parameter variations compared to the historical period. By identifying the influential parameters that affect the projected carbon sink's uncertainty, we help improve the terrestrial biosphere models used for simulating the future land carbon sink.

A compilation of the results from the three main chapters, and research outlook are provided in the upcoming chapter.

Chapter 5

Conclusions

Some of the uncertainties in Land surface models (LSM) are due to uncertainty in input parameters. These uncertainties can propagate through the model and influence the simulated outputs. In this research, I have systematically quantified these parametric uncertainties using a two-step global sensitivity analysis (GSA) approach. By applying this approach within the context of CLASSIC, I identified the most influential parameters and/or processes that drive the variability in carbon cycle and energy flux variables across different biomes and climate scenarios. The following paragraphs summarize the important findings and implications of this research.

5.1 Research Questions

The main research questions posed in this work were:

1. Is there a common set of parameters that substantially influence the majority of ecosystem output variables simulated at an eddy covariance site?

2. Which parameters substantially affect the uncertainty of the historical carbon sink for different biomes?

3. Which parameters substantially affect the uncertainty of future carbon sink projections for different biomes?

General Findings

The preliminary qualitative Morris screening test revealed that only about 15–17% of the input parameters had any influence for any given setting. The number of influen-

tial parameters identified through the subsequent quantitative variance-decomposition based Sobol' method varied across the different chapters, as briefed in the following subsections.

Question 1

In Chapter 2, CLASSIC was forced using available meteorological observations at a tropical broadleaf eddy covariance site. GSA was performed for the 11-year means for a broad range of output variables. Only two parameters were found to be influential. The two parameters were the maximum carboxylation rate ($vmax$) and canopy extinction coefficient (kn). These two parameters were influential for not just gross primary productivity (GPP), but for a wide range of output variables ranging from carbon and water cycle variables to turbulent and radiative heat fluxes. The influential parameter subset was very small and as mentioned, had only two parameters, and it was found that $vmax$ and kn were the only parameters to have robust interactive effects. By combining and studying the conditional influences of $vmax$ and kn on GPP, it was noted that GPP reduces for fixed values of $vmax$, and bigger values of kn.

Question 2

In Chapter 3, CLASSIC was forced using reanalysis data. The GSA was performed for two statistical measures namely, the 30-year mean and 30-year trend. The numbers of influential parameters identified through the Morris and Sobol' methods were close for the historical carbon sink. The ranking of parameters through the Sobol' method was not possible because of the sampling uncertainty in terms of the overlapping confidence intervals for multiple parameters. The large sampling uncertainties for the 30-year NBP mean and 30-year NBP trend were noticed even after substantial computational effort.

By grouping parameters based on their associated processes, it was observed that photosynthesis, rooting, and phenology-related parameters were consistently influential for the historical carbon sink. While the parameters related to physical fluxes, mortality, and allocation were rarely influential. Those parameters related to heterotrophic respiration, fire, and turnover exhibited no influence across biome locations.

The interactive effects were not robustly greater than the individual effect for multiple parameters. Conversely, many past GSA studies have observed both individual and interactive effects among influential parameters in (e.g., Y. Li et al., 2022; Ma et al., 2020; Pappas et al., 2013; Zhu & Zhuang, 2014). Robust interactive effects of a few parameters were evident in Chapter 3, for example, as denoted by *vmax*'s total order effects at five of seven biome locations. The presence of multiple influential parameters complicated the identification of interactions among them, unlike in Chapter 2.

The highly influential parameters identified using the Sobol' method were consistent across both statistical measures. In contrast, parameters with lower Euclidean distance values in the Morris method, but used in the Sobol' method varied between the two measures. The relative influence of each parameter within the targeted parameter set also differed depending on the statistical measure used. To ensure effective model tuning, the selection of influential parameters through GSA should align with the specific optimization problem.

Question 3

In Chapter 4, CLASSIC was forced with bias-adjusted CanESM5 data. GSA was performed for two statistical measures, the projected 20-year means, and the difference between the projected 20-year mean and the historical 20-year mean. Results from this chapter indicate that the influential parameters governing the projected mean carbon sink were more easily identifiable than those for the historical mean carbon sink in Chapter 3, except at the tropical broadleaf site. The future period allows more time for the parameter uncertainties to manifest themselves on the output variable, making it easier to assess the impact of parameter uncertainty on the uncertainty of the output variable.

The influential parameters for the changes in projected 20-year mean values can be identified, though less easily than the projected 20-year mean. The Sobol' method showed similar results for the influential parameters obtained for the two statistical measures. Though not as broad as in Chapter 3, large sampling uncertainties were still seen for the two statistical measures with respect to NBP. The uncertainties were seen despite extensive computational efforts. The broad and overlapping uncertainties made it difficult to robustly rank the parameters through the Sobol' method for the sensitivity of the carbon sink. Parameters related to all processes except fire, were

influential to some extent.

The influence of *vmax* on the projected carbon sink diminishes toward the end of the 21st century. Instead, other parameters, such as the upper photosynthetic threshold temperature (*tup*) at the tropical grassland, the mean root distribution profile (*abar*) at temperate broadleaf, temperate grassland, temperate conifer and boreal deciduous biomes locations, and the quantum efficiency parameter (*alpha_phtsyn*) at tundra, become more influential than *vmax*.

The projected 20-year NBP mean values decrease with higher *vmax* values at certain biome locations, an outcome that is counterintuitive. This outcome happens in the context of increasing temperature under SSP5-8.5, and was explained by increased biomass, which not only absorbs atmospheric CO_2, but also enhances CO_2 release through environmental respiration. The increased biomass provides more fuel for wildfires, thereby adding to the CO_2 release into the atmosphere.

5.2 Research Outlook

The choice of statistical measure should align with the research question. If the objective is to optimize the model's trends, the statistical measure used in the GSA should correspond to trend-based assessments, as influential parameters vary across different statistical approaches (e.g., those used in Chapter 3). Using statistical measures that do not pair with the research objective in GSA and optimization problems may yield less robust results. Conversely, if the research question focuses on optimizing differences between the late historical and late future periods' carbon sink values (as in Chapter 4), it is appropriate to use the influential parameters identified from projected future means.

The results from the GSA study of the terrestrial carbon sink indicate that the influence of *vmax* is reducing over time, and rooting processes are becoming more important. When tuning parameters for the carbon sink, multiple parameters including *vmax* should be used, instead of solely relying on the effects of *vmax*. Simulating a highly process-based, complex LSM like CLASSIC is computationally expensive. For example, the GSA simulations in this study ran for approximately 25 CPU years using 120 processors for just seven grid cells. Scaling such analyses to a global scale or across multiple forcing datasets would require vastly more computational resources, making brute-force approaches infeasible. Optimizing for a particular region may produce worse results elsewhere, and has to be performed for numerous regions globally.

But, computational demand to run the full model on a global scale is impractical.

To overcome these limitations, future GSA and optimization efforts could use Machine Learning (ML)-driven surrogate models. Surrogate models trained on a subset of full-model simulations can rapidly approximate the response of the LSM to parameter perturbations, drastically reducing computational costs (Baker et al., 2022; McNeall et al., 2023, 2020; Petropoulos et al., 2014). Machine learning algorithms could also be used to identify non-linear parameter interactions, to refine parameter uncertainty estimates, and improve optimization efficiency.

Additionally, ML techniques such as reinforcement learning and Bayesian optimization could streamline parameter tuning by iteratively selecting the most informative parameter sets to evaluate, rather than relying on exhaustive sampling. By reducing the dimensionality of the optimization space through GSA and integrating ML-driven surrogate models, future studies can improve computational efficiency and enhance the predictive accuracy of terrestrial carbon sink projections.

5.3 Concluding remarks

By identifying the most influential parameters and the associated processes driving terrestrial carbon cycle variables, this research serves as a foundation for a deeper understanding of CLASSIC and paves the way for better model optimization efforts. Reducing uncertainty in simulated terrestrial carbon fluxes, particularly the carbon sink, is critical for improving the accuracy of assessments such as the Global Carbon Budget (Friedlingstein et al., 2024) and future projections by the Intergovernmental Panel on Climate Change (Canadell et al., 2023). These improvements can, in turn, support more informed climate mitigation strategies.

As the first GSA conducted using CLASSIC, I am sure this work will contribute to the development of more robust terrestrial carbon cycle variables, strengthen future climate projections, and ultimately aid in shaping policies for a more sustainable future.

Appendix A

Appendix

This Appendix contains five sections. The first section comprises of supplemental equations common to all chapters, namely: the equations within the CLASSIC model, dependency conversion using spherical coordinate system, detailed description of the Morris and Sobol' methods, and an example calculation for the Sobol' method. The second section contains supplemental material and figures for Chapter 4. The third section consists of the common tables used through this research work, such as the exact locations of the grid cells used in Chapters 3 and 4 (Table A.1) and input parameters used in the CLASSIC model for all three chapters (Table A.2). The Code and Data Availability is provided in the fourth section. This section contains the repositories where the source code, input data, output data, and figures produced during this dissertation work have been stored. The last section provides a breakdown of the computational demand required for each main chapter.

A.1 Supplemental Equations: Common for All Chapters

A.1.1 Gross Primary Productivity Calculation

The photosynthesis module of the CLASSIC model simulates the gross leaf photosynthesis rate (G_o; mol CO_2 m^{-2} s^{-1}). A few input parameters used in this module are described briefly, as their importance will be analyzed in the main manuscript.

These parameters affect the CO_2 assimilation limited by Rubisco (J_c), light (J_e) and transport capacity (J_s) values simulated by the model. Since our site is an evergreen broadleaf forest, the photosynthetic rates limited by each quantity are described only for C_3 plants. The light-limited CO_2 assimilation rate, J_e (mol CO_2 m^{-2} s^{-1}), given by Melton and Arora (2016) is:

$$J_e = \varepsilon(1-\nu)I\left[\frac{c_i-\Gamma}{c_i+2\Gamma}\right], \tag{A.1}$$

where ν is the leaf scattering coefficient (*omega_phtysn* in Table A.2), I is the incident photosynthetically active radiation (PAR; mol photons m^{-2} s^{-1}), c_i is the leaf interior partial pressure of CO_2 (Pa) and Γ is the compensation point of CO_2 (Pa). The quantum efficiency ε (mol CO_2 (mol photons)$^{-1}$; *alpha_phtsyn* in Table A.2) is defined as the initial slope of the relationship between CO_2 assimilation and irradiance (Farquhar et al., 1980):

$$\varepsilon = \frac{\text{mol of } CO_2 \text{ assimilated}}{\text{mol of photons absorbed}}.$$

The Rubisco-limited assimilation rate, J_c (mol CO_2 m^{-2} s^{-1}), given by Melton and Arora (2016) is:

$$J_c = V_m\left[\frac{c_i-\Gamma}{c_i+K_c(1+\frac{O_a}{K_o})}\right], \tag{A.2}$$

where the Michaelis-Menten constant for O_2 is K_o (Pa) and for CO_2 is K_c (Pa), the partial pressure of O_2 in the atmosphere is O_a (Pa) and the maximum catalytic capacity of Rubisco is V_m (mol CO_2 m^{-2} s^{-1}). The triose phosphate use (TPU) limitation carboxylation rate, J_s (mol CO_2 m^{-2} s^{-1}), given by Melton and Arora (2016) is:

$$J_s = 0.5 \times V_m. \tag{A.3}$$

The maximum catalytic capacity of Rubisco (V_m) equals *vmax* adjusted for temperature and water stresses is defined as (Melton & Arora, 2016):

$$V_m = \frac{vmax\, f_{25}(Q_{10})S_{root}(\theta)\times 10^{-6}}{[1+\exp 0.3(T_c-T_{high})][1+\exp 0.3(T_{low}-T_c)]}, \tag{A.4}$$

where the standard Q_{10} function at temperature 25°C is f_{25}, canopy temperature is

T_c (K), the lower temperature limit for photosynthesis is T_{low} (K; *tlow* in Table A.2), the upper temperature limit for photosynthesis is T_{high} (K; *tup* in Table A.2), $S_{root}(\theta)$ simulates the influence of soil moisture and *vmax* is the maximum carboxylation rate by the Rubisco enzyme (mol CO_2 m^{-2} s^{-1}; *vmax* in Table A.2). The three photosynthetic states calculated above (J_c, J_e, and J_s) are combined to compute G_o (mol CO_2 m^{-2} s^{-1}):

$$J_p = \frac{(J_c + J_e) \pm \sqrt{(J_c + J_e)^2 - 4\beta_1 J_c J_e}}{2\beta_1}, \tag{A.5}$$

$$G_o = \frac{(J_p + J_s) \pm \sqrt{(J_p + J_s)^2 - 4\beta_2 J_p J_s}}{2\beta_2}, \tag{A.6}$$

where β_1 and β_2 are the photosynthetic coupling or curvature coefficients (Table A.2), and the positive root of Eq. A.5 is used in computing Eq. A.6. The minimum of the positive roots from these two equations, G_r (i.e., $\min(J_p, G_o)$) determines if the photosynthetic process is limited by the availability of Rubisco, light, or the transport capacity. The gross leaf photosynthetic rate (G_r) is scaled to obtain the nutrient limited leaf level gross photosynthetic rate, using a down-regulation term Ξ_{N} as (Melton & Arora, 2016):

$$G_{\mathrm{o,N-limited}} = \Xi_N \times G_r, \tag{A.7}$$
$$\Xi_N = \frac{1 + \gamma_{gd} \ln(c_a/c_0)}{1 + \gamma_d \ln(c_a/c_0)},$$

where the atmospheric concentration of CO_2 in ppm is c_a, the pre-industrial concentration of CO_2 (285.0 ppm) is c_0, the parameter for equivalent CO_2 fertilization effect with photosynthetic down-regulation is γ_d (*gamma_m* in Table A.2) and the parameter for equivalent CO_2 fertilization effect without photosynthetic down-regulation is γ_{gd} (*gamma_w* in Table A.2). The leaf level gross photosynthetic rate ($G_{\mathrm{o,N-limited}}$) is finally scaled to the canopy level, G_{canopy} (or GPP) as (Melton & Arora, 2016):

$$G_{\mathrm{canopy}} = G_{\mathrm{o,N-limited}} \times f_{PAR}, \tag{A.8}$$
$$f_{PAR} = \frac{1}{k_n}(1 - \exp^{-k_n \mathrm{LAI}}),$$

where f_{PAR} is the factor for scaling photosynthesis from the leaf to the canopy, k_n (unitless, in Table A.2) represents the rate at which the canopy reduces the availability

of light, and the green leaf area index is given by LAI (m^2 leaf (m^2 ground)$^{-1}$).

The maximum carboxylation rate ($vmax$) and k_n are also used to compute the leaf maintenance respiration, R_{mL}, that is a part of the autotrophic respiration (R_a) from all the living components, and given by Melton and Arora (2016) is:

$$R_{mL} = \varsigma_L vmax f_{25}(Q_{10\mathrm{d,n}}) f_{PAR}, \tag{A.9}$$

where the leaf maintenance respiration coefficient is ς_{L} (unitless, $rmlcoeff$ in Table A.2), $f_{25}(Q_{10\mathrm{d,n}})$ is the function that accounts for the different temperature sensitivities of leaf respiration during the day (d) and the night (n).

A.1.2 Dependency Conversion Using Spherical Coordinates

Parameters such as, the percentage of disturbed biomass that is used in short-term storage as paper (*paper*), in long-term storage as furniture ($furniture$), and that is combusted (*combust*); and carbon allocations to stem (*epsilons*), root (ι_r; *epsilonr*), and leaves (ι_l; *epsilonl*), in Table A.2, depend on each other such that that their sum is constrained to equal unity. The three terms can be denoted as ι_a, ι_b, and ι_c, where

$$\iota_a + \iota_b + \iota_c = 1, \tag{A.10}$$

All parameters inputted to GSA methods must be independent, and thus dependent parameters (the three parameters mentioned) have to be converted to independent variants. The dependent parameters are transformed to spherical coordinates with a unit radius to achieve the required parameter independence (Eq. A.11). Representing $(\iota_a)^{0.5}$ as x, $(\iota_b)^{0.5}$ as y and $(\iota_c)^{0.5}$ as z, we achieve

$$x^2 + y^2 + z^2 = 1. \tag{A.11}$$

By using the spherical coordinate system, we can focus on two independent parameters (the spherical angles) to derive values for all three parameters given by:

$$(\sin\phi\cos\theta)^2 + (\sin\phi\sin\theta)^2 + \cos^2\phi = 1, \tag{A.12}$$

where θ and ϕ are:

$$\theta = \mathrm{atan}\frac{y}{x},$$

$$\phi = \mathrm{asin}\frac{y}{\sin\theta}$$

$$z = \cos\phi.$$

A.1.3 Morris Elementary Effects Method

If Y is the model output given as: $Y = f(\mathbf{X})$, where $\boldsymbol{X}$ is the input vector of n parameters, $\mathbf{X} = \{x_1, x_2, \ldots, x_n\}$, such that $x_i \in [min_i, max_i]$, the elementary effects can be computed by assigning the number of grids-to-jump; and p, the number of grid points. The parameter ranges are then scaled to $[0, 1]$. The parameters are sampled on a fixed grid, with p values spanning the range of each parameter. Step sizes of Δ are used between parameters. The unit hypercube, made of n dimensions/parameters and p grid points per parameter, is denoted Ω. A coarse discretization of Ω (with a smaller p value) is needed because of the very high dimensionality and helps ensure that the entire space is reasonably well sampled, in contrast to the variance based GSA generally conducted on a much smaller number of parameters and for which any value in the uncertainty range can be sampled. For simplicity and a higher probability of selecting parameter values across the uncertainty space, if p is even, Δ can be chosen as:

$$\Delta = \frac{p}{2 \times (p-1)}. \tag{A.13}$$

It can be shown that this discretization results in good sampling of Ω (Saltelli et al., 2008). The elementary effects values for a particular parameter are computed by using two points in a unit hypercube. A base value $\mathbf{x^*}$ is randomly selected for $\mathbf{X}$ in the unit hypercube. The $\mathbf{x^*}$ value is then increased or decreased by Δ in one coordinate, before computing the elementary effects for that coordinate. The sign of the Δ value is chosen such that $\mathbf{X} \pm \Delta\mathbf{e}_j$ still lies in the parameter space Ω, where $\mathbf{e}_j$ is the unit vector in the j^{th} direction. The Δ and p were set to $\frac{2}{3}$ and 4 respectively in this study.

The elementary effects values are computed for a number of trajectories (r) in Ω to better sample the input's variability space. If consecutive evaluations of the j^{th} trajectory are termed $\boldsymbol{x}^l$ and $\boldsymbol{x}^{l+1}$, $l \in \{1, \ldots, n\}$, the elementary effect (EE) associated with the i^{th} parameter is given as (Saltelli et al., 2008):

$$EE_i^j(\mathbf{x}^l) = \frac{f(\mathbf{x}^{l+1}) - f(\mathbf{x}^l)}{\Delta}, \tag{A.14}$$

if the i^{th} component of $\boldsymbol{x}^l$ is increased by Δ and,

$$EE_i^j(\mathbf{x}^{l+1}) = \frac{f(\mathbf{x}^l) - f(\mathbf{x}^{l+1})}{\Delta}, \tag{A.15}$$

if the i^{th} component of $\boldsymbol{x}^l$ is decreased by Δ. The statistical measures: mean μ, absolute mean μ^* and standard deviation σ (or variance σ^2) can be computed for all input parameters after obtaining r trajectories.

$$\mu_i = \frac{1}{r}\sum_{j=1}^{r}(EE_i^j), \tag{A.16}$$

$$\mu_i^* = \frac{1}{r}\sum_{j=1}^{r}\left|EE_i^j\right|, \tag{A.17}$$

$$\sigma_i^2 = \frac{1}{r-1}\sum_{j=1}^{r}(EE_i^j - \mu_i)^2. \tag{A.18}$$

The quantity μ^* represents the linear effects, and σ indicates the non-linear effects of the parameter's variation on the model output (Campolongo & Braddock, 1999). We have used the Euclidean distance (κ) from the origin as the sensitivity measure to identify the influential parameters. The distance from the origin can be computed by:

$$\kappa = \sqrt{\mu^{*2} + \sigma^2}. \tag{A.19}$$

A.1.4 Sobol' Analysis

The influence of individual parameters on the output can be determined by calculating the variance of conditional expectation ($V[E(\cdot|\cdot)]$). To study variations in the output with the uncertainty in a single input parameter ($Y|x_i$), the output can be split into subsets based on quantile ranges of the i^{th} parameter's uncertainty range. For each quantile slice, an average can be computed, representing the conditional expectation ($E_{x_{\sim i}}(Y|x_i)$) of the output when the i^{th} parameter is held constant, while the expectation is estimated by sampling over all other ($\sim i$) parameters. The variance of the conditional expectation, $V_{x_i}[E_{x_{\sim i}}(Y|x_i)]$, quantifies the influence of a single parameter on the output variable when all other parameters change. Similarly, variances of output conditioned on two or more parameters can be computed to investigate the impact of interactions between parameters.

A mathematical formalism to find the contribution of each parameter using condi-

tional variance is given as follows (Saltelli et al., 2008). If the variations of the subset of parameters (k) are independent and if the output $f(\mathbf{X})$ is a square integrable function with variables in $\boldsymbol{X}$ being uniformly distributed in the unit hypercube, the output can be decomposed through a functional analysis of variance also known as ANOVA, into terms of increasing dimensions (Saltelli et al., 2008):

$$f(\mathbf{X}) = f_0 + \sum_{i}^{k} f_i(x_i) + \sum_{i=1}^{k}\sum_{j>1}^{k} f_{ij}(x_i, x_j) + \ldots + f_{12\ldots k}(x_1, x_2, \ldots, x_k). \tag{A.20}$$

For simplicity, $f_i(x_i)$ will be denoted as f_i and so on. These terms are defined using conditional expectations of the output Y (Saltelli et al., 2008):

$$f_0 = E(Y),$$

$$f_i = E_{x_{\sim i}}(Y|x_i) - f_0,$$

$$f_{ij} = E_{x_{\sim i,j}}(Y|x_i, x_j) - E_{x_{\sim i}}(Y|x_i) - E_{x_{\sim i}}(Y|x_j) - f_0,$$

and so on for subsequent terms, where the first order term (f_i) excludes the mean effect ($E(Y)$), the second order term (f_{ij}) excludes individual parameter effects as well as the mean effect, and so on. The output variance $V(Y)$ is given by Saltelli et al. (2008):

$$V(Y) = \sum_{i}^{k} V_i + \sum_{i=1}^{k}\sum_{j>1}^{k} V_{ij} + \ldots + V_{12\ldots k}, \tag{A.21}$$

where $V_i = \mathrm{var}(f_i) = V[E_{x_{\sim i}}(Y|x_i)]$, $V_{ij} = \mathrm{var}(f_{ij}) = V[E_{x_{\sim i,j}}(Y|x_i, x_j)] - V_i - V_j$ and so on. The variance of conditional expectation is a measure of the sensitivity and, thus, the measure of importance. Dividing both sides by $V(Y)$, the sensitivity indices (SI) are given by:

$$\sum_{i}^{k} S_i + \sum_{i}^{k}\sum_{i<j}^{k} S_{ij} + \ldots + S_{12\ldots k} = 1 \tag{A.22}$$

The first or main order sensitivity index (S_i) is given by:

$$SI_{1_i} = \frac{V_{x_i}[E_{x_{\sim i}}(Y|x_i)]}{V(Y)}, \tag{A.23}$$

where

$$0 \leq \sum_{i=1}^{k} S_i \leq 1.$$

Another metric, the total sensitivity index (S_T) denotes the contribution of a single parameter and its interactions to the model output. Saltelli et al. (2008) deduced a way to calculate S_{T_i}, using the interactions of all parameters except, the individual contribution of the ith term ($X_{\sim i}$) given by:

$$SI_{tot_i} = 1 - \frac{V_{x_i}[E_{x_i}(Y|x_{\sim i})]}{V(Y)}. \tag{A.24}$$

S_{T_i} close to zero implies that the influence of a parameter is negligible, and the confidence interval crossing zero implies that even if the mean is away from zero the influence of the parameter is not robust. If $S_{T_i} \simeq 0$, the parameter can be fixed to any value in its given range of uncertainty without appreciably affecting the output of the model.

Here is a detailed example for calculating Sobol' indices using a simple quadratic equation without parameter interactions. This example demonstrates the calculation of expectations and variances, leading to the determination of Sobol' indices. Since there are no parameter interactions, the total sensitivity index will be the same as the first-order sensitivity index.

Consider the following simple quadratic function:

$$Y = f(x_1, x_2) = x_1 + 2x_2^2,$$

where x_1 and x_2 are independent and are uniformly distributed in $[0, 1]$ The expectation of a ($E(a)$) is given as:

$$E(a) = \int_0^1 a\, da,$$

$$E(x_1) = E(x_2) = \frac{1}{2}.$$

Similarly, the square of the expectation of a ($E(a^2)$) is given as:

$$E(a^2) = \int_0^1 a^2\, da,$$

$$E(x_1^2) = E(x_2^2) = \frac{1}{3},$$

and the expectation of a^4 ($E(a^4)$) is given as:

$$E(a^4) = \int_0^1 a^4 \, da,$$

$$E(x_2^4) = \frac{1}{5},$$

From Eqn. A.21, we can write the first term (1st order variances) on the right hand side as:

$$V(Y) = V(x_1) + V(2x_2^2),$$

$$V(a) = E(a^2) - [E(a)]^2,$$

$$V(x_1) = E(x_1^2) - [E(x_1)]^2,$$

and

$$V(x_2^2) = E(x_2^4) - [E(x_2^2)]^2,$$

Substituting values calculated for $E(x_1)$, $E(x_2)$, $E(x_1^2)$, $E(x_2^2)$, and $E(x_2^4)$, we get:

$$V(x_1) = \frac{1}{3} - (\frac{1}{2})^2 = \frac{1}{12},$$

and

$$V(x_2) = \frac{1}{5} - (\frac{1}{3})^2 = \frac{4}{45}.$$

The total variance of the output (Y) is thus:

$$V(Y) = V(x_1) + V(2x_2^2) = \frac{1}{12} + 4 \times \frac{4}{45} = \frac{79}{180}.$$

The 1st-order SI can be calculated from Eqn. 4.4 as:

$$SI_{1_{x_1}} = \frac{\frac{1}{12}}{\frac{79}{180}} = 0.1899,$$

$$SI_{1_{x_2}} = \frac{\frac{16}{45}}{\frac{79}{180}} = 0.8101,$$

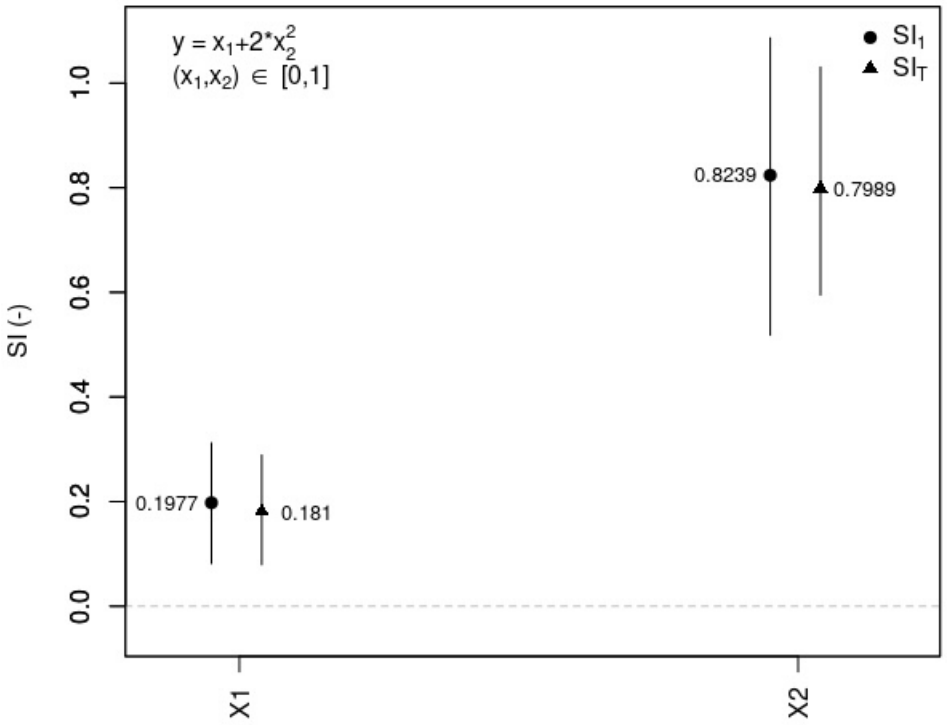

Figure A.1: Sobol indices for the example equation $Y = x_1 + 2 \times x_2^2$, with 512 perturbation points.

and the total-order from Eqn. 4.5 as:

$$SI_{tot_{x_1}} = 1 - \frac{\frac{16}{45}}{\frac{79}{180}} = 0.1899,$$

$$SI_{tot_{x_2}} = 1 - \frac{\frac{1}{12}}{\frac{79}{180}} = 0.8101.$$

To visualize the Sobol' sensitivity indices calculated for the equation in the example, we used the *R* Statistical Software. In this experiment, a perturbation matrix is generated by the *sobol*2002() function of the *sensitivity R* package for 512 perturbation points and 1000 bootstrapping samples. The outputs for each of these parameter combinations are computed and are then quantified. The computed estimates of S_{T_i} are smaller than SI_{1_i} when they should be equal (Figure A.1), which illustrates how this result can manifest just from the perturbation point locations in the search space and the estimators used. Since the confidence intervals overlap, we can assume that SI_{1_i} and S_{T_i} will fall anywhere along the confidence interval ranges.

A.2 Supplemental for Chapter 4

This section contains:

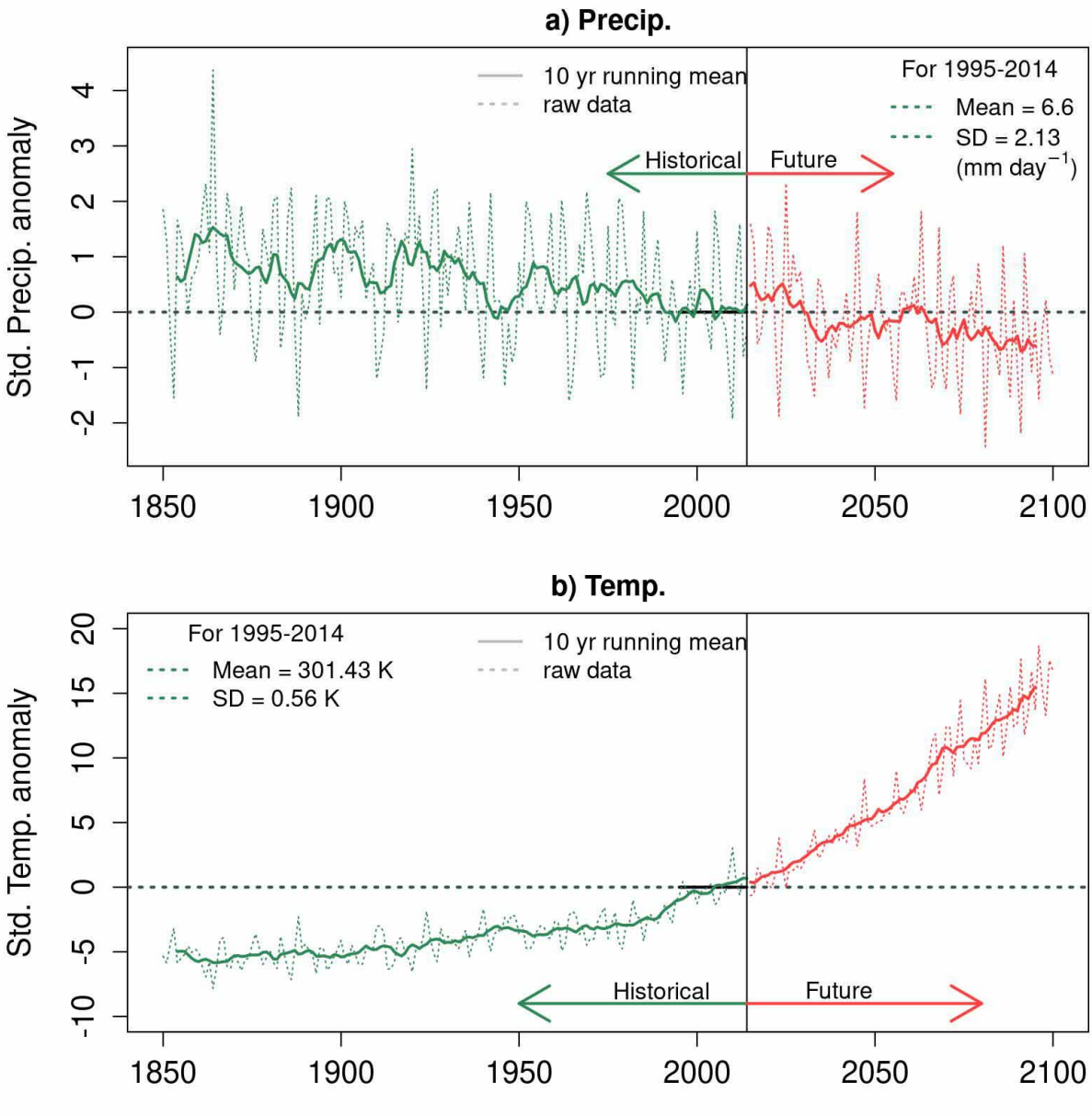

Figure A.2: (a) Standardized precipitation anomalies from 1850-2100 for tropical broadleaf. Green denotes the historical period (1850-2014), red denotes the projected future under SSP5-8.5 conditions (2015-2100). The reference period is from 1995-2014. Dashed lines are raw annual data. Solid lines are 10-year running means. (b) Similar to (a), but for standardized temperature anomalies.

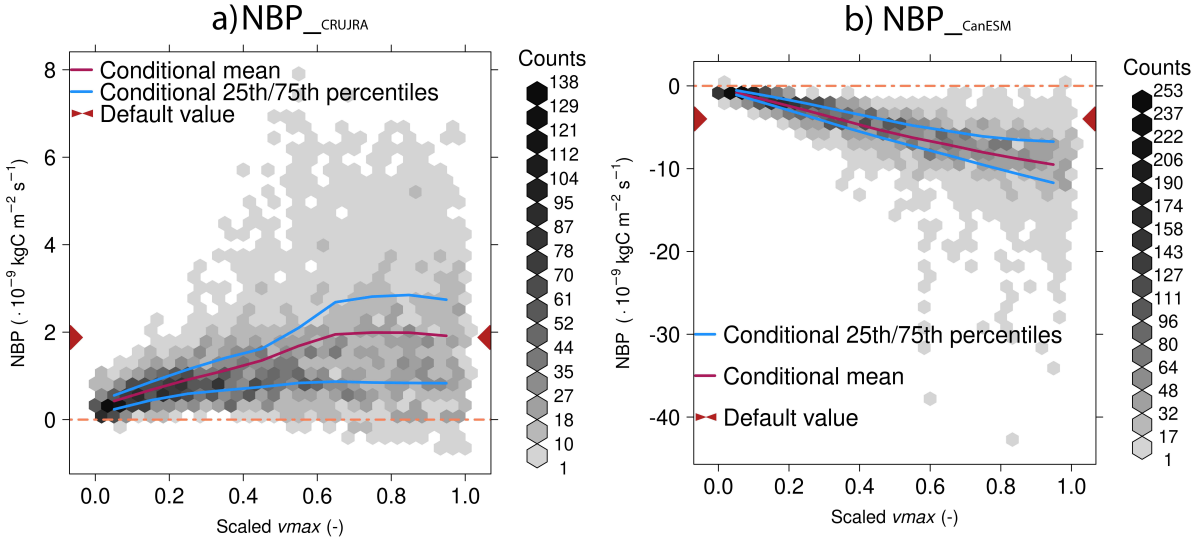

Figure A.3: Conditional distribution figures for the historical (a) 30-year means of NBP when simulated with CRUJRAv2, and (b) 20-year means of NBP when simulated with CanESM5 (10^{-9} kgC m^{-2} s^{-1}) for tropical broadleaf location.

A.2.1 Historical CRUJRAv2 vs CanESM5

From the conditional distribution figures in Chapter 4, we notice that the tropical broadleaf, tropical grassland and boreal deciduous locations predominantly act as sources of atmospheric carbon, while the temperate conifer location acts as a carbon sink. Looking at the conditional distributions of the historical 20-year NBP means, we note that the tropical broadleaf location is a strong sink (Figure A.3b), tropical grassland is a weak source, temperate conifer is a weak sink, and the boreal deciduous is carbon neutral. The conditional historical spreads from Chapter 4 conflict with those from Chapter 3. In Chapter 3 for the historical NBP mean, the tropical broadleaf location was a strong sink (Figure A.3a), tropical grassland was a strong source for smaller *vmax* values and neutral for higher values of *vmax*, temperate conifer was predominately a source, and the boreal deciduous was a weak sink. The input parameters, their uncertainty ranges, and the biome locations do not differ between Chapters 3 and 4. The only changes correspond to the forcing and the number of years used in the statistical measures (i.e., CRUJRAv2, 30-year means in Chapter 3 vs. CanESM5, 20-year means in Chapter 4). For the simulations from Chapter 4 where the CLASSIC model was forced using CanESM5 data, we compared the conditional distribution figures for historical 30-year NBP means (not shown) and the historical 20-year means, and noticed that the spreads were not substantially different. This comparison implies that the difference in the sources and sinks simulated by the CLASSIC model for the same biome locations is solely due to the difference in the

forcing data used. This mismatch was previously studied by Seiler et al. (2024) who forced CLASSIC using CRUJRAv2 and CanESM5 using default parameters. In their study, they noted that forcing the CLASSIC model with CRUJRAv2 data produced a global carbon sink, and a global carbon source when forced with historical CanESM5 data. Through various experiments performed in their study, they observed that the absence of the carbon sink in the latter setting was mainly driven by the exaggerated historical temperature trend in CanESM5.

A further analysis of the components of NBP, such as the gross primary productivity (GPP), autotrophic respiration (Ra) (Figure A.4), heterotrophic respiration (Rh), and CO_2 emissions due to wildfire ($fFire$) (Figure A.5) and was done for the historical 30-year NBP mean simulated by CRUJRAv2 forcing data (Figures A.4a,c and Figures A.5a,c), and for the historical 20-year NBP mean simulated by the bias adjusted CanESM5 forcing data (Figures A.4b,d and Figures A.5b,d). From this analysis, we note that the components of NBP for both the forcing data are always increasing with larger $vmax$ values. The conditional distributions for both settings are similar to the results in Figure 5 (MS). For the simulations with CanESM5 forcing data, it is noted that the sum of ecosystem respiration and emissions of fire exceeds gross primary productivity for larger values of $vmax$, leading to an overall source of carbon (conditional mean ranging from -3.399 to -9.1334 μgC m^{-2} s^{-1} for scaled values of $vmax$ of 0.1 and 0.9 respectively). The opposite applies to the CRUJRAv2-driven simulation (conditional mean NBP ranging from 0.5614 to 2.0064 μgC m^{-2} s^{-1} for scaled values of $vmax$ of 0.1 and 0.9 respectively). The conditional distribution ranges for the respective respiration terms are similar. The CLASSIC model simulates stronger gross primary productivity for the CRUJRAv2 setting, and stronger CO_2 emissions due to forest fires under the CanESM5 forcing. The result from Seiler et al. (2024) mentioned in the previous paragraph supports the theory that the absence of the carbon sink is mainly driven by CO_2 emissions due to forest fires, which could be boosted by the exaggerated historical temperature trend in CanESM5. This result shows that the uncertainty of the carbon sink is also influenced by uncertainty in the forcing, beyond parameter or model uncertainty. The unrealistic historical NBP values for the CanESM5-driven simulation cannot be addressed solely through model tuning.

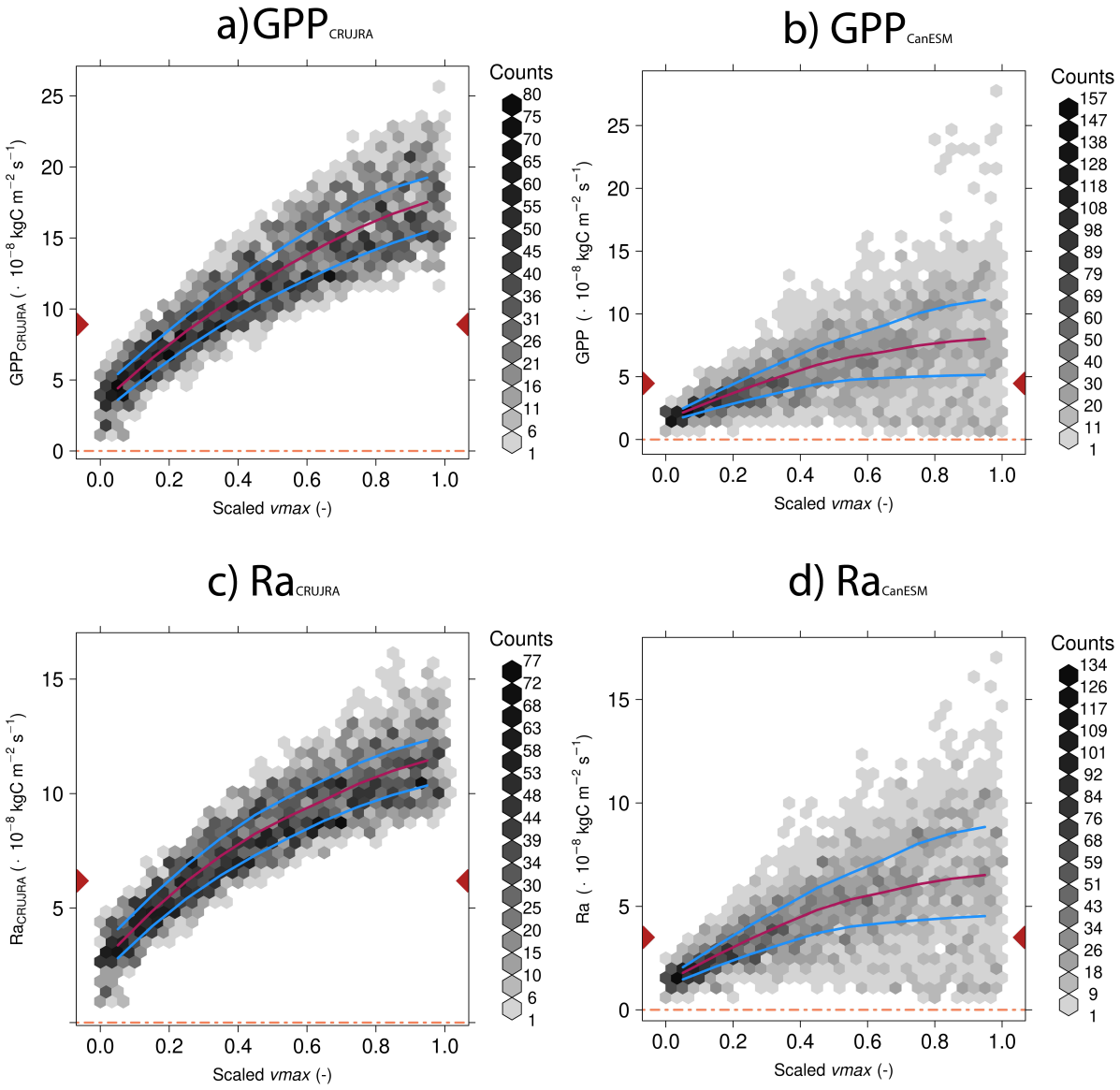

Figure A.4: Conditional distribution figures for the historical (a) 30-year means of GPP when simulated with CRUJRAv2, and (b) 20-year means of GPP when simulated with CanESM5 (10^{-8} kgC m^{-2} s^{-1}), (c) 30-year means of Ra when simulated with CRUJRAv2, and (b) 20-year means of Ra when simulated with CanESM5 (10^{-8} kgC m^{-2} s^{-1}), for tropical broadleaf location.

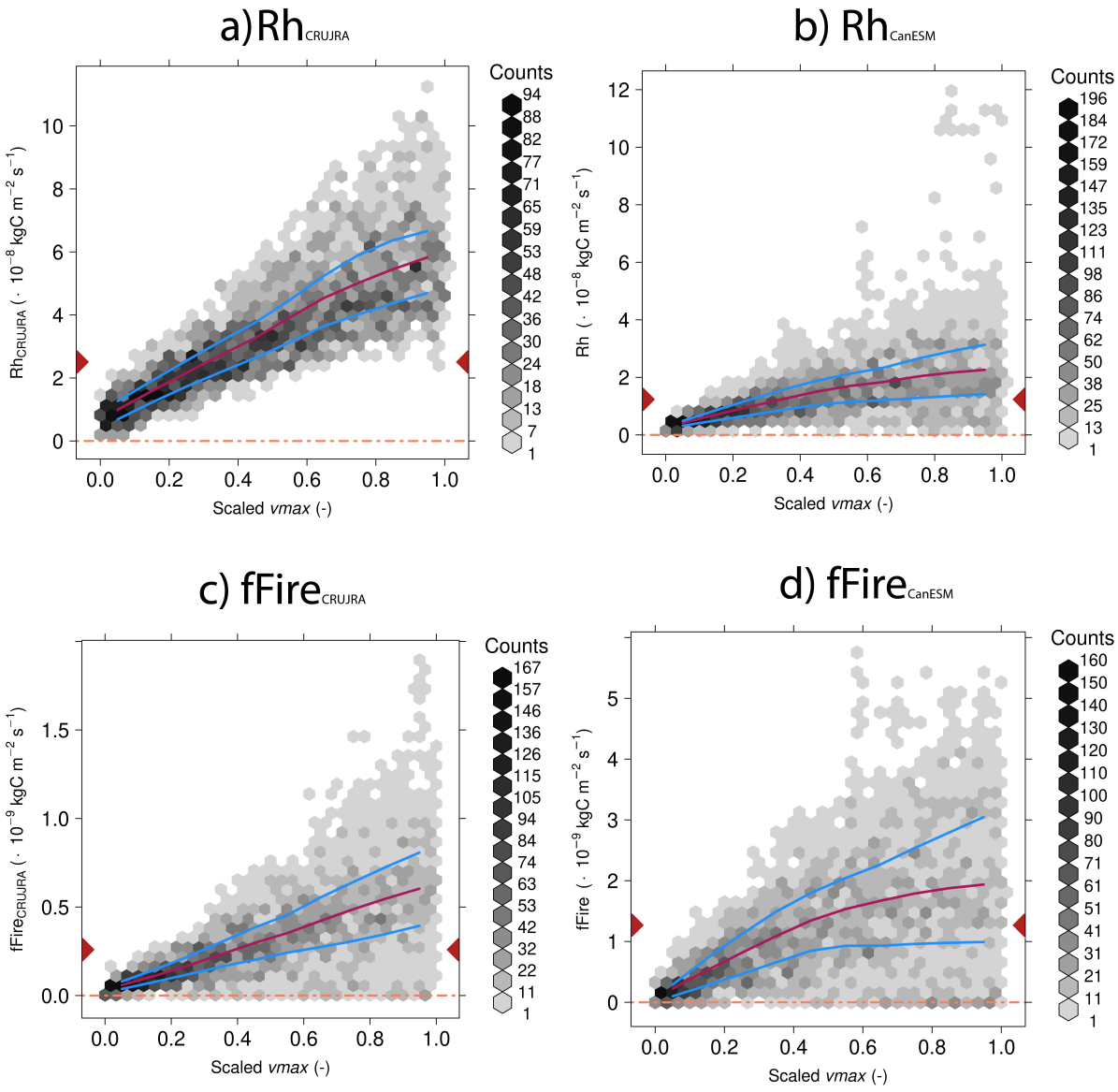

Figure A.5: Conditional distribution figures for the historical (a) 30-year means of Rh when simulated with CRUJRAv2, and (b) 20-year means of Rh when simulated with CanESM5 (10^{-8} kgC m^{-2} s^{-1}), (c) 30-year means of $fFire$ when simulated with CRUJRAv2, and (b) 20-year means of $fFire$ when simulated with CanESM5 (10^{-9} kgC m^{-2} s^{-1}), for tropical broadleaf location.

A.2.2 Different time-periods

We noticed that the inter-decadal variability in the evolution of default NBP for the SSP5-8.5 scenario was high at each biome location (Figure A.6). The time series indicate that the NBP values switched signs for the default state where no parameters were perturbed. A comparison of SI values of the projected changes in 20-year NBP means between the early future (2015-2034) and late historical (1995-2014) time periods are also provided (Figure A.7). The Zenodo link provided in the Section A.4 contains a comparison of SI values (Similar to Figure 4.3) for projected 10- and 20-year NBP means of various time periods. By analysing these figures, we notice that the the subset of highest-ranked influential parameters varies if another future time period, rather than 2081-2100 is used. The parameters may vary if another SSP scenario is used (experiments not conducted).

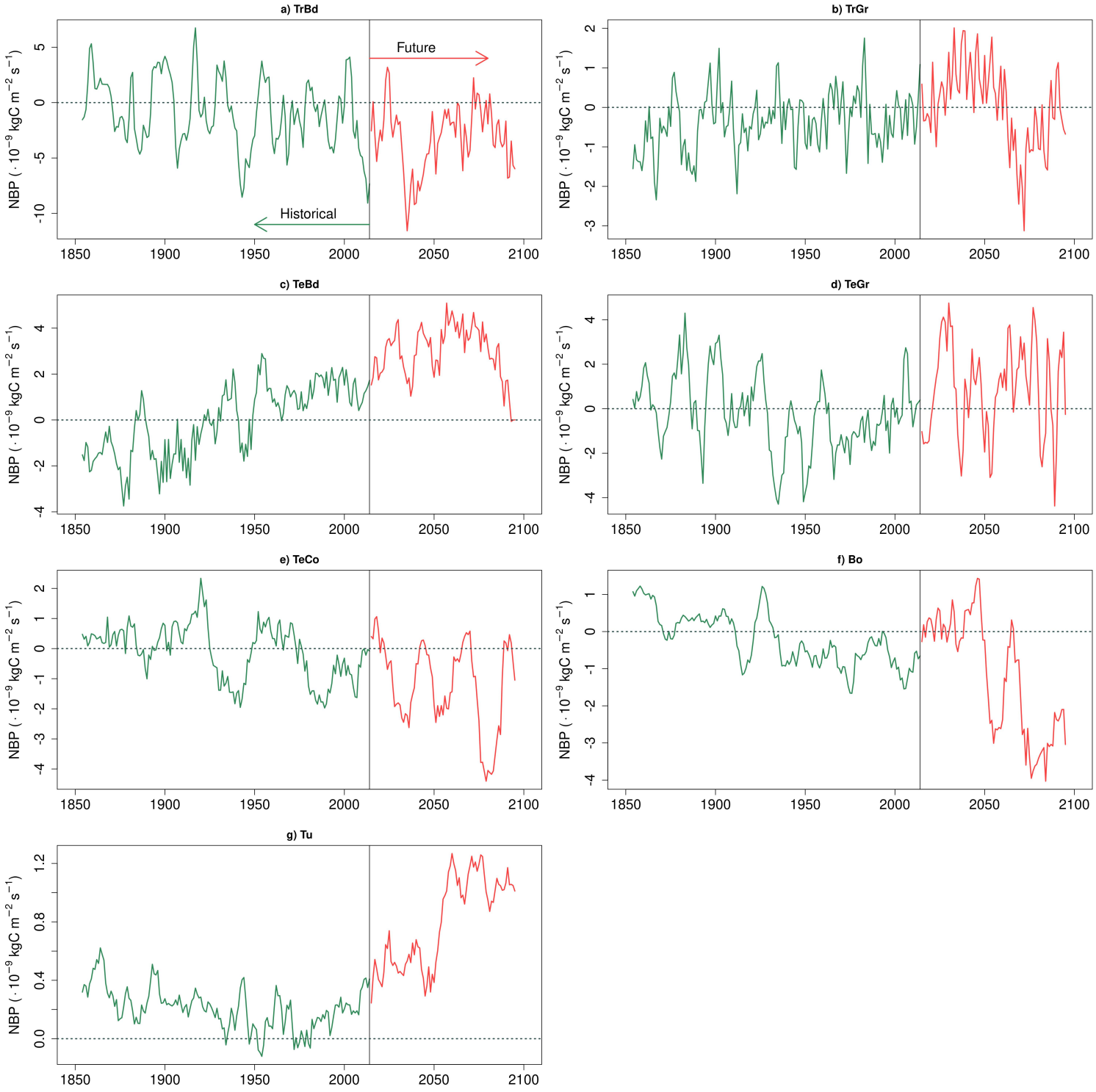

Figure A.6: Evolution of default NBP from the historical (green) to the future period under SSP5-8.5 forcing (red) for the seven biome locations, where only the 10-year running means are depicted.

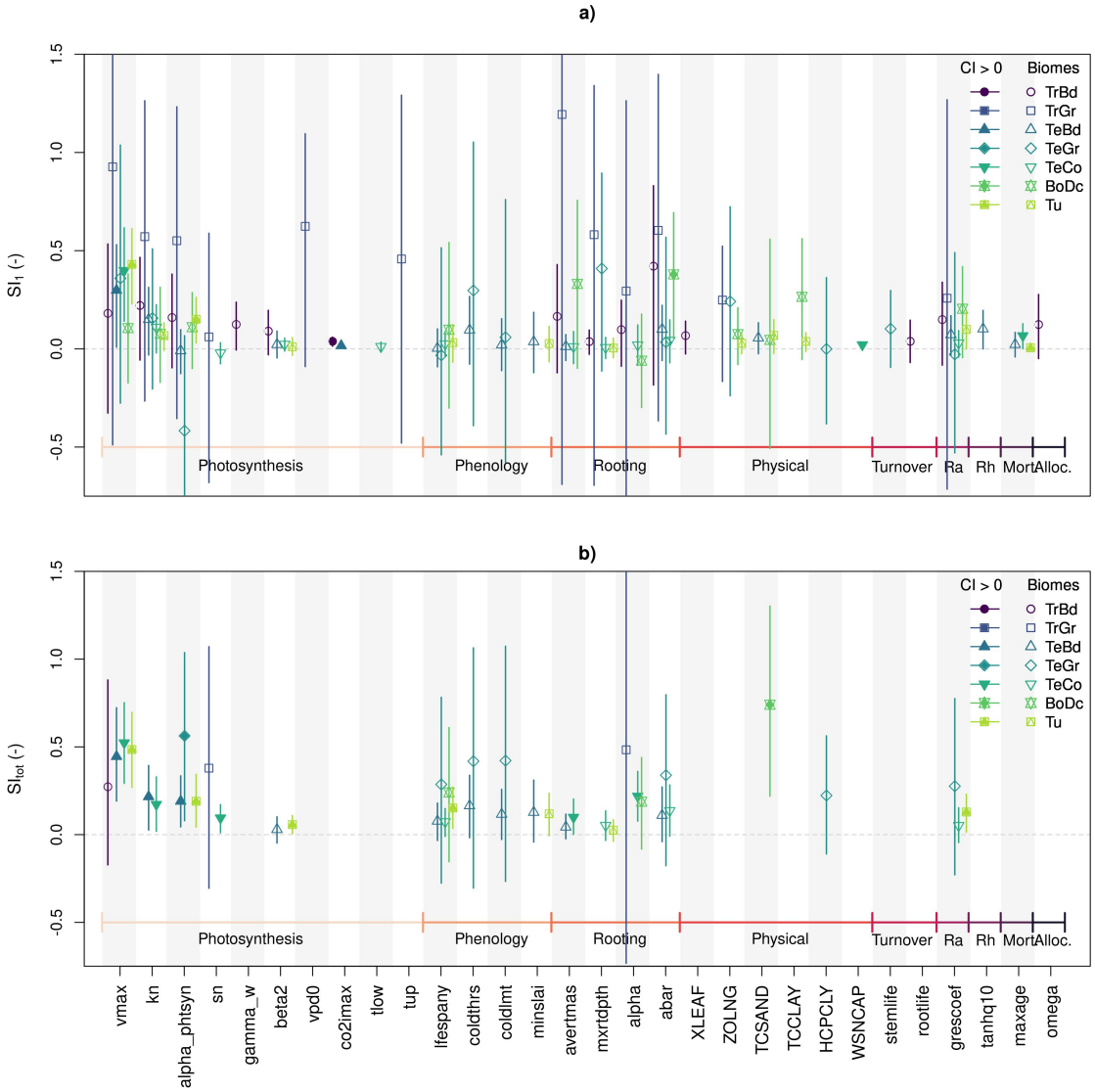

Figure A.7: (a) First and (b) total-order SIs, and their confidence intervals for the top-ranked parameters across biomes (open symbols) for the projected change in 20-year means when 2015-2034 is used instead of 2081-2100 as the future 20-year means. Filled symbols represent robust SIs. Total order indices are plotted only where SI_{tot} greater than SI_1. The parameters are grouped according to the processes.

A.3 Common Tables

Table A.1: Biome grid cells chosen in Chapters 3 and 4 with the latitude, and longitude values, PFT of 1901, and the average soil composition in terms of sand, clay and organic matter for maximum root depth (*mxrtdpth* in Table A.2). Locations where the PFT percentages do not add up to 100 have bareground and/or water as well.

	TrBd	**TrGr**	**TeBd**	**TeGr**	**TeCo**	**BoDc**	**Tu**
Latitude (°N)	0	10	40	40	50	65	66
Longitude (°E)	300	20	280	260	240	120	250
PFT_{1901} (%)							
EvgNdlTr	0.00	0.00	0.80	0.01	74.45	5.01	0.00
DcdNdlTr	0.00	0.00	0.18	0.00	0.04	79.27	0.00
EvgBdlTr	94.58	3.54	0.00	0.00	0.00	0.01	0.01
DcdCBdlTr	0.00	0.00	63.09	0.03	5.59	5.02	2.64
DcdDBdlTr	5.02	3.80	0.00	0.00	0.00	0.00	0.00
C3Cr	0.00	0.00	0.11	0.00	0.00	0.00	0.00
C4Cr	0.00	0.00	0.04	0.00	0.00	0.00	0.00
C3Gr	0.00	0.00	25.74	52.16	13.06	10.13	25.15
C4Gr	0.40	43.87	3.67	36.48	0.00	0.02	0.00
Soil composition (%)							
Sand	44.16	35.19	21.04	23.09	14.42	10.67	10.23
Clay	36.24	33.42	38.98	24.67	49.12	53.81	61.19
Organic matter	1.25	0.78	0.89	1.16	1.76	3.12	1.19

Table A.2: Input parameters, their PFT specific minimum, maximum uncertainty ranges, default values, units, and description as used in the CLASSIC model, and the corresponding references. Parameters not used in Chapter 2, but used in Chapters 3 and 4 are in grey.

Parameter	Minimum	Maximum	Default	Unit	Description	Reference
abar	2.5,2.5,2.5,2.5,2.5, 2.5,2.5,2.5,2.5	5.17,6.446,4.257,3.806,4.367, 4.367,4.367,6.446,5.412	4.70,5.86,3.87,3.46,3.97, 3.97,3.97,5.86,4.92	-	Mean root distribution profile	Arora and Boer (2003)
albnir	17.1,17.1,20.7,26.1,26.1, 30.6,30.6,27,30.6	20.9,20.9,25.3,31.9,31.9, 37.4,37.4,33,37.4	19.0,19.0,23.0,29.0,29.0, 34.0,34.0,30.0,34.0	-	Near IR albedo	-
albvis	2.7,2.7,2.7,4.5,4.5, 5,5,4.5,5.4	3.3,3.3,3.3,5.5,5.5, 6,6,5.5,6.6	3.0,3.0,3.0,5.0,5.0, 5.5,5.5,5.0,6.0	-	Visible albedo	-
ALIRI	0.6	0.9	0.73	-	Near-infrared albedo of ice	Gardner and Sharp (2010)
ALIRO	0.2	0.4	0.3	-	Near-infrared albedo of organic matter	Expert opinion
ALIRWC	0.3686	0.3914	0.38	-	Average background NIR albedo of snow covered canopy	Expert opinion
alpha	0.25,0.25,0.25,0.25,0.25, 0.25,0.25,0.25,0.25	1,1,1,1,1, 1,1,1,1	0.8,0.8,0.8,0.8,0.8, 0.8,0.8,0.8,0.8	-	Parameter determining how the roots grow	Arora and Boer (2003)
alpha_phtsyn	0.05,0.05,0.05,0.05,0.05, 0.05,0.03,0.05,0.03	0.120,0.12,0.12,0.12,0.12, 0.12,0.054,0.12,0.054	0.08,0.08,0.08,0.08,0.08, 0.08,0.04,0.08,0.04	μ mol CO_2 (μ mol photons)$^{-1}$	Quantum efficiency	Skillman (2008)
ALVSI	0.9	1	0.95	-	Visible albedo of ice	Gardner and Sharp (2010)
ALVSO	0.03	0.08	0.05	-	Visible albedo of organic matter	Expert opinion
ALVSWC	0.2619	0.2781	0.27	-	Average background visible albedo of snow covered canopy	Expert opinion
avertmas	0.1,0.1,0.1,0.1,0.1, 0.09,0.09,0.1,0.1	8.7,8.7,8.7,8.7,8.7, 0.11,0.11,3,3	1.85,1.45,2.45,2.10,2.10, 0.10,0.10,0.70,0.70	kg C m^{-2}	Average root biomass	Arora and Boer (2003)
bb	0.009,0.009,0.009, 0.009,0.009,0.009, 0.036,0.009,0.036	0.011,0.011,0.011, 0.011,0.011,0.011, 0.044,0.011,0.044	0.01,0.01,0.01, 0.01,0.01,0.01, 0.04,0.01,0.04	mol m^{-2} s^{-1}	Used in photosynthesis-stomatal conductance coupling.	-
beta1	0.9	0.98	0.95	g species (kg DOM)$^{-1}$	Photosynthesis coupling or curvature coefficients	Expert opinion
beta2	0.9	0.99	0.99	g species (kg DOM)$^{-1}$	Photosynthesis coupling or curvature coefficients	Expert opinion
bmasthrs	3.6,0.9	4.4,1.1	4.0,1.0,	(kgC m^{-2})	Biomass thresholds for determining if deforested area is a forest	-
bmasthrs_fire	0.36,1.08	0.44,1.32	0.4,1.2,	(kgC m^{-2})	Min. and max. veg. biomass thresholds	-
bsratelt	0.40077,0.53874, 0.57051,0.68184,0.62613, 0.54,0.54, 0.4734,0.4734	0.48983,0.65846, 0.69729,0.83336,0.76527, 0.66,0.66, 0.5786,0.5786	0.4453,0.5986, 0.6339,0.7576,0.6957, 0.60,0.60, 0.5260,0.5260	kg C m^{-2} year^{-1}	Litter respiration rates at 15°C	Arora (2003)
bsratesc	0.0234,0.0234, 0.01872,0.01872,0.01872, 0.0315,0.0315, 0.01125,0.01125	0.0286,0.0286, 0.02288,0.02288,0.02288, 0.0385,0.0385, 0.01375,0.01375	0.0260,0.0260, 0.0208,0.0208,0.0208, 0.0350,0.0350, 0.0125,0.0125	kg C m^{-2} year^{-1}	Soil carbon respiration rates at 15°C	Arora (2003)
bsrtroot	0.45,0.2565,0.585, 0.2025,0.0495,0.144,0.144, 0.09,0.09	0.55,0.3135,0.715, 0.2475,0.0605,0.176,0.176, 0.11,0.11	0.5,0.285,0.65, 0.225,0.055,0.16,0.16, 0.1,0.1	kg C m^{-2} year^{-1}	Base respiration rates for root at 15°C	-
bsrtstem	0.081,0.0495, 0.054,0.03015,0.027, 0.03285,0.03285, 0,0	0.099,0.0605, 0.066,0.03685,0.033, 0.04015,0.04015, 0,0	0.0900,0.0550, 0.0600, 0.0335,0.0300, 0.0365,0.0365, 0,0	kg C m^{-2} year^{-1}	Base respiration rates for stem at 15°C	-
CANEXT	-0.375,-1.125,-0.6,-0.6	-0.625,-1.875,-1,-1	-0.5,-1.5,-0.8,-0.8	-	Attenuation coefficient used in calculating the sky view factor for vegetation canopies	Expert opinion
cdlsrtmx	0.09,0.27,0.27,0.36,0.135, 0.135,0.135,0.135,0.135	0.11,0.33,0.33,0.44,0.165, 0.165,0.165,0.165,0.165	0.10,0.30,0.30,0.40,0.15, 0.15,0.15,0.15,0.15	day^{-1}	Max. loss rate for cold stress	-
co2imax	50	3000	2000	Pa	Max. intercellular CO_2 concentration	Leuning (1995)
colda	2.7,2.7,2.7,2.7,2.7, 2.7,2.7,2.7,2.7	3.3,3.3,3.3,3.3,3.3, 3.3,3.3,3.3,3.3	3.0,3.0,3.0,3.0,3.0, 3.0,3.0,3.0,3.0	-	Parameter determining how fast cold temperatures causes leaves to fall	-
coldlmt	3,3	10,10	7,5	days	No. of days for which some temperature has to remain below a given threshold for initiating a process	Expert opinion
coldthrs	-15, 0	-5, 10	-5.0, 8.0	°C	Threshold temperature for initiating leaf fall	X. Lu et al. (2013)

combust	0.135,0.27,0.405	0.165,0.33,0.495	0.15,0.30,0.45,	(kgC m^{-2})	Disturbed biomass that combusts	-
CXTLRG	9.00E+19	1.10E+20	1.00E+20	-	Effective overall extinction coefficient given if visible transmissivity is very small	-
dayschk	3,3,3,3,3, 3,3,3,3	10,10,10,10,10, 10,10,10,10	7,7,7,7,7, 7,7,7,7	days	Number of days to check if net photosynthetic rate is positive before initiating leaf onset	Expert opinion
drgta	2.7,2.7,2.7,2.7,2.7, 2.7,2.7,2.7,2.7	3.3,3.3,3.3,3.3,3.3, 3.3,3.3,3.3,3.3	3.0,3.0,3.0,3.0,3.0, 3.0,3.0,3.0,3.0	-	Determines how fast soil dryness causes leaves to fall	-
drlsrtmx	0.00225,0.0045, 0.0045,0.0045,0.00225, 0.0045,0.0045, 0.0045,0.0045	0.00275,0.0055, 0.0055,0.0055,0.0055, 0.00275,0.0055, 0.0055,0.0055	0.0025,0.005, 0.005,0.005,0.025, 0.005,0.005, 0.050,0.050	day^{-1}	Max. loss rate for drought stress	-
emif_bc	0.504,0.504,0.504,0.504,0.423, 0.504,0.423,0.00,0.504,0.423	0.616,0.616,0.616,0.616,0.517, 0.616,0.517,0.00,0.616,0.517	0.56,0.56,0.56,0.56,0.47, 0.56,0.47,0.00,0.56,0.47	(gspecies $kgDOM^{-1}$)	PFT-specific emissions for black carbon	-
emif_co	95.4,95.4,92.7,95.4,57.6, 95.4,57.6,0.00,95.4,57.6	116.6,116.6,113.3,116.6,70.4, 116.6,70.4,0.00,116.6,70.4	106.0,106.0,103.0,106.0,64.0, 106.0,64.0,0.00,106.0,64.0	"	PFT-specific emissions for CO	-
emif_co2	1418.4,1418.4,1443.6, 1418.4,1488.6,1418.4,1488.6, 0.00,1418.4,1488.6	1733.6,1733.6,1764.4, 1733.6,1819.4,1733.6,1819.4, 0.00,1733.6,1819.4	1576.0,1576.0,1604.0, 1576.0,1654.0,1576.0,1654.0, 0.00,1576.0,1654.0	"	PFT-specific emission factors for CO_2	-
emif_h2	1.62,1.62,2.286,1.62,0.882, 1.62,0.882,0.00,1.62,0.882	1.98,1.98,2.794,1.98,1.078, 1.98,1.078,0.00,1.98,1.078	1.80,1.80,2.54,1.80,0.98, 1.80,0.98,0.00,1.80,0.98	"	PFT-specific emissions for H_2	-
emif_nmhc	5.13,5.13,5.76,5.13,3.33, 5.13,3.33,0.00,5.13,3.33	6.27,6.27,6.99,6.27,4.07, 6.27,4.07,6.27,4.07	5.7,5.7,6.4,5.7,3.7, 5.7,3.7,5.7,3.7	"	PFT-specific emissions for non-methane HCs	-
emif_oc	8.19,8.19,6.03,8.19,2.88, 8.19,2.88,0.00,8.19,2.88	10.01,10.01,7.37,10.01,3.52, 10.01,3.52,10.01,3.52	9.1,9.1,6.7,9.1,3.2, 9.1,3.2,9.1,3.2	"	PFT-specific emissions for total carbon	-
emif_pm25	11.43,11.43,9.45,11.43,4.68, 11.43,4.68,0.00,11.43,4.68	13.97,13.97,11.55,13.97,5.72, 13.97,5.72,13.97,5.72	12.7,12.7,10.5,12.7,5.2, 12.7,5.2,12.7,5.2	"	PFT-specific emissions for particles	-
emif_tc	7.47,7.47,6.48,7.47,3.06, 7.47,3.06,0.00,7.47,3.06	9.13,9.13,7.92,9.13,3.74, 9.13,3.74,9.13,3.74	8.3,8.3,7.2,8.3,3.4, 8.3,3.4,8.3,3.4	"	PFT-specific emissions for total carbon	-
emif_tpm	15.84,15.84,13.23,15.84,7.65, 15.84,7.65,0.00,15.84,7.65	19.36,19.36,16.17,19.36,9.35, 19.36,9.35,19.36,9.35	17.6,17.6,14.7,17.6,8.5, 17.6,8.5,17.6,8.5	"	PFT-specific emissions for total particulate matter	-
epsilonl	0.18,0.054,0.315,0.315,0.225, 0.72,0.72,0.009,0.009	0.22,0.066,0.385,0.385,0.275, 0.88,0.88,0.011,0.011	0.20,0.06,0.35,0.35,0.25, 0.8,0.8,0.01,0.01	-	Base allocation fraction for leaf (epsilon L)	Melton and Arora (2016)
epsilonr	0.585,0.801,0.54,0.495,0.585, 0.045,0.045,0.98,0.98	0.715,0.979,0.66,0.605,0.715, 0.055,0.045,0.99,0.99	0.65,0.89,0.60,0.55,0.65, 0.05,0.05,0.99,0.99	-	Base allocation fraction for root (epsilon R)	Melton and Arora (2016)
epsilons	0.135,0.045,0.045,0.09,0.09, 0.135,0.135,0,0	0.165,0.055,0.055,0.11,0.11, 0.135,0.135,0,0	0.15,0.05,0.05,0.10,0.10, 0.15,0.15,0,0	-	Base allocation fraction for stem (epsilon S)	Melton and Arora (2016)
eta	9,27.72,27.9,45,27, 6.3,6.3,2.7,2.7	11,33.88,34.1,55,33, 7.7,7.7,3.3,3.3	10.0,30.8,31.0,50.0,30.0, 7.0,7.0,3.0,3.0	-	Determines proportion of stem plus wood biomass to leaf biomass and the minimum root : shoot ratio lr min	Ludeke et al., 1994
extnmois_veg	0.27	0.33	0.3,	(-)	Extinction moisture content for veg. fire	-
extnmois_duff	0.45	0.55	0.5,	(-)	Extinction moisture content for duff layer fire	-
f0	0.045	0.055	0.05,	(-)	Fire spread rate in the absence of wind	-
flhrspan	5, 25	30, 55	17.0, 45.0	days	Harvest span	Expert opinion
fracbofg	0.4	0.65	0.55	-	Parameter used to estimate lai of brown leaves. SLA of brown leaves is a fraction of SLA of green leaves	Expert opinion
frco2blf	0,0,0,0 0,0,0,0.486,0.486	0,0,0,0, 0,0,0,0.594,0.594	0.00,0.00,0.00,0.0, 0.00,0.0,0.00,0.54,0.54	(-)	Brown leaf biomass to gases, fraction	-
frco2glf	0.378,0.378,0.378,0.378,0.378, 0,0,0.432,432	0.462,0.462,0.462,0.462,0.462, 0,0,0.528,0.528	0.42,0.42,0.42,0.42,0.42, 0.0,0.00,0.48,0.48	(-)	Green leaf biomass to gases, fraction	-
frco2stm	0.108,0.108,0.108,0.054,0.054, 0.0,0.00,0.00,0.00	0.132,0.132,0.132,0.066,0.066, 0.0,0.00,0.00,0.00	0.12,0.12,0.12,0.06,0.06, 0.0,0.00,0.00,0.00	(-)	Stem biomass to gases, fraction	-
frltrblf	0.00,0.00,0.00,0.0, 0.00,0.0,0.00,0.054,0.054	0.00,0.00,0.00,0.0, 0.00,0.0,0.00,0.066,0.066	0.00,0.00,0.00,0.0, 0.00,0.0,0.00,0.06,0.06	(-)	Brown leaf biomass to litter, fraction	-
frltrbrn	0.27,0.27,0.324,0.324,0.324, 0.0,0.00,0.00,0.378,0.378,	0.330,0.330,0.396,0.396,0.396, 0.0,0.00,0.00,0.462,0.462,	0.30,0.30,0.36,0.36,0.36, 0.0,0.00,0.00,0.42,0.42	(-)	Fraction of litter burned during fire	-
frltrglf	0.18,0.18,0.18,0.18,0.18, 0,0,0.09,0.09	0.22,0.22,0.22,0.22,0.22, 0,0,0.11,0.11	0.20,0.20,0.0,0.20,0.20,0.20, 0.0,0.00,0.00,0.10,0.10	(-)	Green leaf biomass to litter, fraction	-
frltrrt	0.00,0.00, 0.00,0.0, 0.00,0.0,0.00,0.225,0.225	0.110,0.110,0.110,0.110,0.110, 0.0,0.00,0.00,0.275,0.275	0.10,0.10,0.10,0.10,0.10, 0.0,0.00,0.00,0.25,0.25	(-)	Root biomass to litter, fraction	-
frltrstm	0.00,0.00,0.00,0.0, 0.00,0.0,0.00,0.0,0.00	0.660,0.660,0.660, 0.440,0.440, 0.0,0.00,0.00,0.00	0.60,0.60,0.60,0.40,0.40, 0.0,0.00,0.00,0.00	(-)	Stem biomass to litter, fraction	-
frozered	0.05	0.2	0.1	-	Factor to reduce respiration by for temps below tcrit	-
furniture	0.135,0,0	0.165,0,0	0.15,0.0,0.00,	(kgC m^{-2})	Disturbed biomass converted to furniture	-
gamma_m	0.9405	0.9595	0.95	-	Equivalent CO_2 fertilization effect without any photosynthesis down-regulation	-
gamma_w	0.2	0.45	0.35	-	Photosynthesis down regulation parameters equivalent CO_2 fertilization effect	Expert opinion
grescoef	0.15,0.15,0.15,0.15,0.15, 0.15,0.15,0.15,0.15	0.4,0.4,0.4,0.4,0.4, 0.4,0.4,0.4,0.4	0.15,0.15,0.15,0.15,0.15, 0.15,0.15,0.15,0.15,	-	Growth respiration coefficient	Pappas et al. (2013)

HCPCLY	3.00E+05	2.00E+06	2.38E+06	J m^{-3} K^{-1}	Volumetric heat capacity of fine mineral particles	Bonan (2019)
HCPOM	1.52E+06	3.55E+06	2.50E+06	J m^{-3} K^{-1}	Volumetric heat capacity of organic matter	Alnefaie and Abu-Hamdeh (2013)
HCPSND	1.92E+06	2.34E+06	2.13E+06	J m^{-3} K^{-1}	Volumetric heat capacity of sand particles	Bonan (2019)
HCPSOL	1.20E+06	3.56E+06	2.25E+06	J m^{-3} K^{-1}	Volumetric heat capacity of mineral matter	Santanello Jr et al. (2013)
hgrlthrs	9	11	10.0,	flashes km−2 y−1	Higher C-G lightning threshold	-
humicfac	0.4,0.4,0.4,0.4,0.4, 0.1,0.1,0.4,0.4	0.5,0.5,0.5,0.5,0.5, 0.5,0.1,0.1,0.5,0.5	0.42,0.42,0.53,0.48,0.48, 0.10,0.10,0.42,0.42,	-	Humification factor - used for transferring carbon from litter into soil carbon pool	Melton and Arora (2016)
kappa	1.44,1.44,1.44,1.44,1.44, 1.44,1.44,1.08,1.08	1.76,1.76,1.76,1.76,1.76, 1.76,1.76,1.32,1.32	1.6,1.6,1.6,1.6,1.6, 1.6,1.6,1.2,1.2	-	Exponential parameter of allometric relations, required to support green leaf biomass.	Ludeke et al., 1994
kmort1	0.27	0.33	0.3	m^2/gC	Parameter used in growth efficiency mortality formulation	Melton and Arora (2016)
kn	0.4,0.4,0.4,0.4,0.4, 0.4,0.4,0.4,0.4	0.7,0.7,0.7,0.7,0.7, 0.7,0.7,0.7,0.7	0.5,0.5,0.5,0.5,0.5, 0.40,0.48,0.46,0.44	-	Canopy light extinction coefficient	Pappas et al. (2013)
laimax	3.6,2.7,5.4,4.5,4.5, 7.2,7.2,3.6,3.6	4.4,3.3,6.6,5.5,5.5, 8.8,8.8,4.4,4.4	4.0,3.0,6.0,5.0,5.0, 8.0,8.0,4.0,4.0	(m2/m2)	Maximum lai above which a pft always expand	-
laimin	0.9,0.9,1.35,0.9,0.9, 0.9,0.9,0.009,0.009	1.1,1.1,1.65,1.1,1.1, 1.1,1.1,0.011,0.011	1.0,1.0,1.5,1.0,1.0, 1.0,1.0,0.01,0.01	(m2/m2)	Minimum lai below which a pft does not expand	-
lfespany	1.9459,0.3233,0.6466, 0.3233,0.3233,0.1449, 0.5779,0.1449,0.5779	7.2798,1.5,2.5979, 1,1,1.75001, 1.75001,1,1	5.0,1.0,1.5, 1.0,1.0,1.75, 1.75,1.0,1.0	years	Leaf life span	J. Li et al. (2016)
lwrlthrs	0.225	0.275	0.25,	(flashes km^{-2} $year^{-1}$)	Lower C-G lightning threshold	-
lwrthrsh	-50,-7,3,6,3, 3,3,0,3	-48,-3,7,10,7, 7,7,0.1,7	-50.0,-5.0,5.0,8.0,5.0, 5.0,5.0,0.1,5.0	°C	Lower temperature threshold. Used to estimate cold stress related leaf loss rate	-
maxage	100,100,100, 90,50,0, 0,0,0	2500,500,600, 1000,500,0, 0,0,0	250.0,400.0,600.0, 250.0,500.0,0, 0,0,0	years	Maximum plant age. used to calculate intrinsic mortality rate.	Prentice and Helmisaari (1991)
maxsprd	0.342,0.342,0.252,0.252,0.252, 0,0,0.459,0.675	0.418,0.418,0.308,0.308,0.308, 0,0,0.561,0.825	0.38,0.38,0.28,0.28,0.28, 0.00,0.00,0.51,0.75	(km hr^{-1})	Max. fire spread rate	-
minlvfr	0.05	0.2	0.05	-	Minimum live wood fraction	Expert opinion
minslai	0.05,0.05,0.05,0.05,0.05, 0.05,0.05,0.05,0.05	0.5,0.5,0.5,0.5,0.5, 0.5,0.5,0.5,0.5	0.3,0.3,0.3,0.3,0.3, 0.2,0.2,0.2,0.2	-	Minimum storage lai	Expert opinion
mm	9,9,9,9,9, 9,5.99,9,5.99	15,15,15,15,15, 15,6.01,15,6.01	9.0,9.0,12.0,12.0,12.0, 12.0,6.0,12.0,6.0	-	Used in photosynthesis-stomatal conductance coupling.	Expert opinion
mxmortge	0.0045,0.0045,0.0045, 0.0045,0.0045,0, 0,0,0	0.0055,0.0055,0.0055, 0.0055,0.0055,0, 0,0,0	0.005,0.005,0.005, 0.005,0.005,0, 0,0,0	$year^{-1}$	Maximum mortality when growth efficiency is zero	-
mxrtdpth	1,1,1,1,1, 1,0.5,0.5,0.5	7,7,12,5,5, 4,4,7,7	3.0,3.0,5.0,5.0,3.0, 2.0,2.0,1.0,1.0	m	Maximum rooting depth	Canadell et al. (1996)
omega	0.5,0.5,0.5,0.5,0.5, 0.5,0.5,0.5,0.5	0.9,0.9,0.9,0.9,0.9, 0.9,0.9,1,1	0.8,0.5,0.8,0.8,0.8, 0.5,0.5,1.0,1.0	-	Parameter used in allocation formulae	Expert opinion
omega_phtsyn	0.1275,0.1275,0.1275, 0.1275,0.1275,0.1275,0.1445, 0,0.1275,0.1445	0.1725,0.1725,0.1725, 0.1725,0.1725,0.1725,0.1955, 0,0.1725,0.1955	0.15,0.15,0.15, 0.15,0.15,0.15,0.17, 0,0.15,0.17	-	Leaf scattering coefficients	Expert opinion
paper	0.63,0.63,0.495	0.77,0.77,0.605	0.70,0.70,0.55,	(kgC m^{-2})	Disturbed biomass converted to paper	-
parblght	0.09	0.11	0.1,	(-)	Parameter b for lightning fire	-
parmlght	0.72	0.88	0.8,	(-)	Parameter m for lightning fire	-
popdthrshld	270	330	300.0,	(people km^{-2})	Threshold of population density	-
prcnslai	6.75,6.75,6.75,6.75,6.75, 6.75,6.75,2.25,2.25	8.25,8.25,8.25,8.25,8.25, 8.25,8.25,2.75,2.75	7.5,7.5,7.5,7.5,7.5, 7.5,7.5,2.5,2.5	-	Storage/imaginary lai is the percentage of maximum leaf area index that a given root+stem biomass can support	-
reparea	450	550	500.0,	(km^2)	Area representing fire parameterization	-
RHOOM	1100	1500	1.30E+03	kg m^{-3}	Particle density of soil organic matter	Young and Spycher (1979)
RHOSOL	2400	2900	2.65E+03	kg m^{-3}	Particle density of soil mineral matter	Ball et al. (2000)
rmlcoeff	0.0135,0.189,0.0225, 0.0135,0.0135,0.0135, 0.0225,0.0117,0.0225	0.0165,0231,0.0275, 0.0165,0.0165,0.0165, 0.0225,0.0143,0.0275	0.015,0.021,0.025, 0.015,0.015,0.015, 0.025,0.013,0.025	-	Leaf maintenance respiration coefficients	-

roothrsh	1	12	8	°C	Root temperature threshold for initiating leaf onset	Expert opinion
rootlife	12.42,11.88,11.43, 9.81,8.82,2.7,2.7, 0,2.7,2.7	15.18,14.52,13.97, 11.99,10.78,3.3,3.3, 0,3.3,3.3	13.8,13.2,12.7, 10.9,9.8,3.0,3.0, 0,3.0,3.0	years	Turnover timescale for root	-
rtsrmin	0.1,0.1,0.1,0.1,0.1, 0.1,0.1,0.1,0.1	1,1,1,1,1, 1,1,1,1	0.16,0.16,0.16,0.16,0.32, 0.16,0.16,0.5,0.5	-	Minimum rootshoot ratio for support and stability	Melton and Arora (2016)
sn	1,1,1,1,1, 1,1,1,1	5,5,5,5,5, 5,5,5,5	2,2,4,2,2, 2,2,2,2	-	Exponent for soil moisture stress	Expert opinion
SPHICE	1.39E+03	2.5E+03	2.10E+03	J kg^{-1} K^{-1}	Specific heat of ice	-
SPHVEG	500	3500	2.70E+03	J kg^{-1} K^{-1}	Specific heat of vegetation matter	Bonan (2019)
SPHW	4.18E+03	4.22E+03	4.19E+03	J kg^{-1} K^{-1}	Specific heat of water	Kays et al. (1980)
standreplace	0.18,0.18,0.45,0.18,0.135, 0.0,0.00,0.00,0.225,0.225	0.220,0.220,0.550,0.220,0.165, 0.0,0.00,0.00,0.275,0.275,	0.20,0.20,0.50,0.20,0.15, 0.0,0.00,0.00,0.25,0.25	(-)	PFT prevalence for stand replacing fire events	-
stemlife	77.67,77.67,72.45, 72.45,68.22,18,18, 0,0	94.93,94.93,88.55, 88.55,83.33,22,22, 0,0	86.3,86.3,80.5, 80.5,75.8,20.0,20.0, 0,0	years	Turnover timescale for stem	-
tanhq10	1.3,0.5,0.075,46	1.5,0.6,0.075,46	1.44,0.56,0.075,46.0,	-	Constants used in tanh formulation of heterotrophic respiration Q10 determination	-
TCCLAY	0.1	3	2.5	W m^{-1} K^{-1}	Thermal conductivity of fine mineral particles	Bonan (2019)
TCDRYS	0.15	2.25	0.275	W m^{-1} K^{-1}	Thermal conductivity of dry mineral soil	Abu-Hamdeh and Reeder (2000)
TCGLAC	2.18	3.48	2.24	W m^{-1} K^{-1}	Thermal conductivity of ice sheets	-
TCICE	2.21	2.81	2.24	W m^{-1} K^{-1}	Thermal conductivity of ice	Raznjevic (1976)
TCOM	0.15	2.25	0.25	W m^{-1} K^{-1}	Thermal conductivity of organic matter	Abu-Hamdeh and Reeder (2000)
tcrit	-8	0	-1	°C	Temperature below which respiration is inhibited	-
TCSAND	0.1	5	2.5	W m^{-1} K^{-1}	Thermal conductivity of sand particles	Bonan (2019)
TCW	0.522	0.646	0.57	W m^{-1} K^{-1}	Thermal conductivity of water	Kodešová et al. (2013)
thrprcnt	30,30,30,30,30, 30,30,30,30	60,60,60,60,60, 60,60,60,60	40.0,40.0,40.0,50.0,50.0, 50.0,50.0,40.0,40.0	%	Percentage of max. LAI that can be supported, used as a threshold for determining leaf phenology status	Melton and Arora (2016)
tlow	268.1,268.1, 273.1,268.1,268.1, 270.1,277.1, 271.1,278.1	270.1,270.1, 278.1,278.1,278.1, 273.1,279.1, 273.1,283.1	268.1,268.1, 273.1,273.1,273.1, 270.1,278.1, 272.1,283.1	K	Lower temperature limits for photosynthesis	-
tup	307.1,307.1, 318.1,310.1,310.1, 313.1,313.1, 313.1,323.1	315.1,315.1, 323.1,318.1,318.1, 323.1,323.1, 323.1,333.1	307.1,307.1, 318.1,310.1,310.1, 315.1,315.1, 313.1,323.1	K	Upper temperature limits for photosynthesis	-
vmax	16E-06,37E-06, 13E-06,12E-06,12E-06, 15E-06,22E-06, 15E-06,15E-06	123E-06,54E-06, 80E-06,110E-06,110E-06, 121E-06,125E-06, 121E-06,121E-06	42.0E-06,47.0E-06, 35.0E-06,57.0E-06,40.0E-06, 55.0E-06,40.0E-06, 55.0E-06,15.0E-06	mol CO_2 m^{-2} s^{-1}	Max. carboxylation rate	TRY database (Kattge et al., 2020)
VMIN	0.1	0.3	0.1	m s^{-1}	Minimum wind speed	Garratt (1994)
vpd0	1000,1000,1000, 1000,1000,1000, 1000,1000,1000	3000,3000,3000, 3000,3000,3000, 3000,3000,3000	2000.0,2000.0,2000.0, 2000.0,2000.0,1500.0, 1500.0,1500.0,1500.0	Pa	Vapour pressure deficit	Expert opinion
WSNCAP	0.01	0.15	0.04	wt%	Maximum water retention capacity of the snow pack	Expert opinion
XLEAF	0.02,0.02,0.02,0.02	0.1,0.1,0.1,0.1	0.0247,0.0204,0.0456,0.0456	-	Leaf dimension factor used in calculating the leaf boundary resistance	Expert opinion
ZOLNG	-6.908	-0.5108	-4.605	-	Natural log of roughness length of soil	R. Yang and Friedl (2003)
ZOLNI	-9.21	-4.61	-6.215	-	Natural log of roughness length of ice	Expert opinion
ZOLNS	-9.21	-4.61	-6.908	-	Natural log of roughness length of snow	Dantec-Nédélec et al. (2017)
ZORAT	1	5	1	-	The ratio of the roughness length for momentum to the roughness length for heat	Kanda et al. (2007)
ZORATG	1	5	3	-	Ratio of soil roughness length for momentum to roughness length for heat	Kanda et al. (2007)

A.4 Code and Data Availability

The *R* Statistical Software (v3.6.3; (R Core Team, 2020)) was used to conduct this study. The *sensitivity R* package (v1.27.1; (Iooss et al., 2022)) was used to perform the GSA. This *R* package consists of the *morris*() and *sobol*2002() functions which were used for screening and quantitative analysis respectively. The *sobol*() function within the *randtoolbox* R package (v1.31.1; (Christophe & Petr, 2021)) was used to generate quasi-random numbers for the quantitative method.

The repositories available at (1) `https://doi.org/10.5281/zenodo.10582208`, (2) `https://doi.org/10.5281/zenodo.13988579`, and (3) `https://doi.org/10.5281/zenodo.15061387` have a collection of scripts used in this analysis for the three main chapters. These scripts can be used to perturb the name list files, to run the CLASSIC model, and to produce the figures shown in the Results section. The input matrices and the output files have also been included in respective repository. These files can be used to reproduce the results without having to run the CLASSIC model.

The source code and the model data for the CLASSIC model v1.0 used to run all model simulations for the GSA in this dissertation can be downloaded from `https://doi.org/10.5281/zenodo.3522407`, the singularity container with required packages to run the model is at `https://doi.org/10.5281/zenodo.3525249`, and site-level meteorological input files used in Chapter 2 are available through `https://doi.org/10.5281/zenodo.3525336`. The locations of the forcing data used in Chapters 3 and 4 are provided within the respective Chapter. The external open-access components mentioned, have to be downloaded, and if needed, installed to run the CLASSIC model for other locations, but are not necessary for the reproduction of GSA/ parameter uncertainty interaction results shown in the dissertation.

A.5 Computational Demand

Each run presented in this dissertation was independent, and multiple cores were simultaneously used to run the CLASSIC model. The runs presented in Chapter 2 were performed on a single shared server with two CPUs of 8 cores each and one node. The run time for Morris and Sobol' was four weeks using 14 cores, where each run was 45 minutes long. The number of CLASSIC years were 7.83 million. The runs presented in Chapters 3 and 4 were performed on a high performance computer cluster with five nodes and 30 processors. For Chapter 3, the individual run time for each simulation was 40 minutes totalling to 10 CPU years or five weeks in real time using 120 cores for seven biome locations, and the number of CLASSIC years were 80.65 million. Similarly for Chapter 4, individual run times were an hour each, totalling to 15 CPU years or seven weeks using 120 cores for seven biome locations. The number of CLASSIC years were 98.20 million.

References

Abu-Hamdeh, N. H., & Reeder, R. C. (2000). Soil thermal conductivity effects of density, moisture, salt concentration, and organic matter. *Soil science society of America Journal*, *64*(4), 1285–1290. Retrieved from https://doi.org/10.2136/sssaj2000.6441285x

Alnefaie, K. A., & Abu-Hamdeh, N. H. (2013). Specific heat and volumetric heat capacity of some saudian soils as affected by moisture and density. In *International conference on mechanics, fluids, heat, elasticity and electromagnetic fields* (pp. 139–143). Retrieved from https://doi.org/10.46300/91018.2020.7.8

Alton, P., Mercado, L., & North, P. (2006). A sensitivity analysis of the land-surface scheme JULES conducted for three forest biomes: Biophysical parameters, model processes, and meteorological driving data. *Global Biogeochemical Cycles*, *20*(1). Retrieved from https://doi.org/10.1029/2005GB002653

Arora, V. K. (2003). Simulating energy and carbon fluxes over winter wheat using coupled land surface and terrestrial ecosystem models. *Agricultural and Forest Meteorology*, *118*(1-2), 21–47. Retrieved from https://doi.org/10.1016/S0168-1923(03)00073-X

Arora, V. K., & Boer, G. J. (2003). A representation of variable root distribution in dynamic vegetation models. *Earth Interactions*, *7*(6), 1–19. Retrieved from https://doi.org/10.1175/1087-3562(2003)007<0001:AROVRD>2.0.CO;2

Arora, V. K., & Boer, G. J. (2005). A parameterization of leaf phenology for the terrestrial ecosystem component of climate models. *Global Change Biology*, *11*(1), 39–59. Retrieved from https://doi.org/10.1111/j.1365-2486.2004.00890.x

Arora, V. K., Katavouta, A., Williams, R. G., Jones, C. D., Brovkin, V., Friedlingstein, P., … Ziehn, T. (2019). Carbon-concentration and carbon-climate feedbacks in CMIP6 models, and their comparison to CMIP5 models. *Biogeosciences Discussions*, *2019*, 1–124. Retrieved from

https://doi.org/10.5194/bg-17-4173-2020

Arora, V. K., & Scinocca, J. F. (2016). Constraining the strength of the terrestrial CO2 fertilization effect in the canadian earth system model version 4.2 (CanESM4.2). *Geoscientific Model Development*, *9*(7), 2357–2376. Retrieved from https://doi.org/10.5194/gmd-9-2357-2016

Arsenault, K. R., Nearing, G. S., Wang, S., Yatheendradas, S., & Peters-Lidard, C. D. (2018). Parameter sensitivity of the Noah-MP Land Surface Model with dynamic vegetation. *Journal of Hydrometeorology*, *19*(5), 815–830. Retrieved from https://doi.org/10.1175/jhm-d-17-0205.1

Bagnara, M., Gonzalez, R. S., Reifenberg, S., Steinkamp, J., Hickler, T., Werner, C., … Hartig, F. (2019). An R package facilitating sensitivity analysis, calibration and forward simulations with the LPJ-GUESS dynamic vegetation model. *Environmental Modelling & Software*, *111*, 55–60. Retrieved from https://doi.org/10.1016/j.envsoft.2018.09.004

Baker, E., Harper, A. B., Williamson, D., & Challenor, P. (2022). Emulation of high-resolution land surface models using sparse gaussian processes with application to JULES. *Geoscientific Model Development*, *15*(5), 1913–1929. Retrieved from https://doi.org/10.5194/gmd-15-1913-2022

Ball, B., Campbell, D., & Hunter, E. (2000). Soil compactibility in relation to physical and organic properties at 156 sites in UK. *Soil and Tillage Research*, *57*(1-2), 83–91. Retrieved from https://doi.org/10.1016/S0167-1987(00)00145-8

Bastrikov, V., MacBean, N., Bacour, C., Santaren, D., Kuppel, S., & Peylin, P. (2018). Land surface model parameter optimisation using in situ flux data: Comparison of gradient-based versus random search algorithms (a case study using ORCHIDEE v1. 9.5. 2). *Geoscientific Model Development*, *11*(12), 4739–4754. Retrieved from https://doi.org/10.5194/gmd-11-4739-2018

Bonal, D., Bosc, A., Ponton, S., GORET, J.-Y., Burban, B., Gross, P., … Granier, A. (2008). Impact of severe dry season on net ecosystem exchange in the Neotropical rainforest of French Guiana. *Global Change Biology*, *14*(8), 1917–1933. Retrieved from https://doi.org/10.1111/j.1365-2486.2008.01610.x

Bonan, G. (2019). *Climate change and terrestrial ecosystem modeling* [Book]. Cambridge University Press.

Booth, B. B., Jones, C. D., Collins, M., Totterdell, I. J., Cox, P. M., Sitch, S., … Lloyd, J. (2012). High sensitivity of future global warming to land carbon cycle processes. *Environmental Research Letters*, *7*(2), 024002. Retrieved from

https://doi.org/10.1088/1748-9326/7/2/024002

Box, G. E., & Meyer, R. D. (1986). An analysis for unreplicated fractional factorials. *Technometrics*, *28*(1), 11–18. Retrieved from https://doi.org/10.2307/1269599

Bratley, P., Fox, B. L., & Niederreiter, H. (1992). Implementation and tests of low-discrepancy sequences. *ACM Transactions on Modeling and Computer Simulation (TOMACS)*, *2*(3), 195–213. Retrieved from https://doi.org/10.1145/146382.146385

Campolongo, F., & Braddock, R. (1999). The use of graph theory in the sensitivity analysis of the model output: A second order screening method. *Reliability Engineering & System Safety*, *64*(1), 1–12. Retrieved from https://doi.org/10.1016/S0951-8320(98)00008-8

Canadell, J., Jackson, R., Ehleringer, J., Mooney, H., Sala, O., & Schulze, E.-D. (1996). Maximum rooting depth of vegetation types at the global scale. *Oecologia*, *108*, 583–595. Retrieved from https://doi.org/10.1007/BF00329030

Canadell, J., Monteiro, P. M., Costa, M. H., Cotrim da Cunha, L., Cox, P. M., Eliseev, A. V., … Williamson, P. (2023). Intergovernmental panel on climate change (ipcc). global carbon and other biogeochemical cycles and feedbacks. In *Climate change 2021: The physical science basis. contribution of working group i to the sixth assessment report of the intergovernmental panel on climate change* (pp. 673–816). Cambridge University Press. Retrieved from https://www.ipcc.ch/report/ar6/wg1/downloads/report/IPCC_AR6_WGI_FGD_Chapter05.pdf

CCI, E. (2018). *European space agency climate change initiative.* Retrieved from https://climate.esa.int/en/about-us-new/climate-change-initiative/

Chan, K., Saltelli, A., & Tarantola, S. (2000). Winding stairs: A sampling tool to compute sensitivity indices. *Statistics and Computing*, *10*(3), 187–196. Retrieved from https://doi.org/10.1023/A:1008950625967

Chini, L., Hurtt, G., Sahajpal, R., Frolking, S., Klein Goldewijk, K., Sitch, S., … Poulter, B. (2021). Land-use harmonization datasets for annual global carbon budgets. *Earth System Science Data*, *13*(8), 4175–4189. Retrieved from https://doi.org/10.5194/essd-13-4175-2021

Christophe, D., & Petr, S. (2021). randtoolbox: Generating and testing random numbers [Computer software manual]. (R package version 1.31.1)

Ciais, P., Sabine, C., Bala, G., Bopp, L., Brovkin, V., Canadell, J., … ... Vesala, T. (2013). *Carbon and other biogeochemical cycles. Climate change 2013: The physical science basis. contribution of working group I to the Fifth Assessment Report of the Intergovernmental Panel on Climate Change.* Cambridge: Cambridge University Press. Retrieved from https://www.ipcc.ch/report/ar5/wg1/carbon-and-other-biogeochemical-cycles/

Dantec-Nédélec, S., Ottlé, C., Wang, T., Guglielmo, F., Maignan, F., Delbart, N., … Jouzel, J. (2017). Testing the capability of ORCHIDEE land surface model to simulate Arctic ecosystems: Sensitivity analysis and site-level model calibration. *Journal of Advances in Modeling Earth Systems*, *9*(2), 1212–1230. Retrieved from https://doi.org/10.1002/2016MS000860

Deardorff, J. W. (1978). Efficient prediction of ground surface temperature and moisture, with inclusion of a layer of vegetation. *Journal of Geophysical Research: Oceans*, *83*(C4), 1889–1903. Retrieved from https://doi.org/10.1029/JC083iC04p01889

Dietze, M. (2017). Ecological forecasting. In *Ecological forecasting.* Princeton University Press. Retrieved from https://doi.org/10.2307/j.ctvc7796h

Farquhar, G. D., von Caemmerer, S. v., & Berry, J. A. (1980). A biochemical model of photosynthetic CO_2 assimilation in leaves of C_3 species. *Planta*, *149*(1), 78–90. Retrieved from https://doi.org/10.1007/BF00386231

Fisher, R. A., & Koven, C. D. (2020). Perspectives on the future of land surface models and the challenges of representing complex terrestrial systems. *Journal of Advances in Modeling Earth Systems*, *12*(4). Retrieved from https://doi.org/10.1029/2018MS001453

Fisher, R. A., Wieder, W. R., Sanderson, B. M., Koven, C. D., Oleson, K. W., Xu, C., … Lawrence, D. M. (2019). Parametric controls on vegetation responses to biogeochemical forcing in the CLM5. *Journal of Advances in Modeling Earth Systems*, *11*(9), 2879–2895. Retrieved from https://doi.org/10.1029/2019MS001609

Friedlingstein, P., O'sullivan, M., Jones, M. W., Andrew, R. M., Bakker, D. C., Hauck, J., … Zheng, B. (2023). Global carbon budget 2023. *Earth System Science Data*, *15*(12), 5301–5369. Retrieved from https://doi.org/10.5194/essd-15-5301-2023

Friedlingstein, P., O'Sullivan, M., Jones, M. W., Andrew, R. M., Hauck, J.,

Landschützer, P., … Zeng, J. (2024). Global carbon budget 2024. *Earth System Science Data Discussions*, *2024*, 1–133. Retrieved from https://doi.org/10.5194/essd-2024-519

Friend, A. D., Lucht, W., Rademacher, T. T., Keribin, R., Betts, R., Cadule, P., … ... Woodward, F. I. (2014). Carbon residence time dominates uncertainty in terrestrial vegetation responses to future climate and atmospheric CO2. *Proceedings of the National Academy of Sciences*, *111*(9), 3280–3285. Retrieved from https://doi.org/10.1073/pnas.1222477110

Gao, X., Avramov, A., Saikawa, E., & Schlosser, C. A. (2021). Emulation of community land model version 5 (clm5) to quantify sensitivity of soil moisture to uncertain parameters. *Journal of Hydrometeorology*, *22*(2), 259–278. Retrieved from https://doi.org/10.1175/JHM-D-20-0043.1

Gardner, A. S., & Sharp, M. J. (2010). A review of snow and ice albedo and the development of a new physically based broadband albedo parameterization. *Journal of Geophysical Research: Earth Surface*, *115*(F1). Retrieved from https://doi.org/10.1029/2009JF001444

Garratt, J. R. (1994). The atmospheric boundary layer. *Earth-Science Reviews*, *37*(1-2), 89–134. Retrieved from https://doi.org/10.1016/0012-8252(94)90026-4

Gier, B. K., Schlund, M., Friedlingstein, P., Jones, C. D., Jones, C., Zaehle, S., & Eyring, V. (2024). Representation of the terrestrial carbon cycle in CMIP6. *Biogeosciences*, *21*(22), 5321–5360. Retrieved from https://doi.org/10.5194/bg-21-5321-2024

Goll, D. S., Vuichard, N., Maignan, F., Jornet-Puig, A., Sardans, J., Violette, A., … Philippe (2017). A representation of the phosphorus cycle for ORCHIDEE (revision 4520). *Geoscientific Model Development*, *10*(10), 3745–3770. Retrieved from https://doi.org/10.5194/gmd-10-3745-2017

Green, J. K., Seneviratne, S. I., Berg, A. M., Findell, K. L., Hagemann, S., Lawrence, D. M., & Gentine, P. (2019). Large influence of soil moisture on long-term terrestrial carbon uptake. *Nature*, *565*(7740), 476–479. Retrieved from https://doi.org/10.1038/s41586-018-0848-x

Harris, I. (2019). CRU JRA v1. 1: a forcings dataset of gridded land surface blend of climatic research unit (CRU) and japanese reanalysis (JRA) data, January 1901–December 2017, University of East Anglia climatic research unit, centre for environmental data analysis. *University of East Anglia Climatic*

Research Unit, Centre for Environmental Data Analysis, *10*. Retrieved from https://dx.doi.org/10.5285/13f3635174794bb98cf8ac4b0ee8f4ed

Harris, I., Jones, P., Osborn, T., & Lister, D. (2014). Updated high-resolution grids of monthly climatic observations-the CRU TS3. 10 dataset. *International journal of climatology*, *34*, 623–642. Retrieved from https://ueaeprints.uea.ac.uk/id/eprint/47192

Horowitz, C. A. (2016). Paris agreement. *International Legal Materials*, *55*(4), 740–755. Retrieved from https://doi.org/10.1017/S0020782900004253

Hou, T., Zhu, Y., Lü, H., Sudicky, E., Yu, Z., & Ouyang, F. (2015). Parameter sensitivity analysis and optimization of Noah Land Surface Model with field measurements from Huaihe River Basin, China. *Stochastic environmental research and risk assessment*, *29*(5), 1383–1401. Retrieved from https://doi.org/10.1007/s00477-015-1033-5

Hurtt, G., Chini, L., Sahajpal, R., Frolking, S., Bodirsky, B. L., Calvin, K., … Zhang, X. (2017). *Harmonization of global land use scenarios (LUH2): SSP585 v2.1f 2015 - 2100.* Earth System Grid Federation. Retrieved from https://doi.org/10.22033/ESGF/input4MIPs.1662

Iooss, B., Veiga, S. D., Janon, A., Pujol, G., with contributions from Baptiste Broto, Boumhaout, K., … Weber, F. (2022). *sensitivity: Global sensitivity analysis of model outputs* [R package version 1.27.1]. Retrieved from https://CRAN.R-project.org/package=sensitivity

Jones, B., & O'Neill, B. C. (2016). Spatially explicit global population scenarios consistent with the Shared Socioeconomic Pathways. *Environmental Research Letters*, *11*(8), 084003. Retrieved from https://doi.org/10.1088/1748-9326/11/8/084003

Kaminski, T., Knorr, W., Schürmann, G., Scholze, M., Rayner, P., Zaehle, S., … Ziehn, T. (2013). The BETHY/JSBACH carbon cycle data assimilation system: Experiences and challenges. *Journal of Geophysical Research: Biogeosciences*, *118*(4), 1414–1426. Retrieved from https://doi.org/10.1002/jgrg.20118

Kanda, M., Kanega, M., Kawai, T., Moriwaki, R., & Sugawara, H. (2007). Roughness lengths for momentum and heat derived from outdoor urban scale models. *Journal of Applied Meteorology and Climatology*, *46*(7), 1067–1079. Retrieved from https://doi.org/10.1175/JAM2500.1

Kattge, J., Bönisch, G., Díaz, S., Lavorel, S., Prentice, I. C., Leadley, P., … Wirth, C. (2020). TRY plant trait database–enhanced coverage and

open access. *Global change biology*, *26*(1), 119–188. Retrieved from https://doi.org/10.1111/gcb.14904

Kays, W. M., Crawford, M. E., & Weigand, B. (1980). *Convective heat and mass transfer* (Vol. 4) [Book]. McGraw-Hill New York.

Klein Goldewijk, K., Beusen, A., Doelman, J., & Stehfest, E. (2017). Anthropogenic land use estimates for the holocene–HYDE 3.2. *Earth System Science Data*, *9*(2), 927–953. Retrieved from https://doi.org/10.5194/essd-9-927-2017

Knorr, W., Williams, M., Thum, T., Kaminski, T., Voßbeck, M., Scholze, M., … Drusch, M. (2024). A comprehensive land surface vegetation model for multi-stream data assimilation, D&B v1. 0. Retrieved from https://doi.org/10.5194/egusphere-2024-1534

Kobayashi, S., Ota, Y., Harada, Y., Ebita, A., Moriya, M., Onoda, H., … Takahashi, K. (2015). The JRA-55 reanalysis: General specifications and basic characteristics. *Journal of the Meteorological Society of Japan. Ser. II*, *93*(1), 5–48. Retrieved from https://doi.org/10.2151/jmsj.2015-001

Kodešová, R., Vlasakova, M., Fer, M., Tepla, D., Jakšík, O., Neuberger, P., & Adamovskỳ, R. (2013). Thermal properties of representative soils of the czech republic. *Soil and Water Research*, *8*(4), 141–150. Retrieved from https://doi.org/10.17221/33/2013-SWR

Koven, C., Arora, V. K., Cadule, P., Fisher, R. A., Jones, C. D., Lawrence, D. M., … ... Zickfeld, K. (2021). 23rd century surprises: Long-term dynamics of the climate and carbon cycle under both high and net negative emissions scenarios. *Earth System Dynamics Discussions*, *2021*, 1–32. Retrieved from https://doi.org/10.5194/esd-13-885-2022

Kriegler, E., Bauer, N., Popp, A., Humpenöder, F., Leimbach, M., Strefler, J., … Edenhofer, O. (2017). Fossil-fueled development (SSP5): An energy and resource intensive scenario for the 21st century. *Global environmental change*, *42*, 297–315. Retrieved from https://doi.org/10.1016/j.gloenvcha.2016.05.015

Kucherenko, S., & Sytsko, Y. (2005). Application of deterministic low-discrepancy sequences in global optimization. *Computational Optimization and Applications*, *30*(3), 297–318. Retrieved from https://doi.org/10.1007/s10589-005-4615-1

Lange, S., & Büchner, M. (2021). *ISIMIP3b bias-adjusted atmospheric climate input data.* ISIMIP Repository. Re-

trieved from https://doi.org/10.48364/ISIMIP.842396.1 doi: 10.48364/ISIMIP.842396.1

Lawrence, D. M., Fisher, R. A., Koven, C. D., Oleson, K. W., Swenson, S. C., Bonan, G., … Zeng, X. (2019). The community land model version 5: Description of new features, benchmarking, and impact of forcing uncertainty. *Journal of Advances in Modeling Earth Systems*, *11*(12), 4245–4287. Retrieved from https://doi.org/10.1029/2018MS001583

Lee, H., Calvin, K., Dasgupta, D., Krinner, G., Mukherji, A., Thorne, P., … Zommers, Z. (2023). *Climate change 2023: synthesis report. contribution of working groups I, II and III to the sixth assessment report of the intergovernmental panel on climate change*. The Australian National University. Retrieved from https://doi.org/10.59327/IPCC/AR6-9789291691647

Leuning, R. (1995). A critical appraisal of a combined stomatal-photosynthesis model for C_3 plants. *Plant, Cell & Environment*, *18*(4), 339–355. Retrieved from https://doi.org/10.1111/j.1365-3040.1995.tb00370.x

Li, J., Duan, Q., Gong, W., Ye, A., Dai, Y., Miao, C., … Sun, Y. (2013). Assessing parameter importance of the Common Land Model based on qualitative and quantitative sensitivity analysis. *Hydrology and Earth System Sciences*, *17*(8), 3279–3293. Retrieved from https://doi.org/10.5194/hess-17-3279-2013

Li, J., Wang, Y.-P., Duan, Q., Lu, X., Pak, B., Wiltshire, A., … Ziehn, T. (2016). Quantification and attribution of errors in the simulated annual gross primary production and latent heat fluxes by two global land surface models. *Journal of Advances in Modeling Earth Systems*, *8*(3), 1270–1288. Retrieved from https://doi.org/10.1002/2015MS000583

Li, Y., Wang, Y., Sun, Y., & Li, J. (2022). Global sensitivity analysis of the LPJ model for Larix olgensis Henry forests NPP in Jilin Province, China. *Forests*, *13*(6), 874. Retrieved from https://doi.org/10.3390/f13060874

Lu, J., Wang, G., Li, S., Feng, A., Zhan, M., Jiang, T., … Wang, Y. (2021). Projected land evaporation and its response to vegetation greening over china under multiple scenarios in the CMIP6 models. *Journal of Geophysical Research: Biogeosciences*, *126*(9), e2021JG006327. Retrieved from https://doi.org/10.1029/2021JG006327

Lu, X., Wang, Y.-P., Ziehn, T., & Dai, Y. (2013). An efficient method for global parameter sensitivity analysis and its applications to the Australian community land surface model (CABLE). *Agricultural and forest meteorology*, *182*, 292–

303. Retrieved from https://doi.org/10.1016/j.agrformet.2013.04.003

Ma, H., Ma, C., Li, X., Yuan, W., Liu, Z., & Zhu, G. (2020). Sensitivity and uncertainty analyses of flux-based ecosystem model towards improvement of forest GPP simulation. *Sustainability*, *12*(7), 2584. Retrieved from https://doi.org/10.3390/su12072584

Manabe, S. (1969). Climate and the ocean circulation: I. The atmospheric circulation and the hydrology of the Earth's surface. *Monthly Weather Review*, *97*(11), 739–774. Retrieved from https://doi.org/10.1175/1520-0493(1969)097<0739:CATOC>2.3.CO;2

Massoud, E. C., Xu, C., Fisher, R. A., Knox, R. G., Walker, A. P., Serbin, S. P., … ... Vrugt, J. A. (2019). Identification of key parameters controlling demographically structured vegetation dynamics in a land surface model: CLM4. 5 (FATES). *Geoscientific Model Development*, *12*(9), 4133–4164. Retrieved from https://doi.org/10.5194/gmd-12-4133-2019

Matthews, J. R., Möller, V., van Diemen, R., Fuglestvedt, J., Masson-Delmotte, V., Méndez, C., … ... Zanis, P. (2021). Annex VII-Glossary 3. *Notes*, *29*, 30. Retrieved from https://doi.org/10.1017/9781009157896.022.

McNeall, D., Robertson, E., & Wiltshire, A. (2023). Constraining the carbon cycle in JULES-es-1.0. *Geoscientific Model Development Discussions*, *2023*, 1–38. Retrieved from https://doi.org/10.5194/gmd-17-1059-2024

McNeall, D., Williams, J., Betts, R., Booth, B., Challenor, P., Good, P., & Wiltshire, A. (2020). Correcting a bias in a climate model with an augmented emulator. *Geoscientific Model Development*, *13*(5), 2487–2509. Retrieved from https://doi.org/10.5194/gmd-13-2487-2020

Meinshausen, M., Nicholls, Z. R., Lewis, J., Gidden, M. J., Vogel, E., Freund, M., … Wang, R. H. J. (2020). The shared socio-economic pathway (SSP) greenhouse gas concentrations and their extensions to 2500. *Geoscientific Model Development*, *13*(8), 3571–3605. Retrieved from https://doi.org/10.5194/gmd-13-3571-2020

Meinshausen, M., Vogel, E., Nauels, A., Lorbacher, K., Meinshausen, N., Etheridge, D., … Weiss, R. (2016). Historical greenhouse gas concentrations. *Geoscientific Model Development Discussions*, *6*, 1–122. Retrieved from https://doi.org/10.5194/gmd-2016-169

Melton, J., & Arora, V. (2016). Competition between plant functional types in the Canadian Terrestrial Ecosystem Model (CTEM) v.

2.0. *Geoscientific Model Development*, *9*(1), 323–361. Retrieved from https://doi.org/10.5194/gmd-9-323-2016

Melton, J., Arora, V., Wisernig-Cojoc, E., Seiler, C., Fortier, M., Chan, E., & Teckentrup, L. (2019). *The canadian land surface scheme including biogeochemical cycles, zenodo* [Software]. Zenodo. Retrieved from https://doi.org/10.5281/zenodo.3522407

Melton, J., Arora, V. K., Wisernig-Cojoc, E., Seiler, C., Fortier, M., Chan, E., & Teckentrup, L. (2020). CLASSIC v1. 0: The open-source community successor to the Canadian Land Surface Scheme (CLASS) and the Canadian Terrestrial Ecosystem Model (CTEM)–part 1: Model framework and site-level performance. *Geoscientific Model Development*, *13*(6), 2825–2850. Retrieved from https://doi.org/10.5194/gmd-13-2825-2020

Melton, J., Seiler, C., & Fortier, M. (2019). *Singularity software container for the canadian land surface scheme including biogeochemical cycles (classic), zenodo* [Software]. Zenodo. Retrieved from https://doi.org/10.5281/zenodo.3525249

Melton, J., Shrestha, R., & Arora, V. (2015). The influence of soils on heterotrophic respiration exerts a strong control on net ecosystem productivity in seasonally dry Amazonian forests. *Biogeosciences*, *12*(4), 1151–1168. Retrieved from https://doi.org/10.5194/bg-12-1151-2015

Melton, J., Teckentrup, L., & Fortier, M. (2019). *Benchmarking data and outputs for classic v. 1.0, zenodo* [Dataset]. Zenodo. Retrieved from https://doi.org/10.5281/zenodo.3525336

Morokoff, W. J., & Caflisch, R. E. (1994). Quasi-random sequences and their discrepancies. *SIAM Journal on Scientific Computing*, *15*(6), 1251–1279. Retrieved from https://doi.org/10.1137/0915077

Morris, M. D. (1991). Factorial sampling plans for preliminary computational experiments. *Technometrics*, *33*(2), 161–174. Retrieved from https://doi.org/10.1080/00401706.1991.10484804

Niederreiter, H. (1978). Quasi-Monte Carlo methods and pseudo-random numbers. *Bulletin of the American mathematical society*, *84*(6), 957–1041. Retrieved from https://doi.org/10.1090/S0002-9904-1978-14532-7

Niederreiter, H. (1992). *Random number generation and Quasi-Monte Carlo methods* [Book]. SIAM. Retrieved from https://www.ricam.oeaw.ac.at/files/people/siambook$_n$*ied.pdf*

Pappas, C., Fatichi, S., Leuzinger, S., Wolf, A., & Burlando, P. (2013). Sensitivity analysis of a process-based ecosystem model: Pinpointing parameterization and structural issues. *Journal of Geophysical Research: Biogeosciences*, *118*(2), 505–528. Retrieved from https://doi.org/10.1002/jgrg.20035

Parameter optimization for global soil carbon simulations: Not a simple problem. (n.d.).

Pastorello, G., Papale, D., Chu, H., Trotta, C., Agarwal, D., Canfora, E., … Torn, M. (2017). A new data set to keep a sharper eye on land-air exchanges. *Eos, Transactions American Geophysical Union (Online)*, *98*(8). Retrieved from http://doi.org/10.1029/2017EO071597

Pastorello, G., Trotta, C., Canfora, E., Chu, H., Christianson, D., Cheah, Y.-W., … Papale, D. (2020). The FLUXNET2015 dataset and the ONEFlux processing pipeline for eddy covariance data. *Scientific data*, *7*(1), 1–27. Retrieved from https://doi.org/10.1038/s41597-020-0534-3

Petropoulos, G., Griffiths, H., Carlson, T., Ioannou-Katidis, P., & Holt, T. (2014). SimSphere model sensitivity analysis towards establishing its use for deriving key parameters characterising land surface interactions. *Geoscientific Model Development*, *7*(5), 1873–1887. Retrieved from https://doi.org/10.5194/gmd-7-1873-2014

Pitman, A. (2003). The evolution of, and revolution in, land surface schemes designed for climate models. *International Journal of Climatology: A Journal of the Royal Meteorological Society*, *23*(5), 479–510. Retrieved from https://doi.org/10.1002/joc.893

Prentice, I. C., & Helmisaari, H. (1991). Silvics of north European trees: compilation, comparisons and implications for forest succession modelling. *Forest Ecology and Management*, *42*(1-2), 79–93. Retrieved from https://doi.org/10.1016/0378-1127(91)90066-5

R Core Team. (2020). R: A Language and Environment for Statistical Computing [Computer software manual]. Vienna, Austria. Retrieved from https://www.R-project.org/

Raoult, N., Douglas, N., MacBean, N., Kolassa, J., Quaife, T., Roberts, A. G., … Zobitz, J. (2024). Parameter estimation in land surface models: Challenges and opportunities with data assimilation and machine learning. Retrieved from https://doi.org/10.22541/essoar.172838640.01153603/v1

Raznjevic, K. (1976). *Handbook of thermodynamic tables and charts* [Book]. Hemi-

sphere Publishing Corp., Washington, DC.

Reed, S. C., Yang, X., & Thornton, P. E. (2015). Incorporating phosphorus cycling into global modeling efforts: A worthwhile, tractable endeavor. *New Phytologist*, *208*(2), 324–329. Retrieved from https://doi.org/10.1111/nph.13521

Ricciuto, D., Sargsyan, K., & Thornton, P. (2018). The impact of parametric uncertainties on biogeochemistry in the E3SM land model. *Journal of Advances in Modeling Earth Systems*, *10*(2), 297–319. Retrieved from https://doi.org/10.1002/2017MS000962

Rodriguez, D. A., & Espíndola, R. P. (2024). Improving physiological simulations in seasonally dry tropical forests with limited measurements. *Theoretical and Applied Climatology*, 1–14. Retrieved from https://doi.org/10.1007/s00704-024-05050-1

Rosolem, R., Gupta, H. V., Shuttleworth, W. J., Zeng, X., & De Gonçalves, L. G. G. (2012). A fully multiple-criteria implementation of the sobol' method for parameter sensitivity analysis. *Journal of Geophysical Research: Atmospheres*, *117*(D7). Retrieved from https://doi.org/10.1029/2011JD016355

Saltelli, A. (2002). Sensitivity analysis for importance assessment. *Risk analysis*, *22*(3), 579–590. Retrieved from https://doi.org/10.1111/0272-4332.00040

Saltelli, A., Ratto, M., Andres, T., Campolongo, F., Cariboni, J., Gatelli, D., … Tarantola, S. (2008). *Global sensitivity analysis: The Primer* [Book]. John Wiley & Sons. Retrieved from https://doi.org/10.1002/9780470725184

Saltelli, A., Tarantola, S., Campolongo, F., & Ratto, M. (2004). *Sensitivity analysis in practice: A guide to assessing scientific models* [Book]. Wiley Online Library. Retrieved from http://doi.org/10.1002/0470870958

Santanello Jr, J. A., Kumar, S. V., Peters-Lidard, C. D., Harrison, K., & Zhou, S. (2013). Impact of land model calibration on coupled land–atmosphere prediction. *Journal of Hydrometeorology*, *14*(5), 1373–1400. Retrieved from https://doi.org/10.1175/JHM-D-12-0127.1

Schimel, D., Stephens, B. B., & Fisher, J. B. (2015). Effect of increasing CO2 on the terrestrial carbon cycle. *Proceedings of the National Academy of Sciences*, *112*(2), 436–441. Retrieved from https://doi.org/10.1073/pnas.1407302112

Seiler, C., Kou-Giesbrecht, S., Arora, V. K., & Melton, J. (2024). The impact of climate forcing biases and the nitrogen cycle on land carbon balance projec-

tions. *Journal of Advances in Modeling Earth Systems*, *16*(1), e2023MS003749. Retrieved from https://doi.org/10.1029/2023MS003749

Sellers, P., Dickinson, R., Randall, D., Betts, A., Hall, F., Berry, J., … Henderson-Sellers, A. (1997). Modeling the exchanges of energy, water, and carbon between continents and the atmosphere. *Science*, *275*(5299), 502–509. Retrieved from https://doi.org/10.1126/science.275.5299.502

Senapati, N., Jansson, P.-E., Smith, P., & Chabbi, A. (2016). Modelling heat, water and carbon fluxes in mown grassland under multi-objective and multi-criteria constraints. *Environmental Modelling & Software*, *80*, 201–224. Retrieved from https://doi.org/10.1016/j.envsoft.2016.02.025

Shi, Z., Allison, S. D., He, Y., Levine, P. A., Hoyt, A. M., Beem-Miller, J., … Randerson, J. T. (2020). The age distribution of global soil carbon inferred from radiocarbon measurements. *Nature Geoscience*, *13*(8), 555–559. Retrieved from https://doi.org/10.1038/s41561-020-0596-z

Sitch, S., O'sullivan, M., Robertson, E., Friedlingstein, P., Albergel, C., Anthoni, P., … Zaehle, S. (2024). Trends and drivers of terrestrial sources and sinks of carbon dioxide: An overview of the TRENDY project. *Global Biogeochemical Cycles*, *38*(7), e2024GB008102. Retrieved from https://doi.org/10.1029/2024GB008102

Skillman, J. B. (2008). Quantum yield variation across the three pathways of photosynthesis: not yet out of the dark. *Journal of Experimental Botany*, *59*(7), 1647–1661. Retrieved from https://doi.org/10.1093/jxb/ern029

S. N., R. D., Seiler, C., & Monahan, A. H. (2024). A global sensitivity analysis of parameter uncertainty in the CLASSIC model. *Atmosphere-Ocean*, *62*(5), 347–359. Retrieved from https://doi.org/10.1080/07055900.2024.2396426 doi: 10.1080/07055900.2024.2396426

Sobol', I. M. (1967). On the distribution of points in a cube and the approximate evaluation of integrals. *Zhurnal Vychislitel'noi Matematiki i Matematicheskoi Fiziki*, *7*(4), 784–802. Retrieved from https://doi.org/10.1016/0041-5553(67)90144-9

Sobol', I. M. (1976). Uniformly distributed sequences with an additional uniform property. *USSR Computational Mathematics and Mathematical Physics*, *16*(5), 236–242. Retrieved from https://doi.org/10.1016/0041-5553(76)90154-3

Sobol', I. M. (1998). On Quasi-Monte Carlo integrations. *Mathematics and computers in simulation*, *47*(2-5), 103–112. Retrieved from

https://doi.org/10.1016/S0378-4754(98)00096-2

Sobol', I. M., & Kucherenko, S. S. (2005). On global sensitivity analysis of Quasi-Monte Carlo algorithms. *Monte Carlo methods and applications*, *11*(1), 83–92. Retrieved from https://doi.org/10.1515/1569396054027274

Swart, N. C., Cole, J. N., Kharin, V. V., Lazare, M., Scinocca, J. F., Gillett, N. P., … Winter, B. (2019). The Canadian Earth System Model version 5 (CanESM5. 0.3). *Geoscientific Model Development*, *12*(11), 4823–4873. Retrieved from https://doi.org/10.5194/gmd-12-4823-2019

Tang, J., & Zhuang, Q. (2009). A global sensitivity analysis and Bayesian inference framework for improving the parameter estimation and prediction of a process-based Terrestrial Ecosystem Model. *Journal of Geophysical Research: Atmospheres*, *114*(D15). Retrieved from https://doi.org/10.1029/2009JD011724

Varney, R. M., Friedlingstein, P., Chadburn, S. E., Burke, E. J., & Cox, P. M. (2024). Soil carbon-concentration and carbon-climate feedbacks in CMIP6 earth system models. *Biogeosciences*, *21*(11), 2759–2776. Retrieved from https://doi.org/10.5194/bg-21-2759-2024

Verbeeck, H., Samson, R., Verdonck, F., & Lemeur, R. (2006). Parameter sensitivity and uncertainty of the forest carbon flux model FORUG: A Monte Carlo analysis. *Tree physiology*, *26*(6), 807–817. Retrieved from https://doi.org/10.1093/treephys/26.6.807

Verseghy, D. (2017). CLASS-The Canadian Land Surface Scheme (v. 3.6. 2). *Climate Research Division, Science and Technology Branch, Environment Canada*, *35*.

Wagener, T., & Pianosi, F. (2019). What has global sensitivity analysis ever done for us? A systematic review to support scientific advancement and to inform policy-making in Earth system modelling. *Earth-science reviews*, *194*, 1–18. Retrieved from https://doi.org/10.1016/j.earscirev.2019.04.006

Wallach, D., & Genard, M. (1998). Effect of uncertainty in input and parameter values on model prediction error. *Ecological Modelling*, *105*(2-3), 337–345. Retrieved from https://doi.org/10.1016/S0304-3800(97)00180-4

Wang, Y., Law, R., & Pak, B. (2010). A global model of carbon, nitrogen and phosphorus cycles for the terrestrial biosphere. *Biogeosciences*, *7*(7). Retrieved from https://doi.org/10.5194/bg-7-2261-2010

Wu, K., Hu, Z., Wang, X., Chen, J., Yang, H., & Yuan, W. (2024). Widespread increase in sensitivity of vegetation growth to climate variability on the tibetan plateau. *Agricultural and Forest Meteorology*, *358*, 110260. Retrieved from

https://doi.org/10.1016/j.agrformet.2024.110260

Xiao, J., Davis, K. J., Urban, N. M., & Keller, K. (2014). Uncertainty in model parameters and regional carbon fluxes: A model-data fusion approach. *Agricultural and Forest Meteorology*, *189*, 175–186. Retrieved from https://doi.org/10.1016/j.agrformet.2014.01.022

Xing, X., Wu, M., Zhang, W., Ju, W., Tagesson, T., He, W., … Jiang, F. (2023). Modeling china's terrestrial ecosystem gross primary productivity with BEPS model: Parameter sensitivity analysis and model calibration. *Agricultural and Forest Meteorology*, *343*, 109789. Retrieved from https://doi.org/10.1016/j.agrformet.2023.109789

Yang, Q., Dan, L., Lv, M., Wu, J., Li, W., & Dong, W. (2021). Quantitative assessment of the parameterization sensitivity of the Noah-MP land surface model with dynamic vegetation using ChinaFLUX data. *Agricultural and Forest Meteorology*, *307*, 108542. Retrieved from https://doi.org/10.1016/j.agrformet.2021.108542

Yang, R., & Friedl, M. A. (2003). Determination of roughness lengths for heat and momentum over boreal forests. *Boundary-Layer Meteorology*, *107*, 581–603. Retrieved from https://doi.org/10.1023/A:1022880530523

Yang, X., Thornton, P., Ricciuto, D., & Post, W. (2014). The role of phosphorus dynamics in tropical forests–a modeling study using CLM-CNP. *Biogeosciences*, *11*(6), 1667–1681. Retrieved from https://doi.org/10.5194/bg-11-1667-2014

Yang, Y., Bloom, A. A., Ma, S., Levine, P., Norton, A., Parazoo, N. C., … Saatchi, S. (2022). CARDAMOM-FluxVal version 1.0: a FLUXNET-based validation system for CARDAMOM carbon and water flux estimates. *Geoscientific Model Development*, *15*(4), 1789–1802. Retrieved from https://doi.org/10.5194/gmd-15-1789-2022

Young, J., & Spycher, G. (1979). Water-dispersible soil organic-mineral particles: I. Carbon and nitrogen distribution. *Soil Science Society of America Journal*, *43*(2), 324–328. Retrieved from https://doi.org/10.2136/sssaj1979.03615995004300020017x

Zhang, W., Jansson, P.-E., Sigsgaard, C., McConnell, A., Jammet, M. M., Westergaard-Nielsen, A., … Elberling, B. (2019). Model-data fusion to assess year-round CO2 fluxes for an arctic heath ecosystem in West Greenland (69 N). *Agricultural and Forest Meteorology*, *272*, 176–186. Retrieved from

https://doi.org/10.1016/j.agrformet.2019.02.021

Zheng, Y., Zhang, L., Xiao, J., Yuan, W., Yan, M., Li, T., & Zhang, Z. (2018). Sources of uncertainty in gross primary productivity simulated by light use efficiency models: Model structure, parameters, input data, and spatial resolution. *Agricultural and forest meteorology*, *263*, 242–257. Retrieved from https://doi.org/10.1016/j.agrformet.2018.08.003

Zhu, Q., & Zhuang, Q. (2014). Parameterization and sensitivity analysis of a process-based terrestrial ecosystem model using adjoint method. *Journal of Advances in Modeling Earth Systems*, *6*(2), 315–331. Retrieved from https://doi.org/10.1002/2013MS000241